Process-based modelling
of the methane balance
in periglacial landscapes

Dissertation

zur Erlangung des akademischen Grades doctor rerum naturalium

(Dr. rer. nat.)

vorgelegt dem Rat der Chemisch-Geowissenschaftlichen Fakultät der Friedrich-Schiller-Universität Jena

von Dipl.-Math. techn. Sonja Kaiser

geboren am 03. 07. 1981 in Karl-Marx-Stadt

Gutachter:

1. Prof. Dr. Christian Beer, Stockholm University, Sweden

2. Prof. Dr. Martin Heimann, MPI for Biogeochemistry Jena, Germany

3. PD Dr. Axel Kleidon, MPI for Biogeochemistry Jena, Germany

Tag der Verteidigung: 06. 12. 2017

Table of Contents

Deutsche Kurzfassung

Es wurde ein detailliertes, prozessbasiertes Methanmodul für ein globales Landoberflächenmodell entwickelt. Es ist allgemein genug, um in Permafrostregionen genauso wie in Feuchtgebieten außerhalb von Permafrostgebieten angewandt zu werden. Methanproduktion, Oxidation und Transport mittels aufsteigender Gasblasen, Diffusion und Pflanzen werden repräsentiert. In diesem Modell wurde Sauerstoff in die Diffusion, den Transport mittels Pflanzen und in zwei Oxidationsprozesse explizit einbezogen, von denen einer Bodensauerstoff benutzt, während der andere Sauerstoff benutzt, der über die Wurzeln verfügbar ist. Permafrost- und Feuchtgebietsböden zeigen spezielles Verhalten, wie zum Beispiel einen veränderlichen Bodenporenraum aufgrund von Gefrier- und Auftauvorgängen oder eine variable Wasserspiegeltiefe durch den sich stark ändernden Bodenwassergehalt. Dies wurde direkt in die mit Methan in Beziehung stehenden Prozesse integriert. Eine detaillierte Anwendung an dem Tundrastandort Samoylov, Lenadelta, Russland, der sich durch Frostmusterböden auszeichnet, wird zu Evaluierungszwecken genutzt. Die Anwendung auf Samoylov zeigt auch Unterschiede in der Wichtigkeit von verschiedenen Transportprozessen und in der Methandynamik unter variierenden Bodenfeuchte-, -eis- und -temperaturbedingungen während verschiedener Jahreszeiten und auf verschiedenen Mikrostandorten. Diese Mikrostandorte sind der erhöhte feuchte Rand und das abgesenkte nasse Zentrum des Polygons. Die Evaluierung zeigt eine ausreichend gute Übereinstimmung mit den Feldbeobachtungen, obwohl das Modul nicht spezifisch an diese Daten angepasst worden ist. Dieses Methanmodul ist so konzipiert, daß das erweiterte Landoberflächenmodell aktuelle und zukünftige Methanflüsse von kalthumiden Landschaften

skalenübergreifend modellieren kann. Zusätzlich kann der Beitrag von Methan zu Kohlenstoff-Klima-Rückkopplungsmechanismen quantifiziert werden, wenn es mit einem Atmosphärenmodell gekoppelt benutzt wird.

In einem zweiten Schritt wurde eine weiterentwickelte Version des zugrundeliegenden Landoberflächenmodells, inklusive eines verbesserten Methanmoduls, für regionale, das zukünftige Klima betreffende Experimente genutzt. Die Modifikationen beinhalten Veränderungen in der Hydrologie, dem Kohlenstoffabbau und der Methanproduktion, der Reihenfolge der Transportprozesse und dem Transport mittels Pflanzen. Zusätzlich wurde ein neuer Transportprozess einbezogen, die Diffusion von Gasen durch Schnee. Das so weiterentwickelte Modell wurde am großräumigen Gebiet um das Lenadelta zwischen 71° und 74° N sowie 123° und 130° O angewandt. Detaillierte Analysen der Bodenatmungs- und Methanprozessflüsse, ihrer räumlichen Verteilung sowie Veränderungen über die Zeit und im jahreszeitlichen Wechsel werden präsentiert. Sie zeigen die Relevanz der Methan- verglichen mit den Kohlenstoffdioxidemissionen des Bodens, die Muster von Gebieten mit günstigen Bedingungen für Methanemissionen sowie den Anstieg von Gasflüssen und der Länge der Emissionssaison aufgrund des Klimawandels. Folglich kann das präsentierte prozessbasierte Methanmodul im Rahmen des Landoberflächenmodells ein nützliches Werkzeug zum Studium der Variabilität der Methanemissionen aufgrund von verschiedensten Einflußfaktoren, räumliche und zeitliche Skalen übergreifend, sein. Wenn es mit einem vollständigen Erdsystemmodell gekoppelt wird, kann es Einsichten in die Rolle von Methan in den Kohlenstoffkreislauf-Klima-Rückkopplungsmechanismen liefern.

Abstract

A detailed process-based methane module for a global land surface scheme has been developed which is general enough to be applied in permafrost regions as well as wetlands outside permafrost areas. Methane production, oxidation and transport by ebullition, diffusion and plants are represented. In this model, oxygen has been explicitly incorporated into diffusion, transport by plants and two oxidation processes, of which one uses soil oxygen, while the other uses oxygen that is available via roots. Permafrost and wetland soils show special behaviour, such as variable soil pore space due to freezing and thawing or water table depths due to changing soil water content. This has been integrated directly into the methane-related processes. A detailed application at the Samoylov polygonal tundra site, Lena River Delta, Russia, is used for evaluation purposes. The application at Samoylov also shows differences in the importance of the several transport processes and in the methane dynamics under varying soil moisture, ice and temperature conditions during different seasons and on different microsites. These microsites are the elevated moist polygonal rim and the depressed wet polygonal centre. The evaluation shows sufficiently good agreement with field observations despite the fact that the module has not been specifically calibrated to these data. This methane module is designed such that the advanced land surface scheme is able to model recent and future methane fluxes from periglacial landscapes across scales. In addition, the methane contribution to carbon cycle – climate feedback mechanisms can be quantified when running coupled to an atmospheric model.

In a second step, a further developed version of the underlying land surface scheme, including an enhanced methane module, has been used for regional future climate experiments. The alterations include changes in the hydrology, the carbon decomposition and methane production, the order of the transport processes and the transport via plants. Additionally, a new transport process has been included, the diffusion of gases through snow. The thus further developed model has been applied at the larger area of the Lena River Delta between 71° and 74° N as well as 123° and 130° E. Detailed analyses of the soil respiration and methane process fluxes, their spatial distribution as well as changes with time and in the seasonal behaviour are presented. They show the relevance of the methane fluxes compared to the carbon dioxide emissions from the soil, the pattern of regions with favourable conditions for methane emissions as well as the increase of the gas fluxes and the emission season length due to climate change. Thus, the presented process-based methane module within the framing of the land surface scheme may be a useful tool for studying the variability of the methane emissions due to various influencing factors across spatial and temporal scales. When coupled to a full Earth system model, it can provide insights into the role of methane in the carbon cycle – climate feedback mechanisms.

Chapter 1

Introduction

1.1 Permafrost ecosystems

In high latitudes, and also at high altitudes, temperatures can stay cold enough during the course of the year to prevent the ground from thawing even in summer. If the ground stays frozen for at least 2 years, by definition it is called permafrost (Osterkamp, 2001; French, 2007). Landscapes that exhibit permafrost may still show biological life associated with the part of the ground that thaws during summer. These ecosystems however are limited by the short period of warm temperatures to grow and maintain themselves. When temperatures drop, the soil freezes again after just a short period of unfrozen conditions. Then, almost all biological processes come to a hold and may only start again once the temperatures rise above 0℃. Former biologically active soil parts, that are rich in organic carbon, freeze and may stay frozen over time periods of many years.

Another consequence of permafrost is the possibility of waterlogged soils. Frozen soil, moreover frozen water rich soil, contains a lot of ice. This ice prevents rain, meltwater or other sources of liquid water from draining into deeper parts of the ground (Woo, 2012). If additionally the terrain is flat enough to prevent efficient runoff, very high soil water contents are possible. Under these circumstances, a lot of very special landscape phenomena may arise (Yershow, 1998). One of those is

patterned ground and more specifically, ground polygons. When the soil freezes, it also shrinks, and therefore cracks evolve. If then temperatures rise and meltwater or rain enters the soil, this water accumulates in the cracks. When freezing again, the water expands to ice, which widens the crack, while the soil nearby shrinks again (Péwé, 2016). The displaced material in the vicinity of the crack is lifted but in the course of the development also mixed with the soil nearby. In this way, over many years, patterns evolve with polygonal areas that are surrounded by elevated ridges. These areas are called the centres of the polygons, and the ridges are their rims (Fig. 1.1).

ICE WEDGE POLYGONS
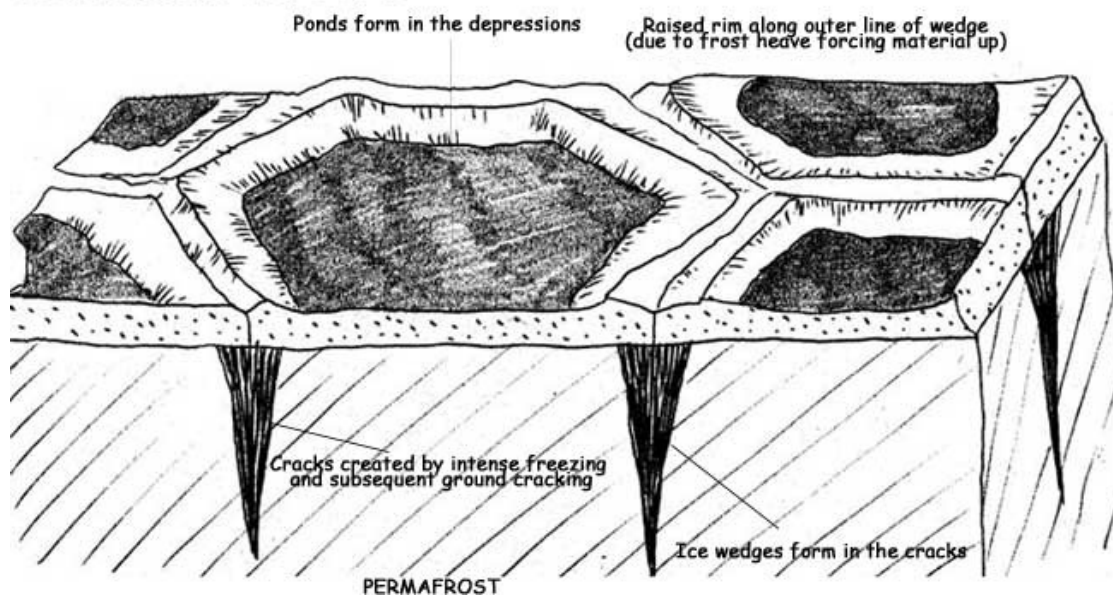
Figure 1.1: Ice wedge polygons, unknown.

Under waterlogged conditions, also the decomposition of organic carbon is reduced. Ordinary microbiotic life needs oxygen for living. If its availability is greatly reduced, only specialised microorganisms will survive. The archaea, that live under these conditions, are able to produce methane by breaking up the available organic carbon in their metabolism. If an area with less water but more oxygen exists on top of the waterlogged soil part, a lot of bacteria will use this methane for their metabolism.

1.2 The methane balance

Knowledge of atmospheric methane concentrations is a key factor in several global-scale environmental research fields. Besides acting as a highly potent greenhouse gas and thus influencing global climate change (Schwietzke et al., 2016), methane also contributes to degrading the ozone layer. Its average atmospheric lifetime is about 12.4 years, and its current atmospheric concentration in the Arctic is about 1850 ppbV (Ito and Inatomi, 2012). Concentrations have been reported as rising slowly but steadily since the onset of industrialisation, and, after a hiatus at the

Table 1.1: Bottom-up estimates of the global methane emission sources.

	Min	Mean	Max
Natural			
Wetlands	26.1	32.0	41.9
Geological, oceans	4.87	7.96	11.1
Freshwater, lakes, rivers	1.18	5.90	10.8
Wild animals	2.21	2.21	2.21
Termites	0.295	1.62	3.24
Hydrates	0.295	0.885	1.33
Wildfires	0.147	0.442	0.737
Permafrost	0.000	0.147	0.147
Anthropogenic			
Fossil fuels	12.5	14.2	15.5
Ruminants	12.8	13.1	13.9
Landfills, waste	9.88	11.1	13.3
Rice agriculture	4.87	5.31	5.90
Biomass burning, biofuels	4.72	5.16	5.75

Single source bottom-up estimates of the global methane emissions for the period of 2000 to 2009 according to Ciais et al. (2013) in %, rounded to three non-zero digits. The absolute value of the sum of the global methane sources, thus 100 % in this calculation, is 678 [542 to 852] $TgCH_4\,a^{-1}$.

beginning of the 21st century, have recently been found to be rising again (Nisbet et al., 2016). These recent dynamics in the global atmospheric methane budget are still not fully explained (Saunois et al., 2016), emphasising the fact that future trajectories of methane and its role in global climate change are also highly uncertain. The global warming potential of methane is 84 to 86 times that of carbon dioxide over an integration period of 20 years and 28 to 34 times over 100 years (Myhre et al., 2013). Accordingly, even though its absolute mixing ratios are quite low compared to carbon dioxide, it makes up for about 20 % of the increase in the radiative forcing since preindustrial times from all greenhouse gases (Tan and Zhuang, 2015). Thus, for the radiation balance and the chemistry of the atmosphere, it is important to understand land–atmosphere exchanges of methane.

Despite wetlands cover only about 5 to 8 % of the terrestrial land surface (Mitsch and Gosselink, 2007), they are with about 32 % the biggest single source of the global methane emissions (Table 1.1). Only the smallest portion (0.147 %) of that comes from permafrost. However, this number reflects the knowledge about the global methane budget for the period of 2000 to 2009 documented in Ciais et al. (2013), but very little is known about direct methane emissions from permafrost, and the uncertainty of even this estimate is high (EPA, 2010). Table 1.2 shows some estimates of the share of different regions of the global wetland area in comparison to their respective share of the global wetland methane emissions.

Table 1.2: Regional share of wetlands and their methane emissions.

	Areal share		Emissions share	
$> 50\,°$ N	> 50	Khalil (1993)	12	Bloom et al. (2010)
$> 30\,°$ N	60	Walter et al. (2001)	30	Bloom et al. (2010)
$23\,°$ S – $23\,°$ N	33	Bloom et al. (2010)	$52 - 58$	Khalil (1993);
				Matthews and Fung (1987)

Estimates of the regional share of the global wetland area and their share of the global wetland methane emissions in %.

In terms of the amount of carbon, the total atmospheric increase of methane is only about 3.18 [1.58 to 4.63] ‰ of that of carbon dioxide (Ciais et al., 2013). But because the global warming potential of methane is that much higher than that of carbon dioxide, the effect of this atmospheric increase of methane might be 9.86 [4.41 to 15.6] to 27.0 [13.2 to 39.9] % of the effect of the atmospheric increase of carbon dioxide. On the other hand, 4.13 [3.35 to 5.07] % of the total methane emissions are emissions from wetlands north of 50° N (Bloom et al., 2010; Ciais et al., 2013). These numbers use data from 2000 to 2009 for the global methane budget and from 2003 to 2005 for the methane budget of wetlands north of 50° N. Still, for the latter, only wetlands and e.g. no permafrost emissions are taken into account. However, under conditions of climate warming, resulting in thawing of permafrost, stored soil carbon will get available to decomposition, and may thus contribute to higher emissions in these wetland areas. Still, it is unclear, how much of that will be methane in contrast to carbon dioxide.

1.3 Methane in the soil

In soils that are very moist or even inundated, there is only very little oxygen available for heterotrophic metabolism. Consequently, heterotrophic decomposition is slowed down, and a lot of organic carbon remains undecomposed in the soil. Under these conditions, archaea can grow that are able to live without oxygen but produce methane in their metabolism by breaking up the available organic carbon (Thauer, 1998). Actually, archaea are the only known organisms that can produce methane.

This archaean methane production builds the source of the methane considered here. Despite the focus was laid on the biological pathway, there is also the possibility of pyrogenically produced methane as well as a geological metamorphic process that may produce methane abiotically underground. This also takes place under anoxic conditions, but deep in the Earth mantle far from the atmosphere (Martin et al., 2009; Proskurowski et al., 2008). Biologically produced methane for the most part is produced anaerobically by the methanogens, those archaea that use methanogenesis as their metabolism to gain energy, (Madigan et al., 2014),

though there are some marine microorganisms that are able to produce methane aerobically (Kamat et al., 2013; Karl et al., 2008). Three main pathways of anaerobic methanogenesis are known. While most of the methanogens use the reduction of carbon dioxide, the fermentation of acetate is responsible for about 70 % of the biologically produced methane on Earth (Lessner, 2009). The third pathway is the disproportionation of several small organic compounds that have methyl groups. Because this methane module is part of a land surface scheme, this work focuses only on the anaerobic biologic methane production, the methanogenesis of the archaea.

The produced methane may be transported within the soil, but also some amounts may be oxidised before reaching the soil surface and escaping to the atmosphere (Schütz et al., 1989). In particular, there may exist regions in the soil, that are less saturated with water and therefore may contain some amount of oxygen. In these soil parts, methanotrophic bacteria can live that use the oxygen and the methane for their metabolism. This bacterial methane consumption is the main sink of the methane considered here.

The gas transport within the soil may happen via different pathways. One of those is the transport via plants. Where vascular plants grow their roots within the waterlogged soil parts, they need to provide oxygen for their roots' metabolism. For this purpose, they developed big air-filled channels within their tissue. Those channels are called aerenchyma and can transport air within the plants even to their finest roots. However, plants always also loose a little bit of oxygen into the soil due to leakage (Končalová, 1990). This way, oxygen can enter the soil, but inversely, methane can also leave the soil in the reverse pathway as a quick bypass to the waterlogged soil. This always depends on the difference of the gas concentrations between the air and the soil.

Because of the close vicinity of oxygen and possibly high methane concentrations, the root zone of the vascular plants is another oxidation sink, independent of the

water saturation level of the soil. The bacteria living next to the plants' roots can use this additional oxygen to oxidised methane for their metabolism.

Another possibility of gas transport in the soil is the ebullition. If the liquid water in the soil is saturated with methane to a certain point, it is also possible, that bubbles form and methane is transported upwards, which is called ebullition. Ebullition is able to transport large amounts of methane in very short time if the soil porosity is high, but it is a rather discontinuous process and happens more in single events.

The third transport pathway, the molecular diffusion, is transporting methane as well as oxygen from higher to lower concentrations, regardless if higher concentrations are on top in the atmosphere or at the bottom deep down in the soil. Diffusion is the slowest transport process, but it is always there, regardless if plants are growing or if the water level is high or not.

In winter, when snow hinders the free exchange of gases with the atmosphere, two different approaches are possible to follow. Snow can simply by definition hinder any exchange with the atmosphere if enough of it has accumulated. But it is also possible to allow another transport process, the diffusion through the snow as long as it is there (Smagin and Shnyrev, 2015). While the first approach may only be a coarse approximation, adding another transport process may be a better option, despite still not very well defined.

Especially in permafrost ecosystems, parts of the soil might be frozen for longer periods. These soil parts may contain a lot of organic carbon, because decomposition needs liquid water to work. When these frozen soils thaw, the available material for decomposition may increase greatly (Khvorostyanov et al., 2008b).

But frozen soils, moreover in regions with very high soil water contents, also tend to contain a lot of ice (Brown et al., 2001). Ice is able to hinder the gas transport

by acting as barrier. And it reduces the pore space of the soil, so that it also induces gas transport if the concentrations rise because of freezing.

1.4 Possible permafrost carbon – climate change feedback mechanism

As long as the soil is frozen, the organic material that is contained therein is not decomposed. Climate change with higher temperatures and more precipitation in the Arctic in general (ACIA, 2004) may lead to warmer soils and, during summer, even thawing of organic material that has been accumulated over centuries. Once this material is available to microorganisms, it may be decomposed. The resulting decomposition gases carbon dioxide and methane add to a positive feedback with the changing climate. However, the partitioning between methane and carbon dioxide depends very much on the moisture conditions.

RCP (Representative Concentration Pathway) scenarios are used to describe different scenarios of the development of greenhouse gas concentrations in the Earth's atmosphere, expressed as additional radiative forcing due to elevated concentrations of the greenhouse gases in 2100 compared to preindustrial times. Three of these scenarios will be used in this work: RCP 2.6 ($+2.6\,\mathrm{W\,m^{-2}}$), RCP 4.5 ($+4.5\,\mathrm{W\,m^{-2}}$) and RCP 8.5 ($+8.5\,\mathrm{W\,m^{-2}}$).

Koven et al. (2015) estimate a methane emissions increase of 35 % for the high warming scenario RCP 8.5 until the year 2100 compared to 2010. This corresponds to approximately 10 to 27 % of additional greenhouse gas forcing, despite the amount of additional methane (5.3 to $14\,\mathrm{Tg\,CH_4\,yr^{-1}}$) is low compared to the additional amount of carbon dioxide ($638\,\mathrm{Tg\,C\,yr^{-1}}$). In their study, Schneider von Deimling et al. (2015) estimate, that under the high warming scenario in the 21st century a plus of 1474 (836 to 2614) Tg methane might be released from permafrost soils to the atmosphere, compared to 87 (42 to 141) PgC of carbon dioxide. Because of the multiple times higher global warming potential of methane compared

to carbon dioxide, these few percent of methane may still cause up to 40 % of the total radiative forcing that is caused by gases released from permafrost. Schuur et al. (2015) state, that an estimated amount of only 2.3 % of the total future emissions from permafrost soils would be methane. At the same time, this small amount has the effect of increasing the global warming potential of all released permafrost carbon by 35 % to 48 %, just by considering, that a small part of the decomposed carbon is not released as carbon dioxide but as methane.

Thus, despite the amount of emitted methane might look rather small, as the effect of the methane in the atmosphere is not at all neglectable, also small amounts are important to study. In the end, if strong warming because of increased greenhouse gas concentrations in the atmosphere occurs, permafrost will react with thawing and that way expose even more organic carbon to be decomposed and released to the atmosphere, which again leads to further warming, a positive feedback.

1.5 Earth system models

Earth system models try to simulate the whole planetary system of the Earth. To be able to deal with the complexity of the network of all the processes on Earth, this is still done rather coarse nowadays. The biggest components, e.g. the oceans, the ice, the atmosphere and the land surface, are submodels of Earth system models. Accordingly, JSBACH (Jena Scheme for Biosphere Atmosphere Coupling in Hamburg) is the land surface scheme of MPI-ESM (Max Planck Institute Earth System Model).

In general, the purpose of these kind of models is to generate an image of the system, within which particular processes, their consequences and interactions can be studied. Furthermore, models allow to test the validity of spatial or temporal extrapolations of knowledge gained by local and / or short-term observations.

It is obvious, that with only the existing knowledge being able to be put into the models, and, moreover, the constraint that most often models have to con-

centrate on main processes instead of being able to simulate everything, what a model will give as answer will never be more than a guess based on the existing knowledge that was put into the model in contrast to representing the truth. Usually, comparing model results to field measurements gives an idea about the properties of those results that are more trustable than others. Still, because of the unknowns and elisions, these comparisons themselves are not trivial or easy.

Environmental conditions are highly heterogeneous in permafrost regions, where landscapes are often characterised by small-scale mosaics of wet and dry surfaces (Sachs et al., 2008). The heterogeneous aerobic and anaerobic conditions in permafrost soils, in concert with elevated soil carbon stocks (Hugelius et al., 2014), set the conditions for large and spatially heterogeneous methane emissions in these areas (Schneider et al., 2009). Such strongly varying environmental and soil conditions as well as processes that influence the methane production and emissions are challenges in a process-based model with a bottom-up approach for methane balance estimation, simply because of the complexity of the network of processes to consider as well as their unclear interactions. But also always limited computational resources do not allow for an appropriately high spatial resolution to model all relevant processes in adequate detail.

However, process-based modelling approaches are powerful tools that help to quantify recent and future methane fluxes on a large spatial scale and over long time periods in such remote areas. They can give first estimates for regions where field measurements are missing and help to understand the effects of climate change on permafrost methane emissions. In addition, the effect of methane emissions on climate, and hence feedback mechanisms, can be analysed using an Earth system model. For such purposes, a methane module for an Earth system model has to be process-based and working under most environmental conditions, including permafrost.

Currently existing process-based methane models have usually been developed for applications in temperate or tropical wetlands, without considering permafrost-

specific biogeophysical processes, such as e.g. freezing and thawing soil processes (e.g. Zhu et al., 2014; Schuldt et al., 2013). In other cases, they are embedded within a vegetation model, which cannot easily be coupled to an atmospheric model (e.g. Schaefer et al., 2011; Wania et al., 2010; Zhuang et al., 2004). Some models have been designed, no matter of the later use, only for small-scale applications (e.g. Xu et al., 2015; Mi et al., 2014; Khvorostyanov et al., 2008a; Walter and Heimann, 2000) or adopt an empirical approach (e.g. Riley et al., 2011). Highly simplified models might be less reliable for global applications (e.g. Jansson and Karlberg, 2011; Christensen et al., 1996) because of oversimplification in simulating the complexity of the methane processes.

Especially the model of Walter and Heimann (2000) proved, despite being already highly process-based, not flexible enough for the intended utilisation. Particularly, the whole model was built with a fixed but very fine layer structure, that was also implicitly merged with all the formulas. Consequently, while it was not feasible to run the model within a global Earth system model due to computation time constraints, it was also not possible to easily decrease the computation time by using less but thicker soil layers. To achieve this, the whole structure of the model would have had to be changed as well (T. Kleinen, personal communication, 2012).

Furthermore, this model did not use the most appropriate diffusion equation, and, moreover, the used diffusion coefficient was constant. It was not depending on soil moisture, just separating between soil layers filled with soil water or soil air, and thus creating a hard boundary between those groups of layers. This caused issues that made subsequent adjustments necessary to make the model work (B. Walter, personal communication, 2012), which made diffusive processes difficult to handle. Because the use of a constant diffusion coefficient also changes the structure of the needed diffusion equation and consequently the procedure of its solving, simply making the diffusion coefficient variable would have caused more issues than it would have solved.

The transport of methane through plants was modelled within this framework as rate of the methane concentration in the soil instead of as a diffusive process. Also, the oxidation of methane linked to the plants was just represented as an arbitrary fraction of the transport through plants. Furthermore, it lacked the feedback of the methane oxidised in plants back to the concentrations in the soil. Also the ebullition was modelled based on a threshold instead of being process-based. So, in order to provide a process-based representation of the methane transport thus it was not possible to use these ideas like represented in this model.

Another issue was the intended use also in permafrost areas. Permafrost features were not incorporated in the model of Walter and Heimann (2000). And because the effects of permafrost, first of all the ice content in the soil, have deep impact, e.g. via the changing pore space, on the gas concentrations and the transport possibilities, it was not possible to simply integrate these effects into the existing model or even to use the model without the representation of these effects, if the aim is to study e.g. the interactions between permafrost and methane.

Last but not least, the aim of this work was not to present another methane model but a methane module that is integrated into a land surface model with permafrost and wetland soils. It should be applicable at global scales and be at the same time process-based. Thus, the applicability in an integrated, global context was mandatory. Without that, the intended utilisation would not have been possible to realise, because an isolated offline methane model cannot serve all the intended use cases.

Thus, in sum, it turned out to be beneficial to use the good ideas of Walter and Heimann (2000) and also those of Wania et al. (2010), enrich these with the newest knowledge and findings, take the special needs of permafrost environments additionally into account and built out of all that a new module within a land surface model.

To be able to provide a land surface model that

- is applicable at global scales,

- covers permafrost-specific biogeophysical processes,

- can be coupled to the other components of an Earth system model, and

- includes a detailed process-based methane module

would be of high value to the research community. The work presented here may be seen as a step towards this goal. All the existing models have their own advantages and serve their own purpose. But for the above-described intention, there was the necessity to build another one, to be able to comprehend the mechanisms in the network of the methane processes within biogeophysical environments including permafrost.

1.6 Research aims and outline of this work

The aim of this work is to gain insights into the complex behaviour and the various interactions of the methane-related processes in the soil with the extension to not only study the methane balance in temperate or tropical wetlands, but also in periglacial landscapes. Recent methane emissions as well as the different transport pathways shall be studied at process level. The effect of the physical preconditions and environmental factors, including also permafrost related features, as well as of their interconnections on methane production, oxidation and the different transport processes shall be studied in a process-based way. Furthermore, also the interactions between the gas transport processes themselves as well as the relation of the methane emissions to the soil respiration fluxes shall be looked at in detail.

Among the questions to be answered within this work are:

- Which flux patterns do the methane processes show?

- How much is the annual methane budget?

- Which methane processes are dominating under which environmental conditions?

- Which environmental conditions are the most influential and / or the most important ones for the methane emissions?

- How much is the share of methane in the soil respiration fluxes?

- Which characteristics does the seasonal cycle have?

- How large are the year to year variations of the emissions?

- What are the consequences of climate change on the methane emissions?

To answer these questions and to help to disentangle the complex network of methane-related processes, a new methane module that is running as part of a land surface scheme of an Earth system model is introduced in Chapter 2. This module is general enough for global applications, including terrestrial permafrost ecosystems.

The platform chosen to develop the methane module is the JSBACH land surface scheme of the MPI-ESM. The starting point was a model version that has a carbon balance (Reick et al., 2013) and a 5-layer hydrology (Hagemann and Stacke, 2015) and that includes permafrost as described in Ekici et al. (2014). A parallel development by Schuldt et al. (2013) incorporated wetland carbon cycle dynamics and was also integrated into the model version presented in this work. The bases for the methane-related processes were the works by Walter and Heimann (2000) and Wania et al. (2010).

The methane module presented in this work represents the gas production, oxidation and relevant transport processes in a process-based fashion. Special focus was also placed on the connections with permafrost and wetland. Among other processes, this new methane module takes into account the size variation of the pore spaces in the soil column in relation to the freezing and thawing cycles, influencing directly the methane concentration in the soil. Furthermore, in this module the oxygen content is explicitly taken into account, enabling two process-based oxidation processes: bulk soil methane oxidation and rhizospheric methane oxidation.

Sect. 2.1 describes the newly developed methane module like it was used for a site-level study, and Sect. 2.2 presents a further developed JSBACH version with an enhanced methane module, which was used for regional future climate experiments.

In Chapter 3, the results of this work are shown. Sect. 3.1 presents the results of the site-level study at a typical polygonal tundra site in the north of the Sakha (Yakutia) Republic, Russia. The first half of the questions mentioned above will be answered there. This detailed evaluation on site level shall also show the possibilities and limitations of the new module. Detailed demonstrations of the behaviour of the various processes are given. This shall lead to some insights into the question of environmental factors that govern recent methane emissions the most.

In Sect. 3.2, results of the regional future climate projections for the larger area of the Lena River Delta are presented. This is a broader application of the enhanced methane module with the benefits of a further developed JSBACH model framework. By applying this new model on a regional scale for a time frame starting in the mid of the last century and lasting until the end of the current century, regional as well as time related and even future climate scenario related variations in the different methane processes' fluxes can be studied. Consequently, the second half of the questions mentioned above will be answered there. Thus, some insights on how the methane emissions might respond to climatical changes until 2100 can be gained there.

The first part of the Abstract, parts of Sect. 1.2, 1.5 and 1.6, Sect. 2.1, 2.3, 3.1, 4.1, parts of Chapter 5 as well as Appendix A have already been published in Kaiser et al. (2017). Furthermore, parts of Sect. 2.2 are used in the manuscript of Castro-Morales about the year-round simulated permafrost methane emissions in Northeast Siberia.

Chapter 2

Methods

The methane module presented in this work is embedded in the JSBACH model. As JSBACH is a global land surface scheme, the ultimate application of the methane module is also global. Consequently, it works at the same temporal and surficial resolution as JSBACH, which is hourly time step and 0.5 ° grid cell size, including the possibility of separating the grid cell into several tiles of arbitrary fraction. For the site-level study, a methane module version has been used that is described in Sect. 2.1 and that uses an own variable depth resolution, that is independent of the one of JSBACH.

Both the methane module and the JSBACH model have been developed further before they have been used for the regional future climate experiments. Because the depth resolution of JSBACH had also been made flexible, in the new JSBACH version, the methane module uses the same depth resolution as JSBACH. The description of the alterations and enhancements made during the development process from the one to the other model version is given in Sect. 2.2.

2.1 Methane module description

The methane module presented in this section and used for the site-level study includes methane production, oxidation as well as different transport processes (Fig. 2.1). There are two oxidation pathways included, one taking place in the bulk soil, the other in the rhizosphere. The included transport processes are ebullition,
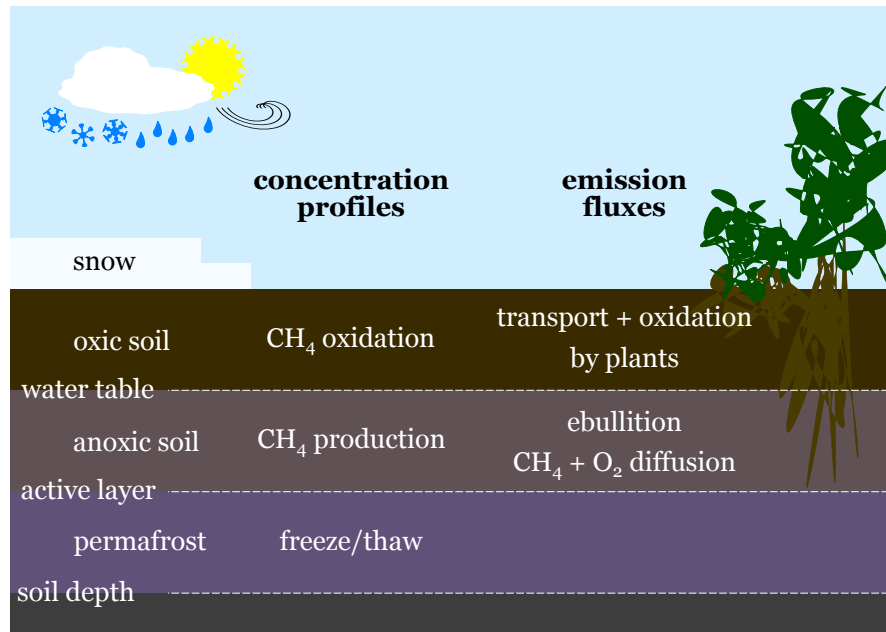
Figure 2.1: The methane processes represented in the methane module that is presented in this section.

diffusion and plant transport. Necessary structural changes in the layer architecture compared to JSBACH and with respect to the hydrology are also included.

The interface between JSBACH and the methane module is shown in Fig. 2.2. The data that JSBACH uses as atmospheric forcing, the other modules which the methane module depends on as well as the used input and output variables of the methane module are named. The atmospheric forcing consists of air temperature, precipitation, relative humidity, short- and long-wave downward radiation and wind speed, all at hourly time step and grid cell resolution, as well as a constant carbon dioxide concentration of 368.67 ppm. The modules that provide input variables for the methane module are the JSBACH forcing module, the soil module, that includes a 5-layer hydrology and the procedures for permafrost calculation, as well as the carbon balance module Bethy.

The forcing module provides information about the vegetation, thus the maximal leaf area index (LAI), the phenology type, the information, if there are C3 or C4

plants, the rooting depth as well as the LAI itself. Furthermore, the air pressure is available through this module as well as information about the soil, thus the soil depth, the volumetric soil porosity and the volumetric field capacity. All these data is provided for every grid cell or tile and constant, except the air pressure and the LAI, which are available at hourly time step.

Atmospheric forcing

* air temperature
* precipitation
* relative humidity
* short- + long-wave downward radiation
* wind speed
* CO_2 concentration

JSBACH

JSBACH forcing

* maximal LAI
* phenology type
* C3 flag
* soil depth
* rooting depth
* vol. soil porosity
* vol. field capacity
* air pressure
* LAI

Soil module with 5-layer hydrology and permafrost

* layer number + geometry
* soil temperature
* surface temperature
* snow height
* rel. soil moisture content
* rel. soil ice content
* rel. soil pore moisture content
* wilting point

C-balance Bethy

* decomposed soil carbon

Methane module

Output

CH4 + O2 concentration profile + process fluxes

Figure 2.2: The interface between JSBACH and the methane module presented in this section.

From the soil module, the layer number and geometry are used, as well as thermal and hydrological variables. Those are the soil and surface temperature, the snow height, the relative soil moisture and ice content, the relative soil pore moisture content and the relative soil moisture content at the wilting point. All these data is provided for every grid cell or tile at hourly time step, except the layer number and geometry as well as the relative soil moisture content at the wilting point, which are constant.

The carbon balance module, finally, delivers the amount of decomposed soil carbon at hourly time step for every grid cell or tile. Variables with a depth dimension, thus the layer number and geometry, the soil temperature, the relative soil moisture as well as ice content are provided for the five JSBACH layers with heights of 6.5, 25.4, 91.3, 290.2 and 570.0 cm. The amount of decomposed soil carbon has only three layers that are variable in height. All these variables have to be recalculated to the finer depth resolution of the layers that the methane module uses.

The output of the methane module includes methane and oxygen concentration profiles as well as process fluxes for both gases, thus methane production, bulk soil and rhizospheric oxidation, ebullition, diffusion as well as plant transport, all at hourly time step, grid cell or tile resolution and, in case of the concentration profiles, depth resolution of the fine layers.

Please note, that in Sect. 2.2 enhancements of the here presented methane module will be provided.

2.1.1 Preconditions for the methane processes

For a numerically stable representation of gas transport processes in soils, a much finer vertical soil structure is required than what is normally used for thermal and hydrological processes in JSBACH. Therefore, a new soil layering scheme has been implemented for the methane module. This scheme is variable and allows fine layers (of the order of a few centimetres), but still inherits the hydrological and

thermal information contained in the coarse scheme. The number and height of layers can be chosen arbitrarily, also allowing non-equidistant choices.

Internally, the module uses midpoints and lower boundaries of the layers as well as distances between midpoints. At the bottom, the layering scheme is truncated at depth to bedrock. The layers where

- the plant roots end, i.e. the rooting depth lies,
- the water table lies and
- the minimum daily water table over the previous year lies (permanent saturated depth)

have also been determined. These layers have a specific function for methane production and various transport processes. Details will be given below in the respective sections.

Specific layers are determined by comparing the midpoints of the layers to rooting depth, water table or minimum daily water table over the previous year, respectively. If one of these lies between two layer midpoints, the layer with the upper midpoint is chosen to be the specific layer for that. If the depth under consideration and the midpoint of a layer are the same, the corresponding layer is chosen.

For model evaluation, fine layers with a height of 10 cm have been used. For all the layers of the new soil layering scheme, the soil temperature is interpolated linearly from the coarse JSBACH layering scheme. From these values, the previous day's mean soil temperature is also calculated. In addition to geometry and soil temperature, each layer has its own hydrological parameters, as described in the next section, and various state variables describing the different gases' concentrations.

2.1.2 Adjusted hydrological preconditions

For the fine layers, several hydrological values have to be determined using the relative soil moisture and ice content from the coarse JSBACH layering scheme. Fine-scale layer values are derived such that known values at common layers are

kept and only those layers that span more than one input layer get values of the weighted mean of the involved coarse-layer values. The relative soil water content is then defined by the sum of the relative soil moisture and ice content.

Subtracting the relative ice content from the volumetric soil porosity leads to the ice-corrected volumetric soil porosity. With this, the relative moisture content of the ice-free pores can be defined, which is calculated by division of the relative soil moisture content by the ice-corrected volumetric soil porosity. Finally, the relative air content of the ice-free pores is defined as 1 minus the relative moisture content of the ice-free pores.

The water table is calculated following Stieglitz et al. (1997). From the uppermost soil layer, the water table is located in the immediate layer above the first one with a relative soil water content of at least 90 % of field capacity. This definition was used because the current hydrology scheme in JSBACH does not allow one to consider a water content of soils higher than field capacity or standing water (Hagemann and Stacke, 2015). Instead, water content exceeding field capacity is removed by runoff and drainage. In this context, the current model implementation considers only mineral soil (field capacity: 0.435; porosity: 0.448); i.e. no peat layers exist in this version. The dimensionless but ice-uncorrected field capacity is used because the relative soil water content already includes ice. The water table depth is then defined as

$$w = \begin{cases} b, & \text{if } r_w \leq 0.7 \cdot fc \\ b - \frac{r_w - 0.7 \cdot fc}{fc - 0.7 \cdot fc} \cdot h, & \text{if } r_w > 0.7 \cdot fc \ . \end{cases} \qquad (2.1)$$

Here, b is the lower boundary of the soil layer of interest with height h and relative soil water content r_w. fc is the field capacity. If even the uppermost layer has a relative soil water content of at least 90 % field capacity, the water table is located at the surface. The mean water table of the previous day is used where appropriate to keep consistency with the daily time step of the carbon decomposition routine. The minimum of this daily mean water table over the previous 365 days is used as the permanently saturated depth.

At a given time step, the soil column, which contains the water table depth and the permanently saturated depth, is divided into three strata that are, from the top,

- the unsaturated zone above the water table,
- the saturated zone below the water table (located above the annual minimum water table depth) and
- the permanently saturated zone (located below the annual minimum water table depth).

Evidently, this stratification is hydrological, while the layering scheme is purely numerical. Thus, each stratum may contain several soil layers. For carbon decomposition, the mean temperatures of the previous day at the midpoints of these three strata are needed. These values are derived analogously to the temperatures in the fine layers by interpolating the mean temperatures of the previous day linearly.

With these three strata, carbon that may experience unsaturated conditions is split into an unsaturated and a saturated pool by the water table. In addition, a permanently saturated carbon pool is defined by the permanently saturated depth. This scheme is similar to what Schuldt et al. (2013) proposed.

The decomposition of carbon is determined similarly to Schuldt et al. (2013), though appropriate temperatures are used for each of the three strata. Furthermore, the decomposition times for the three carbon pools have been adjusted to ensure that the two pools under partially oxic conditions are relatively stable, neither accumulating nor decomposing great portions within a few years, and the last pool slowly accumulating. In numbers, the former two pools change only about $1\,\mathrm{mol\,m^{-2}}$ each within the calculation period from 14 July 2003 to 11 October 2005. The decomposition timescales used are 80, 400 and 30 000 years for the unsaturated, currently saturated and permanently saturated stratum's carbon pool.

Though the rate of organic matter decomposition at the evaluation site is not known, the present-day amount of carbon in the soil is known (Sect. 2.1.3). Considering short timescales only, the above-described approach should give reasonable amounts of decomposed carbon in the three strata. This way, the input to the methane routine, the amount of decomposed carbon per time step in each stratum, is provided daily.

2.1.3 Methane production

Initial values of methane and oxygen concentrations have been derived using reported gas concentrations in free air for oxygen and methane. For oxygen, the global mean value for 2012 is used ($8.56\,\mathrm{mol\,m^{-3}}$, http://cdiac.ornl.gov/tracegases.html). The value for methane is defined as the March 2012 value ($77.06\,\mu\,\mathrm{mol\,m^{-3}}$, http://agage.eas.gatech.edu/data.htm).

The initial gas concentrations in the soil profile are determined assuming equilibrium condition between free ambient air as well as the air and moisture in the soil pore space. Thus, Henry's law with the dimensionless Henry constant is applied. The dimensionless Henry constant is defined as the ratio of the concentration of gas in moisture to its concentration in air (Sander, 1999). The chosen temperature dependence values, which are $\mathrm{d}\left(\ln k_{H\,\mathrm{CH_4}}\right)\left(\mathrm{d}(T^{-1})\right)^{-1} = 1900\,\mathrm{K}$ and $\mathrm{d}\left(\ln k_{H\,\mathrm{O_2}}\right)\left(\mathrm{d}(T^{-1})\right)^{-1} = 1700\,\mathrm{K}$, as well as the Henry constants at standard temperature (25 °C), which are $k_{H\,\mathrm{CH_4}}^{25} = 0.0013\,\mathrm{mol\,dm^{-3}\,atm^{-1}}$ and $k_{H\,\mathrm{O_2}}^{25} = 0.0013\,\mathrm{mol\,dm^{-3}\,atm^{-1}}$, are all from Dean (1992).

The calculated initial values for methane and oxygen concentrations in the soil profile can be transformed into gas amounts and vice versa. During methane transport process calculation, concentration values are widely used. In between time steps, however, the volume of ice is recalculated and therefore the relative ice-free pore volume changes. Thus, concentration values also change, but only the gas amounts stay constant. Therefore, at the beginning of each methane module execution, the total gas amounts that have been saved at the end of the previous

time step are divided by the current relative ice-free pore volume to recalculate the current concentration values.

The final products of the decomposition of soil carbon are carbon dioxide and methane. Depending on the soil hydrological conditions, carbon dioxide or methane are produced from the decomposing carbon pools that belong to the three strata described above. These decomposition results are distributed over fine-scale layers of the whole soil column. Because no direct vertical information about the amount of decomposing carbon is available, equal decomposition velocity in all layers of one stratum is assumed. Thus, once the decomposed amount of carbon per stratum is known, the decomposed amount of carbon per layer per stratum depends on the amount of available carbon in that layer only. And the carbon content in the soil layers for Samoylov has been prescribed from measurements by Zubrzycki et al. (2013), Harden et al. (2012) and Schirrmeister et al. (2011), taking local horizontal variations of polygonal ground (Sachs et al., 2010) into account.

The amount of soil carbon per layer has been prescribed based on measurements for the first metre of the soil profile by Zubrzycki et al. (2013). The values of the six measurement depths were averaged over the 16 different centre and 6 rim cores. These resulting averages have been interpolated to 1 cm values for rim and centre accordingly. The means of the corresponding 1 cm values are then used for the modelling layers within the first metre of the soil profile.

As Zubrzycki et al. (2013) only give values for the first metre, additional information for the rest of the soil profile is needed. Schirrmeister et al. (2011) give an estimate for Lena River Delta soil carbon content of $553.33\,\mathrm{kg\,m^{-2}}$ with a soil depth of 18.25 m, which is converted in a volumetric estimate of $30.32\,\mathrm{kg\,m^{-3}}$. Harden et al. (2012) give quantitative information about the depth distribution of soil carbon up to 3 m. Horizontal variations are accounted for by a partitioning into 65 % rim and 35 % centre (e.g. Sachs et al., 2010).

Using this information, values are assigned to the remaining layers so that the overall mean over all layers, rim and centre mixed in the proposed partitioning, gives the volumetric estimate gained from Schirrmeister et al. (2011). Hereby, the information from Harden et al. (2012) about the variability over depth, which is a slight decrease until 1.7 m and a slight increase thereafter, is taken into account.

As the uppermost values for this, at a depth of 1.05 m, the means of the deepest measured values are taken as 21.24 kg m⁻³ for the rim and 35.00 kg m⁻³ for the centre. As values at the turning point, at depths of 1.65 to 1.75 m, the ceiled mean values of the first metre are used, which are 20 kg m⁻³ for the rim and 34 kg m⁻³ for the centre. In between, the values are interpolated linearly, and then, towards the depth, extrapolated linearly, to meet the criterion of overall fitting to the value of Schirrmeister et al. (2011) as mentioned above.

The initial amount of carbon in the pools is obtained from the sum of carbon in each layer of the strata. In this case, the first and second strata share one carbon pool which is split after calculation of the mean water table over the previous day. The amount of carbon per layer is divided by the amount of carbon per stratum. These weights are used for distributing the amounts of decomposed carbon from strata to layers. In addition, the share of initially produced carbon dioxide and methane is set assuming all decomposed carbon above the water table and half of it below the water table get carbon dioxide:

$$c_{prod}^{\mathrm{CH_4}} = 0.5 \cdot \frac{f_C}{\sum_{sl} f_C} \cdot \frac{C_s}{h \cdot v_p} \ . \tag{2.2}$$

Here, sl means all layers in the stratum, and C_s is the decomposed carbon in the stratum. f_C is the soil carbon content of the layer with height h, and v_p is the ice-corrected volumetric soil porosity. Mass conservation is done if the stratum is too small to get a layer assigned, so that the associated carbon is not neglected. The gas fluxes for methane and carbon dioxide are calculated via the sums of the respective amounts, and the produced gases are added to their respective pools in the layers.

2.1.4   Bulk soil methane oxidation

Only part of the oxygen in the soil is assumed to be available for methane oxidation. In layers above the mean water table over the previous day, available oxygen is reduced by the amount that corresponds to the amount of carbon dioxide which is produced by heterotrophic respiration but not more than 40 % of the total oxygen content. An additional 10 % of oxygen is assumed to be unavailable and also reduced. In layers below the water table, the amount of oxygen is reduced by 50 %. This approach is similar to Wania et al. (2010).

For methane oxidation itself, a Michaelis–Menten kinetics model is applied, that uses the same parameter values as Walter and Heimann (2000). Also the Q_{10} temperature coefficient is similar to the one used by them, but with a reference temperature of 10 °C rather than the annual mean soil temperature. Reaction velocities of both, methane and oxygen, are taken into account by using an additional equivalent term with the concentration of oxygen and $K_m^{O_2} = 2\,\mathrm{mol\,m^{-3}}$, which is chosen to be the average concentration of oxygen at the water table. Furthermore, methane and oxygen follow a prescribed stoichiometry:

$$ c_{oxid}^{CH_4} = \min\left(V_{max} \cdot \frac{c^{CH_4}}{K_m^{CH_4} + c^{CH_4}} \cdot \frac{c^{O_2}}{K_m^{O_2} + c^{O_2}} \cdot Q_{10}^{\frac{T-10}{10}} \cdot \mathrm{d}t, \ 2 \cdot c^{O_2}, \ c^{CH_4} \right) \ . \quad (2.3) $$

c denotes the concentration of oxygen or methane in the layer. T is the soil temperature in the layer, and $\mathrm{d}t$ is the time step. The total gas fluxes for methane, oxygen and carbon dioxide are again calculated as the sums of the respective amounts.

2.1.5   Ebullition of methane

The implementation of the ebullition of methane largely follows the scheme from Wania (2007). Ebullition is the transport of gas via bubbles that form in liquid water within the soil and transport methane rapidly from their place of origin to the water table. The amount of methane to be released through ebullition is determined by that amount of the present methane that can be solute in the present

liquid water. This amount depends on the overall amount of methane present in the layer, but also on the storage capacity of the present liquid water.

In a first step, the concentration of methane in soil air is assumed to be in equilibrium with the concentration in soil water. Thus, by application of Henry's law, the present methane can be partitioned into the potentially ebullited methane concentration in soil air and the potentially solute methane concentration in soil water. The dimensionless Henry solubilities at current soil temperature conditions are used for this. As an initial approximation, all methane is assumed to be in soil air and potentially ebullited. Thus, first, the potentially solute methane in soil water can be determined, but it will also be overestimated because of this approximation. Therefore, second, an updated potentially ebullited concentration of methane in soil air is determined by subtracting the potentially solute methane from the total methane. Unlike what was proposed in Wania (2007), these two steps are iterated until stable-state conditions are reached.

In a second step, to calculate the maximal amount of methane that can be soluble in the present soil water, the Bunsen solubility coefficient from Yamamoto et al. (1976) is applied. By considering the available pore volume, this gives the volume of methane that can maximally be dissolved. The ideal gas law results in the maximally soluble amount of methane. For that, the soil water pressure in layers below the water table needs to be derived. This is determined from soil air pressure and the pressure of the water column, using the basic equation of hydrostatics. For this, the specific gas constant of moist air and the soil air pressure in layers above the water table are required. For the air pressure calculation, the barometric formula is used. Hereby, the first layer uses the air pressure at the soil surface, and deeper layers use the above layer's soil air pressure. The specific gas constant of moist air finally needs the saturation vapour pressure and relative soil air moisture, both in layers above the water table. The former is calculated following Sonntag and Heinze (1982), and the latter is set to 1 if the relative water content is at least at the wilting point and to 0.9 elsewhere.

Now, the maximally soluble concentration of methane is derived by dividing the maximally soluble amount of methane by the available pore volume. Thus, the concentration of methane that is solute and in equilibrium with methane in the air is the lesser of the following two concentrations: the potentially solute methane that was calculated in the first step, and the maximally soluble methane that was calculated in the second step. Finally, the actually ebullited methane is the difference between all methane and solute methane,

$$c_{ebul}^{CH_4} = c^{CH_4} - \min\left(k_{H\,CH_4} \cdot c_{gas}^{CH_4}, \ \frac{\beta \cdot p_w}{R \cdot T}\right) \ , \tag{2.4}$$

with $k_{H\,CH_4}$ being the Henry solubility, $c_{gas}^{CH_4}$ the methane concentration that can potentially be ebullited, β the Bunsen solubility coefficient, p_w the soil water pressure and T the soil temperature. All these variables relate to the layer, and R is the gas constant.

The ebullited methane is removed from the layers and, if the water table is below the surface, added to the first layer above the water table. In this case, the ebullition flux to atmosphere is zero, and the methane is still subject to other transport or oxidation processes in the soil. Otherwise, if the water table is at the surface and if snow is not hindering, it is added to the flux to atmosphere. Snow is assumed not to hinder if snow depth is less than 5 cm. If, finally, the water table is at the surface but snow is hindering, ebullited methane is put into the first layer and the ebullition flux to atmosphere is zero like in the first case.

2.1.6   Gas diffusion

For the diffusion of methane and oxygen, Fick's second law with variable diffusion coefficients is applied. The possibility of a non-equidistant layering scheme is specifically taken into account. Diffusion is a molecular motion due to a concentration gradient, with a net flux from high to low concentrations. For soil as a porous medium, moreover with changing pore volumes because of different contents of ice, the ice-corrected soil porosity of the layers also has to be accounted

for in the equation system directly as a factor (Schikora, 2012). The discretisation of the computational system is done with the Crank–Nicholson scheme with weighted harmonic means for the diffusion coefficients. While ice is treated as non-permeable for gases, the diffusion is allowed to continue if the soil is frozen but not at field capacity; i.e. there is no simple cut at 0 ℃. During every model time step of 1 hour, two half-hourly diffusion steps are calculated to prevent instabilities like oscillations or unrealistic behaviour like negative concentrations. The diffusion-specific time step can be decreased further if necessary and if an adjustment of the layering scheme is not desired. The possibility of these effects results from the tight connection between layering scheme, time step and diffusion coefficients.

As an initial condition, free ambient air, soil air and moisture phase are assumed to be in equilibrium. The boundary condition at the bottom of the soil column is always of Neumann type; i.e. no flux is assumed. At the top of the soil column, boundary conditions are assumed to depend on snow depth. If there are at least 5 cm of snow, no flux is assumed, and therefore the Neumann type also is applied at the top. However, if there are less than 5 cm of snow, ambient air conditions are assumed to hold at the boundary, and therefore a Dirichlet type with a gas concentration in free air is applied:

$$\boldsymbol{v}_p \cdot \frac{\partial \boldsymbol{c}}{\partial t} = \frac{\partial}{\partial x}\left(\boldsymbol{D} \cdot \frac{\partial \boldsymbol{c}}{\partial x}\right) \; ; \quad c = c_{air} \; , \quad x \in \Gamma_D \; ; \quad \frac{\partial c}{\partial x} = 0 \; , \quad x \in \Gamma_N \; . \quad (2.5)$$

Here, $\boldsymbol{v}_p$ is the volumetric soil porosity, $\boldsymbol{c}$ denotes the gas concentration, t is the time, x is the depth, $\boldsymbol{D}$ denotes the diffusion coefficient, Γ_D is the boundary with Dirichlet type boundary conditions, and Γ_N is the boundary with Neumann type boundary conditions.

Following Collin and Rasmuson (1988), the diffusion coefficients of methane and oxygen in the soil layers are calculated by adding the diffusion coefficients in soil moisture times the dimensionless Henry solubility to the diffusion coefficients in soil air. Both are weighted by the relative pore moisture or air content, and the ice-corrected soil porosity of the modelling layers is also considered. The exponents

for this are estimated with Newton's method. For fast convergence, an appropriate starting value has been chosen that was found to be 0.62. The dimensionless Henry solubilities for methane and oxygen at the current soil temperatures are applied, and the diffusion coefficients in soil air and moisture are derived.

The diffusion coefficients in soil air can be seen as such in free air at soil temperature and pressure. They are calculated following Massman (1998) from values at the soil surface with depth-variable soil temperature and pressure. The latter one arises from soil air and water pressure. The values of diffusion coefficients in free air at the soil surface are calculated from values at $0\,°\mathrm{C}$ and $1\,\mathrm{atm}$ (Massman, 1998).

The diffusion coefficients in soil moisture can be seen as such in free water at soil temperature and pressure. They are calculated differently for the two gas species. For methane, Jähne et al. (1987) is used, whereas for oxygen, Boudreau (1996) is used with the calculation of the dynamic viscosity of water following Matthaus as quoted by Kukulka et al. (1987),

$$D = \left(1 - \frac{r_m}{v_p}\right)^2 \cdot (v_p - r_m)^{2 \cdot \epsilon_a} \cdot D^a_{(0,1)} \cdot \left(\frac{T}{T_0}\right)^{1.81} \cdot \frac{p_1}{p_s} + k_H \cdot \left(\frac{r_m}{v_p}\right)^2 \cdot r_m^{2 \cdot \epsilon_w} \cdot D^w \ . \quad (2.6)$$

Here, r_m is the relative soil moisture content, v_p the ice-corrected volumetric soil porosity, ϵ_a and ϵ_w the exponents from Collin and Rasmuson (1988) for air and water, T the soil temperature, p_s the soil air or water pressure in atm and k_H the Henry constant. All these variables relate to the layer. $D^a_{(0,1)}$ is the diffusion coefficient in free air at $T_0 = 273.15\,\mathrm{K}$ and standard pressure $p_1 = 1\,\mathrm{atm}$, and D^w is the diffusion coefficient in water under the conditions of the layer. The latter two for methane and oxygen are defined as

$$
\begin{aligned}
D^a_{\mathrm{CH4}\,(0,1)} &= 1.952 \cdot 10^{-5}\,\mathrm{m^2\,s^{-1}} \ , & D^w_{\mathrm{CH4}} &= A \cdot exp\left(-\tfrac{E_a}{R \cdot T}\right) \ , \\
D^a_{\mathrm{O2}\,(0,1)} &= 1.820 \cdot 10^{-5}\,\mathrm{m^2\,s^{-1}} \ , & D^w_{\mathrm{O2}} &= \left(0.2604 + 0.006383 \cdot \tfrac{T}{\mu}\right) \cdot 10^{-9}\,\mathrm{m^2\,s^{-1}} \ .
\end{aligned}
$$
$$(2.7)$$

with A and E_a from Jähne et al. (1987), and R being the gas constant. T is once more the temperature and μ the dynamic viscosity of water, both of the layer.

To establish the boundary conditions for the system properly, for both the upper and lower boundaries of the soil column, one additional computational point has to be added to the computational system. Also for the boundary conditions, but just for computational reasons, two virtual points at the same distance from the upper or lower boundary as the first or last inner point are needed outside the computational domain. These points have as properties their location and diffusion coefficient only, which are the same as those of the first or last layer. The layer heights are used as weights for the weighted harmonic means of the diffusion coefficients at the borders between the layers. If just boundary points are involved, half of the layer heights are used as weights.

The solution of the diffusion equation system is obtained by the `tridag_ser` and `tridag_par` routines from Press et al. (1996) in Numerical Recipes.

By subtracting the gas concentrations after diffusion from those before for methane and vice versa for oxygen, concentration changes are derived with positive values for lost methane and gained oxygen. Multiplying the concentration changes by their respective pore volumes as usual and summing the resulting amounts over the layers gives the total fluxes of methane and oxygen.

2.1.7   Gas transport via plants

Gas transport via plants is first calculated for oxygen entering the soil. Then, another oxidation mechanism with this newly gained oxygen takes place (see Sect. 2.1.8). After that, the transport of methane via plants is modelled. The transport via plants happens through the plant tissue that contains big air-filled channels, the aerenchyma, to foster aeration of the plant's roots. However, because plants need the oxygen that reaches their roots for themselves, their root exodermis acts as an efficient barrier against gas exchange.

In this model configuration, gas transport by plants is assumed to happen only via the phenology type grass with a C3 photosynthetic pathway. The contribution

to methane emissions due to the degradation of labile root exudates is not taken into account here. The potential role of this process is reviewed in Sect. 4.1.2. Furthermore, the gas transport via plants will occur only if snow is not hindering, i.e. if there are less than 5 cm of snow. This is justified by the consideration of snow crinkling the culms such that transport is not possible anymore. A diffusion process from aerenchyma through the root tissue to soil is assumed as a key process, and it is described by Fick's first law. Gas transport is fast inside the air-filled aerenchyma; hence, atmospheric air conditions can be assumed there.

The diffusion flux via the plants is determined from the oxygen concentration gradient between ambient air and the root zone soil layers. The diffusion coefficients of methane and oxygen in the exodermis are unknown but can be assumed to be slightly lower than in water (e.g. Kutzbach et al., 2004; Končalová, 1990). Therefore, their values are set to be 80 % of their respective values in soil water at the given soil temperatures and pressures, $D_r = 0.8 \cdot D_w$.

The oxygen flux entering the soil is furthermore constrained by the surface area of root tissue, $A_r^{tot} = A_r \cdot q_p$, which is determined from the surface area of a single plant's roots, $A_r = l_r \cdot d_r \cdot \pi$, multiplied by plant density, $q_p = \frac{t_{ph}}{t_p}$. Here, l_r is the root length, d_r the root diameter, both in metres, t_{ph} the number of tillers per square metre depending on phenology and t_p the number of tillers per plant. Finally, the number of tillers per square metre is influenced by plant phenology, which is determined from the leaf area index (LAI), using $t_{ph} = \max(t_m) \cdot \frac{LAI}{\max(LAI)}$, with t_m being the number of tillers per square metre.

The thickness of the exodermis is set to 0.06 mm (Kutzbach et al., 2004). The number of tillers per square metre for rim and centre are given by Kutzbach et al. (2004). The number of tillers per plant is set to 1. While the mean accumulated root length of one plant is derived from Shaver and Billings (1975) to be 0.739 m, the root diameter is derived from Kutzbach et al. (2004) to be 1.9 mm.

The root tissue is assumed to be distributed equally between all root-containing layers; thus, $A_r^{rl} = A_r^{tot} \cdot \frac{h}{\sum_{rl} h}$, with h denoting the layer height and rl all layers with roots. The travel distance, $\mathrm{d}x$, is set to the thickness of the exodermis in metres because this is the limiting factor. The plant transport per layer is thus modelled as

$$n_{plant}^{\mathrm{O_2}} = D_r^{\mathrm{O_2}} \cdot \left(c_{air}^{\mathrm{O_2}} - c^{\mathrm{O_2}} \right) \cdot \frac{1}{\mathrm{d}x} \cdot \mathrm{d}t \cdot A_r^{rl} \ . \tag{2.8}$$

Here, $c_{air}^{\mathrm{O_2}}$ is the concentration of oxygen in free air and $\mathrm{d}t$ the time step length. For every soil layer, the resulting amount of oxygen is converted into concentration and added to the oxygen pool. As usual, the flux of oxygen into the soil is calculated by the total soil column balance.

After plant transport of oxygen, additional methane can be oxidised by the amount of oxygen that leaves the roots (Sect. 2.1.8). The remaining methane is then available for plant transport, which is modelled exactly as for oxygen, with one exception: It is necessary to account for the fraction of roots able to transport gases, $f_r = \frac{dom_{CarexA.}}{dom_{VascularP.}}$. This can be thought of as a measure of distance between the methane and the transporting roots. With increasing amounts of roots being able to transport gases, the distance for methane to travel to them is getting smaller and transport is generally enhanced. To account for that, f_r is set for rim and centre, respectively, as the fraction of the dominance measure for *Carex aquatilis* divided by the dominance of vascular plants (Kutzbach et al., 2004). The plant transport of methane is thus modelled as

$$n_{plant}^{\mathrm{CH_4}} = D_r^{\mathrm{CH_4}} \cdot \left(c^{\mathrm{CH_4}} - c_{air}^{\mathrm{CH_4}} \right) \cdot \frac{1}{\mathrm{d}x} \cdot \mathrm{d}t \cdot A_r^{rl} \cdot f_r \ . \tag{2.9}$$

The variables' definitions are the same as for oxygen and $c_{air}^{\mathrm{CH_4}}$ is the concentration of methane in free air. A similar effect will be taken into account for oxygen when it is allowed to oxidise only methane near the transporting roots. To determine the flux out of the soil, the differences of methane concentrations in the soil subtracted by the concentration in ambient air are used. For every layer, the amount of methane is converted into concentration and removed from the methane pool. Again, the total methane flux out of the soil is calculated by summing up individual layer balances.

2.1.8 Rhizospheric methane oxidation

The oxygen gained by the transport via plants is assumed to foster methane oxidation next to their roots. Thus, if oxygen is leaving these roots, the same oxidation routine as described above in Sect. 2.1.4 is applied to calculate how much additional methane is oxidised by this oxygen. Obviously, only gas concentrations in layers with roots will be influenced. Because the amount of vegetation with roots that are able to supply oxygen varies between rim and centre, the dominance measure (f_r from Sect. 2.1.7) is applied again as a factor to account for the distance to these roots:

$$c_{plox}^{CH_4} = \min \left(V_{max} \cdot \frac{f_r \cdot c^{CH_4}}{K_m^{CH_4} + f_r \cdot c^{CH_4}} \cdot \frac{c_{plant}^{O_2}}{K_m^{O_2} + c_{plant}^{O_2}} \cdot Q_{10}^{\frac{T-10}{10}} \cdot dt, \, 2 \cdot c_{plant}^{O_2}, \, f_r \cdot c^{CH_4} \right).$$
$$(2.10)$$

The variables' definitions are the same as for the bulk soil methane oxidation, f_r is the fraction of roots in the layer that are able to transport gases, and $c_{plant}^{O_2}$ is the concentration of oxygen transported by plants. Carbon and oxygen pools are adjusted accordingly. The total exchange with the atmosphere is determined by summing the total amount of gas that is calculated by multiplying the concentrations by their pore space.

2.2 Enhanced model description

For the second part of this work, the regional future climate experiments, an enhanced model version has been used. The differences of this model version compared to the model version used for the site-level study will be presented in this section.

The most important changes concerning the methane module itself compared to the one described in Sect. 2.1 are the addition of a representation of the diffusion of gases through snow as explicit transport pathway, the enhanced description of the plant transport as well as the change in the order of the transport processes. Furthermore, the atmospheric forcing for JSBACH is now provided daily, including

the carbon dioxide concentration, but still at the same grid cell resolution of 0.5 °.
The JSBACH version itself contains two main additions, the modules TOPMOD-
EL and YASSO, that contribute to the input for the methane module (Fig. 2.3).

The horizontal hydrology module TOPMODEL (Kleinen et al., 2012) delivers at
hourly time step the inundated fraction of a grid cell or tile and furthermore the
relative soil pore moisture content and the relative soil moisture content that were

Atmospheric forcing
* air temperature
* precipitation
* relative humidity
* short- + long-wave downward radiation
* wind speed
* CO_2 concentration

JSBACH

JSBACH forcing
* maximal LAI
* phenology type
* C3 flag
* soil depth
* rooting depth
* vol. soil porosity
* wilting point
* air pressure
* LAI

Soil module with permafrost
* layer number + geometry
* soil temperature
* surface temperature
* snow height
* rel. soil ice content

Topmodel
* inundated fraction
* rel. soil pore moisture content
* rel. soil moisture content

C-balance Yasso
* decomposed soil carbon

Methane module

Output
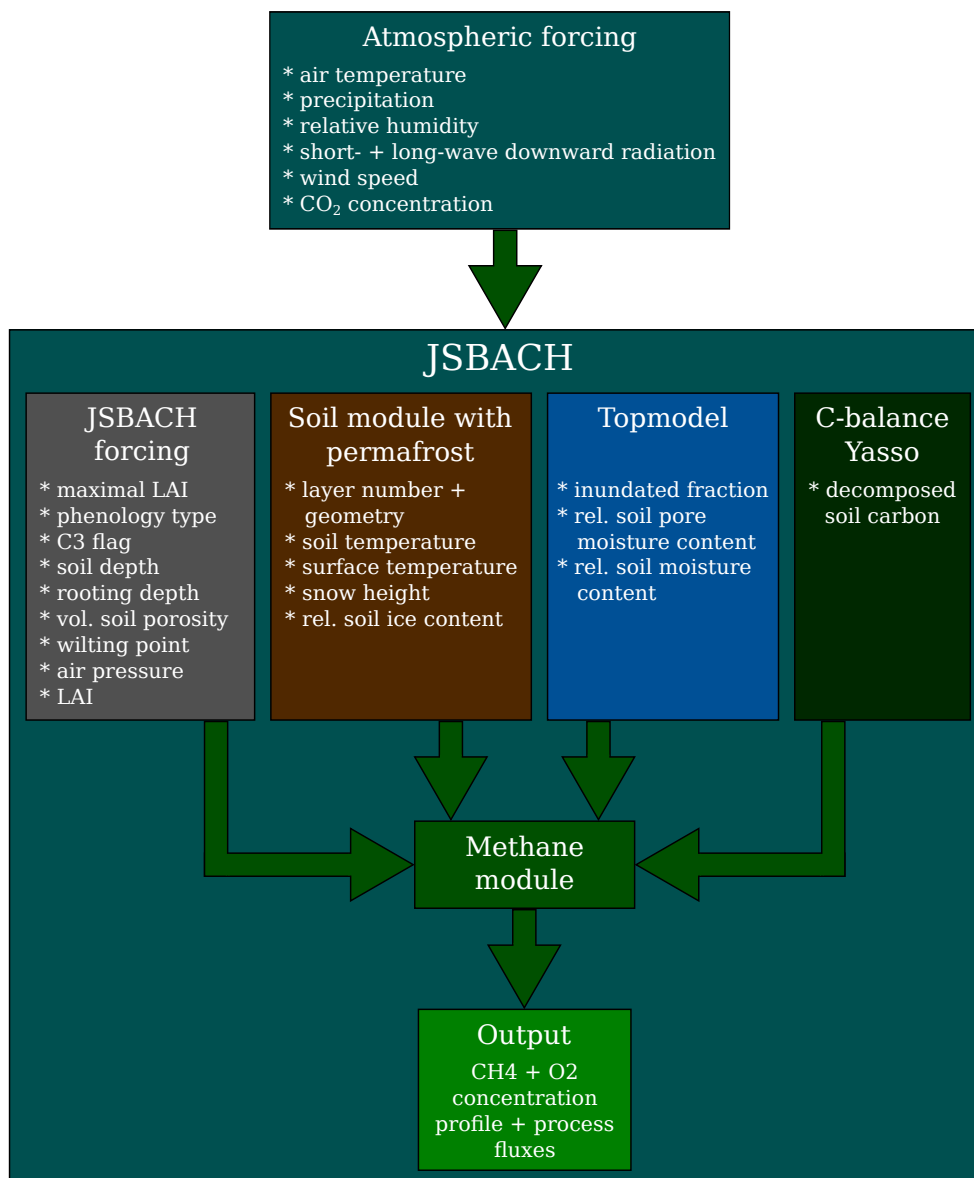CH4 + O2 concentration profile + process fluxes

Figure 2.3: The interface between altered JSBACH and the enhanced methane module.

formerly provided by the soil module. TOPMODEL thus leads to some changes in the hydrological concept. On the other hand, the soil carbon module YASSO (Goll et al., 2015) provides for each grid cell or tile at hourly time step the decomposed soil carbon, but only in two category values instead of the former three over depth and comes thus with a change in methane production.

The output of the methane module includes again methane and oxygen concentration profiles as well as process fluxes for both gases, all at hourly time step and grid cell resolution. However, the depth resolution of JSBACH changed and the methane module now uses the same depth resolution as JSBACH, which is 11 layers with heights of 6.5, 11.7, 21.1, 37.9, 68.2, 122.8, 221.1, 397.9, 716.3, 1289.3 and 2320.8 cm.

This regional configuration of the JSBACH model was further developed and adapted for the larger area of the Lena River Delta in collaboration with Castro-Morales.

2.2.1   Changes in the hydrological concept

The hydrology scheme of the JSBACH version, that was used for the site-level study, worked exclusively vertically and was therefore not able to represent the apparent differences between the wet and dry areas at the small scales of polygonal landscape structures. Thus, in the experiments, lateral water flow from rim to centre was mimicked through the execution of two separate model runs with different settings for rim and centre, where the redistribution of excess water from the rim to the centre was a key aspect.

The JSBACH version, that was used for the regional simulations, aims to enhance that situation by providing the new horizontal hydrology module TOPMODEL, that calculates the inundated fraction of a grid cell. With the grid cell divided into an inundated and a not inundated part, the need to run the model twice, once for rim and once for centre, with manipulated hydrology for the centre, is

obsolete. However, in this model version, the methane module is only applied at the inundated fraction of the grid cell. Now, the assumption holds, that there is no anoxic soil part in the not inundated area, and only in the inundated area, methane production would therefore be possible. The methane module is consequently only applied at that part, and there, the water table lies always at or above the soil surface. Consequently, it is not possible, to discriminate between soil strata, that are above the water table or below, currently below or always below. In contrast, the ice-free pore space is always filled to 95 % with water.

Still, only mineral soils are considered. But the used value for snow density changed to $330\,\mathrm{kg\,m^{-3}}$. All these changes in the hydrological concepts are obligatory to be used by the methane module.

2.2.2 Change in the production

While in the model version that was used in the site-level study, the fraction of anoxic decomposed carbon that becomes methane was 50 %, in this version, this share was set to 10 %.

2.2.3 Order of the transport processes

In the methane module as it was used in the site-level study, the different transport processes were sorted by their velocity (Table 2.1). The process that should allow for the fastest transport was the first, and the one that should allow for the slowest transport was the last.

Changing the enveloping JSBACH to a version, that has among others a further developed hydrological scheme, made this order suboptimal. The reason for this is, that the altered hydrology allowed the desired higher soil moistures, which in turn should lead to a different partitioning between the methane transport processes than in a drier environment without that possibility. It was found, that the nature of the transport processes was not allowing this as long as the formerly used order of them was kept.

Table 2.1: Order of the methane processes.

Site level	Regional
Production	Production
Bulk soil methane oxidation	Bulk soil methane oxidation
Ebullition	Plant transport of oxygen
Diffusion	Rhizospheric methane oxidation
Plant transport of oxygen	Plant transport of methane
Rhizospheric methane oxidation	Diffusion
Plant transport of methane	Ebullition
	Diffusion through snow

The order of the methane processes in the model version used for the site-level study and in the one used for the regional simulations.

However, field observations (e.g. Knoblauch et al., 2015) demonstrated the high importance of gas transport through plants. Therefore with this new JSBACH version, the order of the transport processes has been adjusted in a way that gives plant transport priority.

2.2.4   Gas transport via plants

Compared to the previous version of the methane module, the plant transport has been modified. Before, a predefined but poorly justified value for the mean accumulated root length of a gas transporting vascular plant was used to calculate the surface area of the root tissue per layer depth of root-containing layers (A_r^{rl} of Eq. 2.8). Now, the surface area is calculated based on the available soil volume, assuming a certain fraction of the soil to be root biomass.

The volume of the soil column, reduced by the pore volume, is fractionated into a mineral soil part and a root part. The root part is modelled as one cylinder per plant tiller. By applying the cylinder volume for the roots that fill the given soil part, the surface area of the roots per layer depth of the root-containing layers in $\mathrm{m^2\,m^{-2}}$ is

$$A_r^{rl} = \frac{4 \cdot V_r}{d_r} \qquad \text{with} \qquad V_r = (1 - v_p) \cdot fr_r \cdot h \cdot \frac{LAI}{\max(LAI)} \quad . \tag{2.11}$$

Here, d_r is the root diameter and V_r denotes the volume of soil that is filled with roots. It varies with the growing state of the plants via the changing LAI and depends on the volumetric soil porosity v_p, the fraction fr_r of the soil volume that is filled by roots and the layer height h.

Due to the overall increased plant transport, it became necessary to restrict it to a reasonable range. Reasonable means, that because of physical constraints, it should not be possible, that diffusion continues to change the concentrations once the concentration gradient is zero. At zero concentration gradient, the concentrations in the soil pores are in equilibrium with the concentrations in the air within the roots. Because in the soil pores, there may also be water with dissolved gases, the overall concentration in the soil pores does not have to be equal to the concentration in air to achieve equilibrium. Instead, the relevant concentration is the so-called equilibrium concentration

$$c_{equi} = c_{air} \cdot \left(k_H \cdot \frac{r_m}{v_p} + \left(1 - \frac{r_m}{v_p} \right) \right) \quad , \tag{2.12}$$

that is the concentration of gases in the soil air and water phase combined, that would be in equilibrium with the concentration in air. c_{air} is the concentration in air, k_H is the Henry constant, r_m is the relative soil moisture content, and v_p is the ice-corrected volumetric soil porosity.

Thus, the plant transport has to happen against the boundary of the equilibrium concentration instead of against the air concentration, because once the equilibrium is reached, the diffusion process is not able to change the concentrations anymore. This holds true for both gases, although the restriction works for methane with changed directions compared to for oxygen.

Consequently, the restriction of the plant transport works in the following way:

$$
\begin{cases}
\text{if } c^{\mathrm{O_2}} \leq c^{\mathrm{O_2}}_{equi} & \Rightarrow c^{\mathrm{O_2}}_{plant} > 0 \text{ and } c^{\mathrm{O_2}}_{plant} < c^{\mathrm{O_2}}_{equi} - c^{\mathrm{O_2}} \;, \\
\text{if } c^{\mathrm{O_2}} > c^{\mathrm{O_2}}_{equi} & \Rightarrow c^{\mathrm{O_2}}_{plant} \leq 0 \text{ and } c^{\mathrm{O_2}}_{plant} > c^{\mathrm{O_2}}_{equi} - c^{\mathrm{O_2}} \;, \\
\text{if } c^{\mathrm{CH_4}} \geq c^{\mathrm{CH_4}}_{equi} & \Rightarrow c^{\mathrm{CH_4}}_{plant} > 0 \text{ and } c^{\mathrm{CH_4}}_{plant} < c^{\mathrm{CH_4}} - c^{\mathrm{CH_4}}_{equi}, \\
\text{if } c^{\mathrm{CH_4}} < c^{\mathrm{CH_4}}_{equi} & \Rightarrow c^{\mathrm{CH_4}}_{plant} \leq 0 \text{ and } c^{\mathrm{CH_4}}_{plant} \geq c^{\mathrm{CH_4}} - c^{\mathrm{CH_4}}_{equi}.
\end{cases}
\tag{2.13}
$$

In case of flux into the soil (first and fourth line), the zero concentration gradient may not be exceeded from below, while in case of flux out of the soil (second and third line), it may not be exceeded from above. Please note, that plant transport was defined positive as methane flux out of the soil but oxygen flux into the soil.

There are a few parameters that were used with changed values compared to the previous model version. For the dominance measure of *Carex aquatilis*, the value that has been used for the centre configuration before was used in this model version. The value of the root diameter was set to $3.8\,\mathrm{mm}$, and the newly introduced root fraction was set to 0.5. The number of tillers per square metre and the number of tillers per plant are not used anymore.

To conclude, it may be stated, that the modifications of the plant transport lead not only to a more process-based version, but also some parameters that are difficult or impossible to measure have been eliminated.

2.2.5   Diffusion through snow

The character of the restriction that snow had on the gas exchange in the previous methane module version was more like error compensation. To improve this situation, its behaviour was changed to become more process-based. The main idea is, that one can also look at snow as a barrier of a physically similar kind like the root exodermis of the plants. Diffusion through this barrier is possible and modelled by Fick's first law just like the plant transport.

If there is at least $5\,\mathrm{cm}$ of snow on the ground, diffusion through snow replaces all the other pathways for the exchange of gases between the soil and the atmosphere. It is an almost identical formulation like that one for the plant transport:

$$n_{snow}^{\mathrm{O_2}} = D_s^{\mathrm{O_2}} \cdot \left(c_{equi}^{\mathrm{O_2}} - c^{\mathrm{O_2}} \right) \cdot \frac{1}{\mathrm{d}x} \cdot \mathrm{d}t \ . \tag{2.14}$$

The travel distance, $\mathrm{d}x$, in this case is the snow height in metres. The diffusion coefficient of oxygen through snow, $D_s^{\mathrm{O_2}}$, is set to $60\,\%$ of its diffusion coefficient in air at soil temperature and pressure of the first soil layer. Of course, it would have been better to use the diffusion coefficients at temperature and pressure in the middle of the snow instead of using the first soil layer's values, but these values were not available yet. Moreover, when calculating the pressure within the soil, snow was also not accounted for. Thus, despite the above-described values have been used here, these shortcomings should be removed in further improvements to get a more physical and process-based diffusion through snow.

For methane, the diffusion through snow works in the same way, but with changed direction

$$n_{snow}^{\mathrm{CH_4}} = D_s^{\mathrm{CH_4}} \cdot \left(c^{\mathrm{CH_4}} - c_{equi}^{\mathrm{CH_4}} \right) \cdot \frac{1}{\mathrm{d}x} \cdot \mathrm{d}t \tag{2.15}$$

and also the restriction works exactly like the one for the plant transport.

2.3 Site-level study: Samoylov Island

2.3.1 Site description of Samoylov Island

For the purpose of evaluation, the JSBACH model with the methane module presented in Sect. 2.1 has been applied at the Samoylov island site, located $120\,\mathrm{km}$ south of the Arctic Ocean in the Lena River Delta (Fig. 2.5) in Yakutia (Fig. 2.4), with an elevation of 10 to $16\,\mathrm{m}$ above sea level. The mesorelief of Samoylov is flat, while the microrelief is predominated by low-centre polygons (Fig. 2.6) with the soil surface about $0.5\,\mathrm{m}$ higher at the rim than at the centre. This results in different hydrological conditions also influencing heat conduction. The average

Figure 2.4: Geographical map of Russia, Uwe Dedering. The red square marks the Lena River Delta.
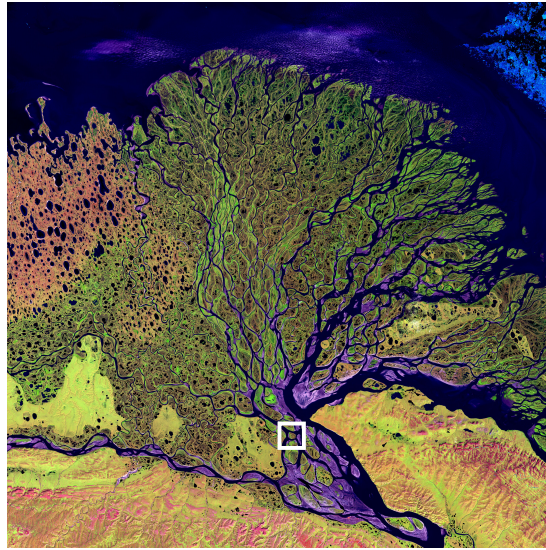

Figure 2.5: The Lena River Delta as false colour composite image using short-wave infrared, infrared and red wavelengths from Landsat 2000, NASA. The white square marks Samoylov island.

Figure 2.6: Polygonal tundra at the Lena River Delta, Peter Prokosch Grida.no.

maximum active layer depth at the dryer but still moist polygonal rims and the wet polygonal centres is about 0.5 m (Boike et al., 2013). While the water table at the polygonal rims is generally well below the soil surface, the polygonal centres are often water-saturated, with water tables at or above the soil surface (Sachs et al., 2008).

The vegetation on Samoylov can be classified as wet polygonal tundra that is composed of mosses, lichens and vascular plants. According to Kutzbach et al. (2004), mosses and lichens grow about 5 cm high and cover about 95 %, while in a second stratum, vascular plants grow about 20 to 30 cm high and cover about 30 % of the area. The most dominant vascular plant, both at the rim and at the centre,

is *Carex aquatilis*, but with a dominance of only 8 % at the rim compared to 25 % at the centre. However, most of the species present at the rim are different from those present at the centre. According to Sachs et al. (2010), the proportions of moist and wet microsites are approximately 65 % moist and 35 % wet. The reader is referred to Sachs et al. (2010) for more details on the study site. Below, moist microsites will be referred to as rim and wet microsites as centre.

2.3.2   Site-level simulation set-up

As a global land surface scheme, the JSBACH model is set up for spatially explicit model runs at larger scales. Accordingly, many assumptions behind the model structures are only valid at large spatial scales. One prominent example here is the hydrology scheme, which works exclusively vertically, and therefore cannot represent lateral water flow from rim to centre, which is a process of major importance in polygonal tundra sites. Other examples include assumptions regarding e.g. the modules for radiation scheme and energy balance (no south- versus north-facing slopes, etc.). Since the ultimate target is to provide a new methane module that can be integrated into global-scale JSBACH simulations, accordingly the structure of the methane module also needs to target spatially explicit experiments. Thus, the site-level runs presented here are landscape-scale spatial runs with a grid cell size of 0.5 ° using input data representing a very small domain.

To still facilitate site-level simulations that capture the general hydrologic characteristics of a polygonal tundra site, the model experiments were split into two separate runs, one for rim and one for centre. A redistribution of excess water from the rim area into polygon centres was added in order to mimic lateral flow. In more detail, the performed experiment consisted of two simulation runs with different settings for rim and centre. The polygon rim is assumed to be a normal upland soil, and a standard JSBACH simulation run was performed. For the polygon centre, runoff and drainage of the rim have been collected and added to centre precipitation. Additionally, for the centre run, runoff and drainage have been switched off until the soil water content reached field capacity.

The sequence of methane processes executed in the module is identical to the above-described order within Sect. 2.1.1 to 2.1.8, and has been sorted according to the velocity of the specific processes, from fast to slow. The impact of changing this sequence on total and component methane flux rates was tested in a separate sensitivity study (not shown). These tests indicated only a minor influence of the sequence to the partitioning of the fluxes between the transport processes compared to the influence of hydrology or the definition of the processes themselves. Still, it cannot be excluded that modelled methane process fluxes may be modified through the chosen order under certain conditions.

The carbon pools for rim and centre were initialised using data from Zubrzycki et al. (2013) and information from Harden et al. (2012), Schirrmeister et al. (2011) and Sachs et al. (2010). The used values for rim and centre for Samoylov are 627.61 and 731.94 mol m^{-2} for the upper carbon pool (i.e. the zone that is made up of the unsaturated and temporarily saturated soil layers) and 16 355 and 25 424 mol m^{-2} for the lower carbon pool (i.e. the permanently saturated zone). Because of the lack of information on how the modelled soil carbon from these two pools is distributed vertically, a depth distribution is applied to the decomposed carbon instead. For all layers within one stratum, equal decomposition velocity is assumed. The relative amounts of measured carbon are applied as a distribution aid for the decomposed carbon. The layers used were 10 cm in height.

The only further settings varying between rim and centre are two vegetation parameters required for the process of plant transport, i.e. the number of tillers per square metre and the dominance of *Carex aquatilis*. Beyond the definitions cited above, the model has not been calibrated to site-specific processes or properties.

To initialise the hydrological conditions, a spin-up of 100 years was done, using 1 year of climate data with the hourly mean conditions from the period of observations. Starting in year 41 of this spin-up, the methane processes were activated. This set-up was chosen to stabilise the hydrological conditions before the methane

processes were included. After finalising the spin-up, the time period of interest has been calculated without restart using the actual climate data.

2.3.3   Parameter sensitivity study

The list of parameters that are required to run the new methane module of JS-BACH has been reviewed and the parameters have been categorised by relevance and available information to support the chosen settings. Based on this survey, a shortlist of 10 parameters was identified, which is shown in Table 3.2. To allow for a uniform processing of all parameters in this list, an uncertainty range of $\pm 10\%$ for each of these settings was assumed. Changing each parameter by these percentages and performing for each of those an individual model run yielded a range of resulting methane emissions according to the influence of each parameter. Model sensitivity towards the setting of the chosen parameters was evaluated through changes in the cumulative methane emissions over the modelled time period that followed the variation of the parameter.

2.3.4   Site-level forcing and evaluation data

The climate forcing data used in the simulations are described in Ekici et al. (2014) and Beer et al. (2014). The spatial resolution was $0.5°$ and the covered time period spanned from 14 July 2003 to 11 October 2005. The climate input consists of air temperature, precipitation, atmospheric relative humidity, short- and long-wave downward radiation and wind speed, all at hourly resolution.

For model evaluation, data from chamber measurements have been used. These data were collected over 39 days from July to September 2006 by Sachs et al. (2010), resulting in 55 single measurements for the rim and 48 for the centre. In addition, eddy-covariance-based fluxes from Wille et al. (2008) have been used, integrating rim and centre. From this, 3340 data points were available for the simulation time period.

2.4   Regional simulations: Lena River Delta

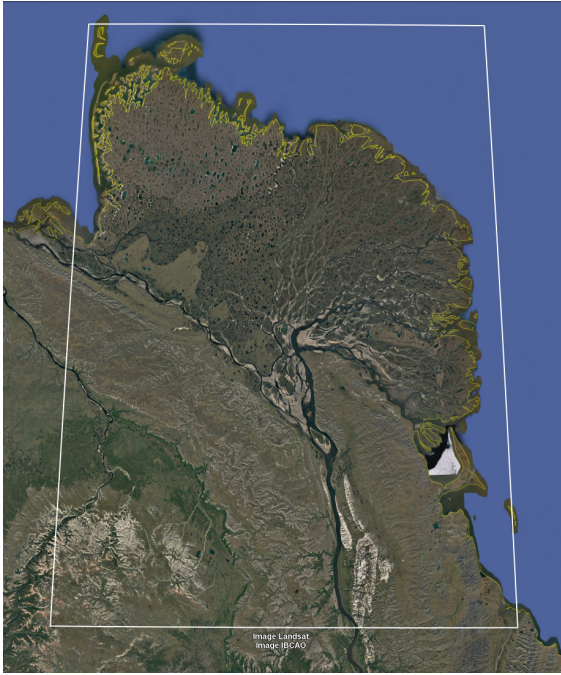## 2.4.1   Description of the Lena River Delta region

Figure 2.7: The Lena River Delta region from the satellite, Landsat and IBCAO. The white rectangle marks the area that has been used for the regional simulations.

Figure 2.8: Terrain of the Lena River Delta region, Google Maps. Please note especially the high share of open water in the delta, the mountain ranges south of it and the river in the southwest.

For the regional simulations, the new model version has been applied at the larger area of the Lena River Delta (Fig. 2.7) in Yakutia. The considered region is located north of the northern polar circle, between 71 ° and 74 ° N as well as 123 ° and 130 ° E. Within this area, the approximately 500 km wide Lena River Delta extends about 150 km into the Laptev Sea, a marginal sea of the Arctic Ocean.
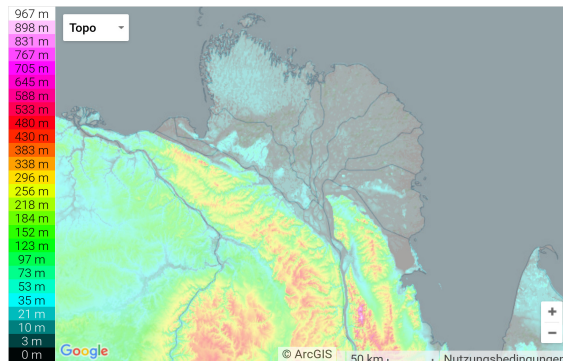
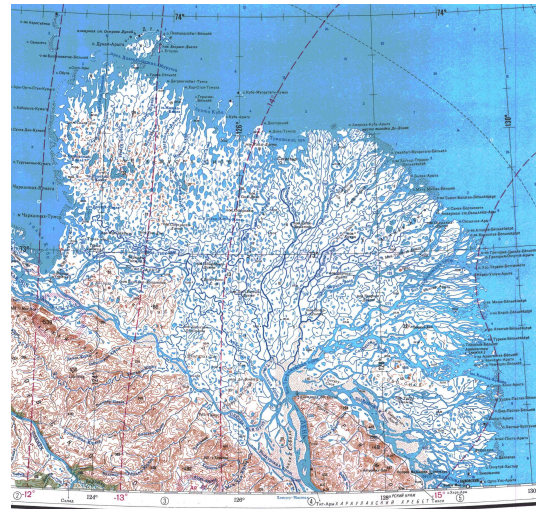Figure 2.9: Topographical heights of the Lena River Delta region, de-de.topographic-map.com.

Figure 2.10: Topographical map of the Lena River Delta, 1:1.000.000, sheet S-51,52, issue 1986, maps51.narod.ru.

To the south of the delta, there are two mountain ranges (Fig. 2.8). One are the Czekanowski Mountains in the southwest, that reach about 450 m height within the considered region (Fig. 2.9). These mountains build the outermost northeastern part of the Central Siberian Plateau. The other one is the Verkhoyansk Range in the southeast, that reaches about 1000 m height within the considered area. These mountains build the outermost northwestern part of the East Siberian Highlands. Coming from the south, the Lena River runs between both of these mountain ranges towards the delta. The delta itself divides into a lot of flat islands (Fig. 2.10), lakes and water channels, that are very variable (Fig. 2.11). In the southwest of the area, to the west of the Czekanowski Mountains, part of the Olenyok River is also included in the considered area. This river also flows towards the Laptev Sea, but in the considered region, only part of its middle course is included.

A variety of vegetation types can be found in the studied region (Fig. 2.12), spanning from barren over tundra to wetland vegetation:

- The vegetation of the Lena River Delta can be classified as wetland vegetation. In the northwest part of the delta, sedge/grass, moss wetlands grow.
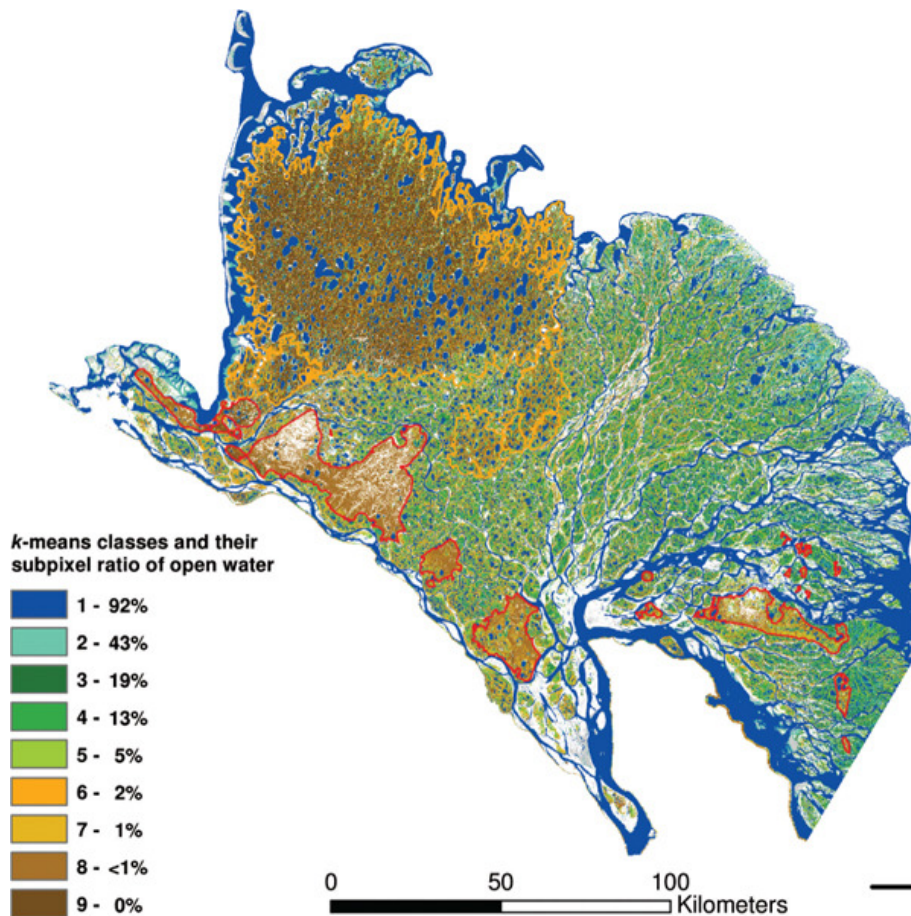
Figure 2.11: Subpixel-scale open water in the Lena River Delta as relative portions versus dry tundra, Muster et al. (2012).

Those are wetlands in the colder areas of the Arctic. They are dominated by sedges, grasses and mosses. The rest of the delta is covered with sedge, moss, dwarf-shrub wetland. This is wetland in the milder areas of the Arctic. It is also dominated by sedges, grasses and mosses, but it includes dwarf shrubs, that are less than 40 cm tall, too.

- In the riparian corridors of the Lena and the Olenyok, complex mixes of vegetation can be found, that may span from bare gravel to fully vegetated.

- The vicinity of the rivers and the lowest altitudinal areas south of the delta in the outermost southwestern part of the considered area are covered with

erect-shrub tundra. Close to the westernmost estuary of the Lena River, it is erect dwarf-shrub tundra. This is tundra, that is dominated by erect dwarf-shrubs, that are mostly less than 40 cm in height. In the other low altitudinal areas south of the delta, low-shrub tundra grows. This is tundra, that is dominated by low shrubs, that are more than 40 cm tall.

- To the south of the vicinity of the westernmost estuary of the Lena River, there is also an area covered with prostrate dwarf-shrub, herb tundra. This is tundra, that is dry with patchy vegetation. The dominant prostrate shrubs are less than 5 cm tall. But there are also graminoids, forbs and lichens.

- In the lower altitudes of the mountain ranges and on two small spots at the western shoreline, graminoid tundras cover the ground. In the spots at the shore, non-tussock sedge, dwarf-shrub, moss tundra grows. This is moist tundra, that is dominated by sedges and dwarf shrubs, that are less than 40 cm tall. But there exists also a well-developed moss layer. And barren patches are common, too. They originate from frost boils and other periglacial features. In the lower altitudes of the mountain ranges, graminoid, prostrate dwarf-shrub, forb tundra grows. This is moist to dry tundra, which has an open to continuous plant cover. Sedges dominate, together with prostrate shrubs, that are less than 5 cm tall.

- In the highest parts of the considered region, to the west of the Lena River in the south of the considered area, barrens dominate. This is dry mountain tundra on non-carbonate or carbonate bedrock. The variety and size of the plants decrease with higher elevation and higher latitude. Relatively uncommon are mesic microsites. Plant communities, that grow on snowbeds, dry fell-fields, screes or windswept, rocky ridges are more common.

- In the southwestern part of the considered region, the treeline is already passed. Thus, trees may generally grow here. This area is already covered with subarctic vegetation.

The Arctic part of the studied region shows several bioclimatic subzones. In the northwest of the delta, the mean July temperature is about 5 to 7 ℃ and the sum-
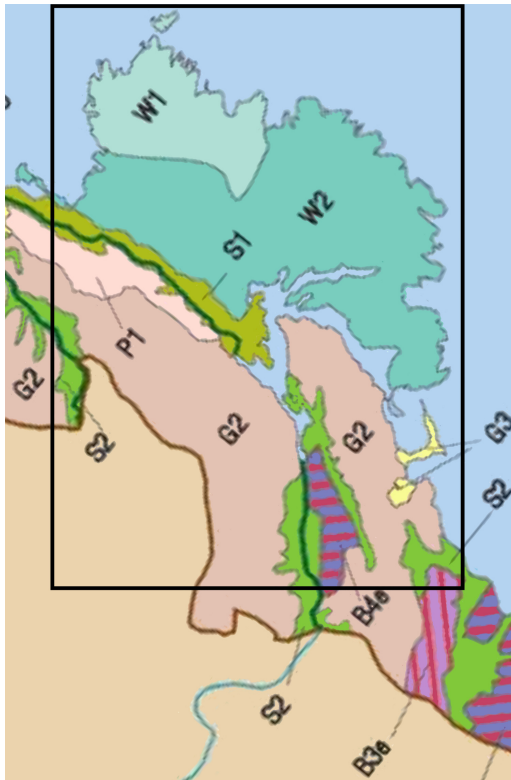
Figure 2.12: Vegetation of the Lena River Delta region, CAVM Team (2003). With the abbreviations: B3e Mountain vegetation on non-carbonate bedrock, southern tundra, B4e Mountain vegetation on carbonate bedrock, southern tundra, G2 Graminoid, prostrate dwarf-shrub, forb tundra, G3 Non-tussock sedge, dwarf-shrub, moss tundra, P1 Prostrate dwarf-shrub, herb tundra, S1 Erect dwarf-shrub tundra, S2 Low-shrub tundra, W1 Sedge/grass, moss wetland, W2 Sedge, moss, dwarf-shrub wetland. The black rectangle marks the studied area. Please see the text for further explanation.

Figure 2.13: Soils of the Lena River Delta region, Jones et al. (2010). With the abbreviations: ARpr Protic Arenosol (yellow), CRcc Calcic Cryosol, CRha Haplic Cryosol, CRhi Histic Cryosol, CRtu Turbic Cryosol (all purple), FLhi Histic Fluvisol (blue), LPli Lithic Leptosol, LPnt Nudilithic Leptosol (both grey), PZet Entic Podzol (green). Please see the text for further explanation.

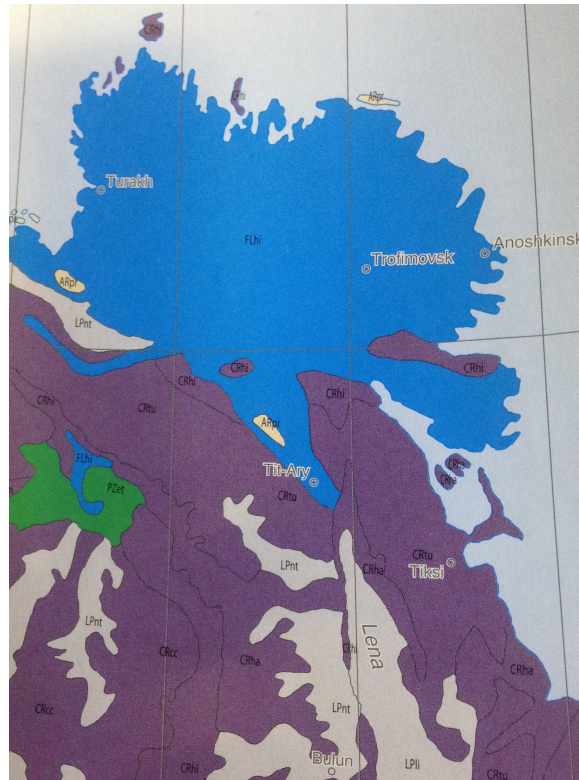mer warmth index is about 9 to 12 °C. The summer warmth index denotes the sum of the mean monthly temperatures higher than 0 °C (CAVM Team, 2003). The rest of the delta has mean July temperatures of about 7 to 9 °C and a summer warmth index of 12 to 20 °C. The soil moisture regime of the delta is wet. To the south of the delta, still in the Arctic climatic zone, the mean July temperatures are about 9 to 12 °C and the summer warmth index is about 20 to 35 °C. The soil moisture regime there is still moist. Only the mountain ranges and the prostate dwarf-shrub, herb tundra are characterised by a soil moisture regime that is dry. The southwest of the considered area belongs already to the subarctic climate zone beyond the treeline. For further information about the region concerning detailed vegetation descriptions, bioclimatic subzones, the elevation zonation of the vegetation and more, the reader is referred to CAVM Team (2003).

A variety of soil types can be found in the studied region (Fig. 2.13):

- The soils of the Lena River Delta are essentially Histic Fluvisols with some small islands of Protic Arenosols at the borders. Fluvisols are young and periodically flooded soils, and they originate from recent river, lake or marine deposits. Histic Fluvisols also have a peaty topsoil. Arenosols are sandy soils that originate from glacier outwashes or wind deposits. Protic Arenosols show no signs of soil development.

- To the south of the delta, the soils are mainly Cryosols and Leptosols with a bigger spot of Podzols in the eastern part of the region, where the Olenyok River influences the landscape. Cryosols are cold permafrost-affected soils.

- In the lower altitudinal regions south of the delta, Histic Cryosols can be found, that are non-cryoturbated and have a peaty topsoil. Turbic Cryosols can be found mainly to the north and to the east, in the lowest altitudes of the mountain ranges. Turbic Cryosols are Cryosols, that show cryoturbation. Haplic Cryosols can be found in the mid altitudes of the mountain ranges. Those soils do not show cryoturbation. In the southwestern part of the area, in the mid altitudes of the Czekanowski Mountains, Calcic Cryosols can be found. Those are soils that accumulate carbonates.

- In the mountains to the south of the delta, Leptosols can be found. Those are shallow soils in mountainous regions or even hard rock at the surface. The highest mountains in the area show Lithic Leptosols, very shallow soils over hard rock. The other high mountain areas in the region show Nudilithic Leptosols, which is bare rock.

- In the vicinity of the Olenyok River, Histic Fluvisols and Entic Podzols can be found. Podzols are acid soils, that build under coniferous forests. Entic Podzols are acid subsoils, that are rich in organic matter, but lack an overlying pale layer.

For more informations about the soils of that region, the reader is referred to Jones et al. (2010).

2.4.2 Simulation set-up for the regional simulations

Because of the altered hydrological scheme, the necessity to run the model twice was omitted. Instead, a regional set-up was used with not just 1 but 6 times 14 0.5 ° grid cells. This included also some grid cells that are classified as water bodies, so that 55 land grid cells remained. Samoylov Island is located in the central one of these remaining land grid cells. Please find maps of the spatial distribution of the grid cells in Sect. 3.2.

The distribution of the decomposed carbon over depth in this version was done following Walter and Heimann (2000). The used model layers are the standard layers of the new Jsbach version. This time, the carbon pools have not been preset, but a real spin-up procedure has been done. In a pre-spin-up, the historical input data for the years 1951 to 1980 have been repeated 10 times to spin up the initial surface conditions for 300 years including the permafrost and the TOPMODEL module. Following that, a first spin-up with the same input data was done for 10 000 years only for the carbon pools generation, thus using only the cbalone module. The cbalone module is a submodel of JSBACH that allows to run the carbon and nitrogen pool calculation offline.

After that, a second spin-up was done with still the same input data by repeating them 20 times to get 600 years to equilibrate the carbon pools with the hydrology. Thus, JSBACH was run with all modules, including permafrost, TOPMODEL and the methane module. However, using data of the years 1951 to 1980 for the spin-up means that the model results will not contain preindustrial data, but only the historic period itself may serve as basis of comparison. Finally, without restart, the historical simulation was carried out with all JSBACH modules by using the full historical dataset from 1951 to 2004. As last step, the three future scenarios RCP 2.6, RCP 4.5 and RCP 8.5 have been calculated for 2005 to 2099, again with all JSBACH modules, using the output of the last time step of the historical run as starting point.

2.4.3   Forcing data for the regional simulations

The used climate input data are the ISI-MIP fast track daily data (Warszawski et al., 2014; Hempel et al., 2013, https://www.isimip.org/documents/17/FastTrack-Protocol.pdf) for 1951 to 2099, with the historical data spanning from 1951 to 2004 and future scenarios for 2005 to 2099. The atmospheric carbon dioxide concentrations for the future scenarios follow three of the representative concentration pathways: RCP 2.6, RCP 4.5 and RCP 8.5; see also Meinshausen et al. (2011). The used 0.5 ° grid cells are those with grid cell centres in latitudes 71.25 ° to 73.75 ° N and longitudes 123.25 ° to 129.75 ° E. The input data for the single grid cells have been provided by Kleinen (unpublished) and consider the vegetation types from 1975 while the soil is saturated to field capacity.

2.4.4   Comparison of methane to carbon dioxide

To compare the methane fluxes to the carbon dioxide emissions from the soil and to the combined soil respiration fluxes, the total fluxes of each species for the historic period of 54 years have been recalculated to the time frame of the future period of 95 years. Then, the increase in the future period compared to the historic period has been converted from amounts of carbon to amounts of carbon dioxide respective carbon dioxide equivalent:

$$
\begin{aligned}
F_{\mathrm{RCP}}^{\mathrm{CO_2}}[\mathrm{CO_2}] &= (F_{\mathrm{RCP}}^{\mathrm{CO_2}}[\mathrm{C}] - F_{\mathrm{Hist}}^{\mathrm{CO_2}}[\mathrm{C}]) \cdot M_{\mathrm{C}}^{-1} \cdot M_{\mathrm{CO_2}} \\
F_{\mathrm{RCP}}^{\mathrm{CH_4}}[\mathrm{CO_2}e] &= (F_{\mathrm{RCP}}^{\mathrm{CH_4}}[\mathrm{C}] - F_{\mathrm{Hist}}^{\mathrm{CH_4}}[\mathrm{C}]) \cdot M_{\mathrm{C}}^{-1} \cdot M_{\mathrm{CH_4}} \cdot GWP \,,
\end{aligned}
\tag{2.16}
$$

where F denotes the total flux of a species for a 95 years time period, either for CO_2 or for CH_4 and either for the historic period or one of the future scenarios. The units are kg of Cx per m^2 and per future time period, thus 95 years. The used quantity for Cx is given in squared brackets. [CO_2e] is one of [CO_2e100a], [CO_2e100aF], [CO_2e20a], [CO_2e20aF], thus the carbon dioxide equivalent for a time horizon of either 100 or 20 years and without or with carbon cycle – climate feedback. M denotes the molar mass of the species and GWP is the global warming potential of methane for a time horizon of either 100 or 20 years and without or with carbon cycle – climate feedback, thus takes one of the numbers 28, 34, 84 or 86.

Chapter 3

Results

3.1 Site-level study

For the site-level study, the methane module version has been used that is described in Sect. 2.1 with the simulation set-up of Sect. 2.3.2 and forcing data named in Sect. 2.3.4.

3.1.1 Modelled water table and permanent saturated depth

The modelled depth of permanent saturation for both, rim and centre, is always at the same level of 31.9 cm. In contrast, the modelled water table changes during the seasons for rim and centre differently (Fig. 3.1). In general, it is higher at the centre than at the rim, though there are few cases in early spring when the rim has a higher water table than the centre. This results from the different soil water contents at the rim and at the centre, which were forced by adding runoff and drainage from the rim to the centre as precipitation and prohibiting runoff and drainage at the centre until the soil water content reached field capacity. Still, in the early part of the thawing season, the water tables at the rim and at the centre are similar. While in general, at the rim, the water table is highest during the early thawing season, at the centre, there is a tendency to high values towards the end of the thawing season. But if the rim shows a high water table, there will generally also be a high water table at the centre. Overall, the water table in the model is changing relatively quickly, due to the quick changes in modelled soil water conditions.
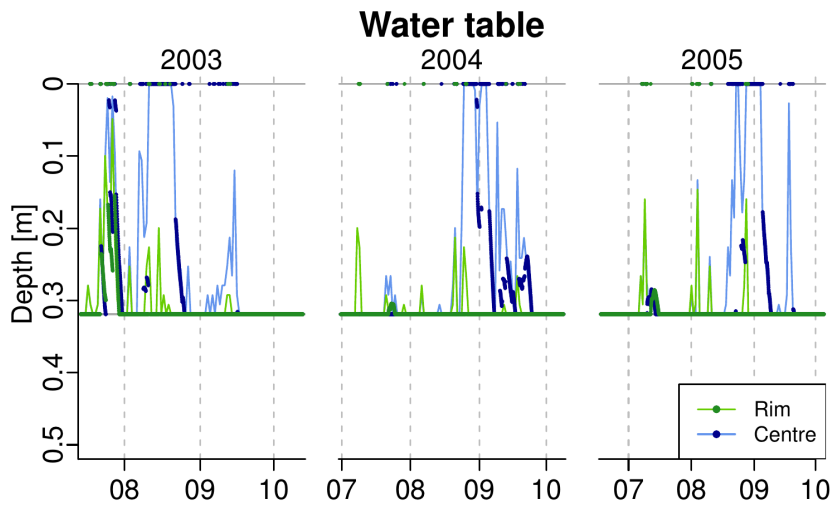
Figure 3.1: Modelled water table at rim and centre as hourly data (points) and daily
means (lines). X axis and dashed lines indicate the first day of the respective
month of the year. Please note the cutouts in between the different years.
Only the summer periods are shown, which means less than 5 cm of snow
are on the ground.

However, JSBACH does not allow one to model soil water content higher than field
capacity or standing water at the surface. Thus, the maximal soil water content
in the model is field capacity. It is obvious that there is a mismatch with the
real situation in the field, where the centre is often water-saturated, with water
tables at or above the soil surface. While measurements of the water table at the
rim give values between 35 and 39 cm (Kutzbach et al., 2004), the mean summer
value in the model is 30.88 cm. For the centre, measurements give values between
-12 and 17 cm (Sachs et al., 2010), while the mean summer value in the model is
24.52 cm. Hence, the model tends to have a slightly higher water table at the rim,
but the calculated water table is too low at the centre. Still, this water table has
been calculated using the unsaturated soil water content. For the interpretation
of the methane module results, it therefore has to be taken into consideration that
JSBACH is currently not capable of filling the entire pore space up to saturation
with water; i.e. a realistic representation of saturated water content like in the
field is not possible.

For additional results concerning modelled physical conditions, such as soil moisture and ice content as well as soil temperatures, the reader is referred to Appendix A.1.

3.1.2 Modelled methane flux in summer and winter
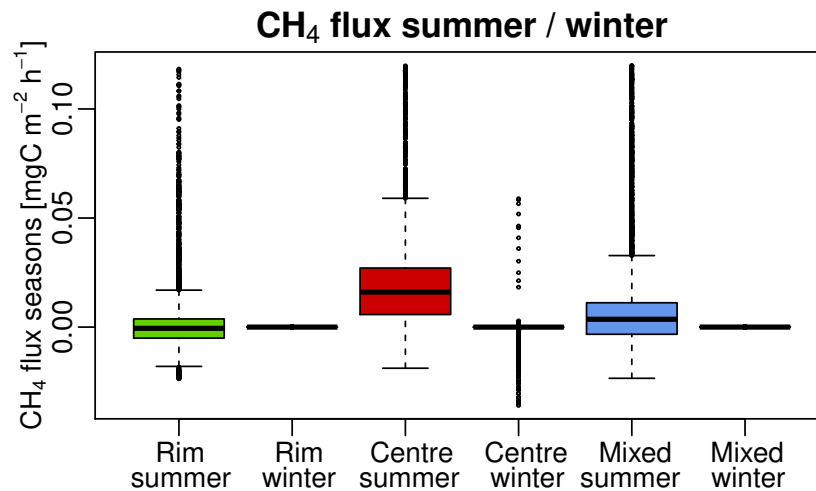
Figure 3.2: Modelled methane flux out of the soil at the rim, centre and a mixed approach of 65 % rim plus 35 % centre, split into summer and winter. Summer means less than 5 cm of snow are on the ground; winter is the remainder. Because of the wide spread of values, from -0.0747 mgC m^{-2} h^{-1} to as high as 86.8 mgC m^{-2} h^{-1}, a portion of 4.66 % values was cut to provide a reasonable picture.

The modelled methane fluxes at the rim and centre are different for the different seasons (Fig. 3.2). While most of the modelled flux is positive (i.e. emission to the atmosphere), there are also uptake events. The spread of the flux is larger for the centre than for the rim in both summer and winter. While the majority of flux values in summer is positive at the centre, it is more balanced at the rim. In winter, the methane flux is almost always zero, following the assumption that snow may hinder the exchange. However, at the centre, there are some rare events when uptake takes place. In the mixed approach, which means 65 % rim and

35 % centre, the overall mean emission is about $0.0813\,\mathrm{mgC\,m^{-2}\,h^{-1}}$ for the summer period. The overall higher emissions at the centre are due to higher moisture and thus more favourable conditions for methane production in concert with lower methane oxidation rates.

3.1.3   Role of different transport processes
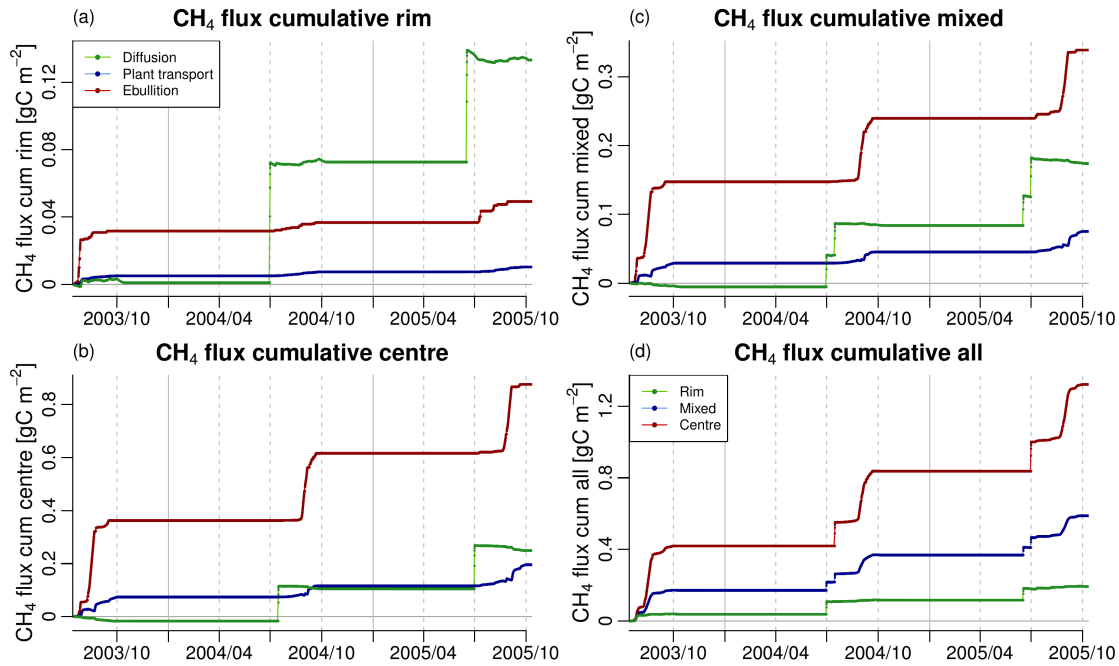
Figure 3.3: Modelled methane flux out of the soil at **(a)** the rim, **(b)** the centre, **(c)** a
mixed approach of 65 % rim plus 35 % centre, split into the different transport
processes, and at **(d)** the rim, the centre and a mixed approach of 65 % rim
plus 35 % centre combined, as a cumulative sum of hourly data (points) and
the daily means (lines). Solid lines indicate 1 January; dashed lines indicate
1 April, 1 July and 1 October of the respective year. Please note the different
scales. Table 3.1 gives the maximal values.

During most of the year, the diffusive methane flux is rather small at the rim
(Fig. 3.3a) and sometimes slightly negative at the centre (Fig. 3.3b). The largest
methane emissions, both at the rim and at the centre, occur during spring. In
this season, the methane that is produced in the topsoil from late autumn on and

accumulated during winter is released in the form of so-called spring bursts upon snow thaw.

Methane transport via plants is smaller than via diffusion, but more pronounced at the centre than at the rim (Fig. 3.3a and b), because plant transport was defined as being slower than diffusion in water and should thus lead to lower emissions under less wet conditions. Despite the exodermis being a very thin layer, it is an efficient barrier against gas exchange, maintaining gases such as oxygen that are necessary for metabolic processes inside the roots. Thus, the diffusion rate through roots is slower than through water, and in turn, diffusion in water is much slower than diffusion in air. Moreover, the soils in the centre were not water-saturated in the model, promoting diffusive methane release through coarse pores. However, the wetter the soil, the more plant transport relative to diffusion should occur, because the more water, the more diffusion is slowed down. While ebullition is the most important process at the centre (Fig. 3.3b), it is diffusion at the rim (Fig. 3.3a). This is due to the drier conditions at the rim that allow a fast diffusion through air, while ebullition is only possible under conditions of high soil moisture. Because in the model higher soil moisture is calculated from the middle to the end of the thawing season, most of the emissions by ebullition and plant transport at the centre occur in this period (Fig. 3.3b).

In the mixed approach, only the diffusion of the rim alters the pattern of the emissions substantially (Fig. 3.3c). In total, the polygon centre accounts for a 6.8 times as large fraction of emissions as the rim due to the higher methane production under wetter conditions (Fig. 3.3d). This means a total share of 78.6 % of the methane emissions in the mixed approach is coming from the centre. Emissions at the rim are highest during spring, while they are highest at the centre during the mid and late season (Fig. 3.3d).

When comparing the total fluxes of the centre to the ones of the rim, diffusion is almost doubled, plant transport is 19 times as high, and ebullition is 18 times as

Table 3.1: Maximal cumulative methane flux.

	Rim	Centre	Mixed
Diffusion	0.139	0.268	0.182
Plant transport	0.0103	0.196	0.0752
Ebullition	0.0492	0.876	0.339
All	0.194	1.32	0.588

Maximal values of the cumulative sums of the modelled methane flux out of the soil over the modelled time period of 821 days for rim, centre and a mixed approach of 65 % rim plus 35 % centre for the different transport processes and combined in $gC\,m^{-2}$, rounded to three non-zero digits.

high (Table 3.1). This results in almost 7 times higher total methane emissions at the centre than at the rim. At the rim, diffusion is more than 13 times as high as plant transport, while at the centre, it is just slightly higher than plant transport. Ebullition is about 4.5 times as high as plant transport both at the rim and at the centre. These differences are again due to the differences in soil moisture content, which allow more production under higher soil moisture and thus also lead to more methane emissions. On the other hand, plant transport is in principle a slower transport process than diffusion in water, but diffusion in water is much slower than diffusion in air. Thus, under drier conditions, diffusion in air will transport the main portion of gas, but under wetter conditions, plant transport may increase relative to diffusion. With reduced soil air, the remaining velocity of the diffusion is almost of the same order of magnitude as the overall velocity of plant transport, in contrast to the velocity of diffusion mainly through air.

Splitting the total methane flux into several transport processes not only allows one to evaluate the relative contribution of each process linked to rim or centre characteristics, but it is also possible to analyse differences in temporal patterns (Fig. 3.4a). As noted above, at the rim, the fluxes are much lower than at the centre (Fig. 3.4b), because less methane is produced under drier conditions, or methane becomes oxidised in the soil column. Ebullition makes up a large portion
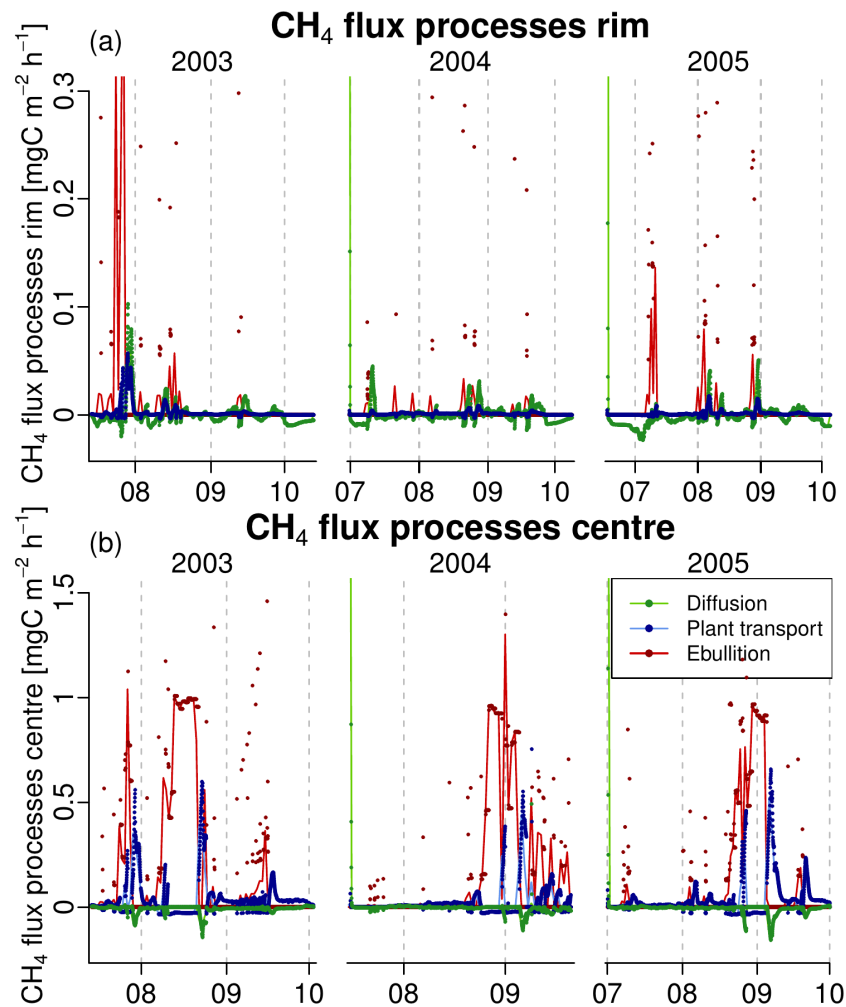
Figure 3.4: Modelled methane flux out of the soil at the **(a)** rim and **(b)** centre as hourly data (points) and daily means (lines), split into the different transport processes. X axes and dashed lines indicate the first day of the respective month of the year. Please note the cutouts in between the different years. Only the summer periods are shown, which means less than 5 cm of snow are on the ground. Please note the different scales. Because of the wide spread of high hourly values, to as high as 39.3 **(a)** and 86.6 **(b)** mgC m^{-2} h^{-1}, a portion of 0.108 % **(a)** and 0.0609 % **(b)** hourly values was cut to provide reasonable pictures. The minima of the hourly values are -0.0234 **(a)** and -0.158 **(b)** mgC m^{-2} h^{-1}.

of the total budget at both microsites at isolated time steps, reflecting the nature of this process, while its total amount for the rim is rather small over longer time frames. At the rim, diffusion represents the second largest methane release but also substantial uptake during the season (Fig. 3.4a). The smallest flux portion at the rim is delivered by plant transport, which also shows some uptake. In contrast, at the centre, plant transport plays a much more pronounced role, and diffusion fluxes are more negative. All these effects occur in the different hydrological regimes at the rim and at the centre.

Furthermore, ebullition can only take place in soils with high soil moisture content, and this is more common at the centre than at the rim. Consequently, substantially more ebullition is found at the centre than at the rim. In the mixed approach, diffusion accounts for about 2.5 times of the emissions of plant transport, while ebullition accounts for 4.5 times of it. Overall, 0.588 g of carbon are emitted by each square metre during the modelled time period from 14 July 2003 to 11 October 2005.

3.1.4 Production versus oxidation

Methane oxidation follows the pattern of methane production as long as enough oxygen is available (Fig. 3.5a). Production, and hence also oxidation, is higher during times of more moist conditions for both, the rim and the centre, and is also higher for the centre than for the rim (Fig. 3.5b). At the centre, a substantial amount of methane is oxidised in the rhizosphere with oxygen that enters the soil via plant transport. This happens when a high amount of methane is produced, which is rather rare at the rim due to lower soil moisture (Fig. 3.5a). During spring, bursts of oxidation occur both at the rim and at the centre because methane produced during the winter and stored below the snow gets in contact with oxygen, or, more precise, fresh oxygen enters the soil and activates the methanotrophs. The different moisture and temperature regimes at the rim and the centre and their dynamics determine these results.
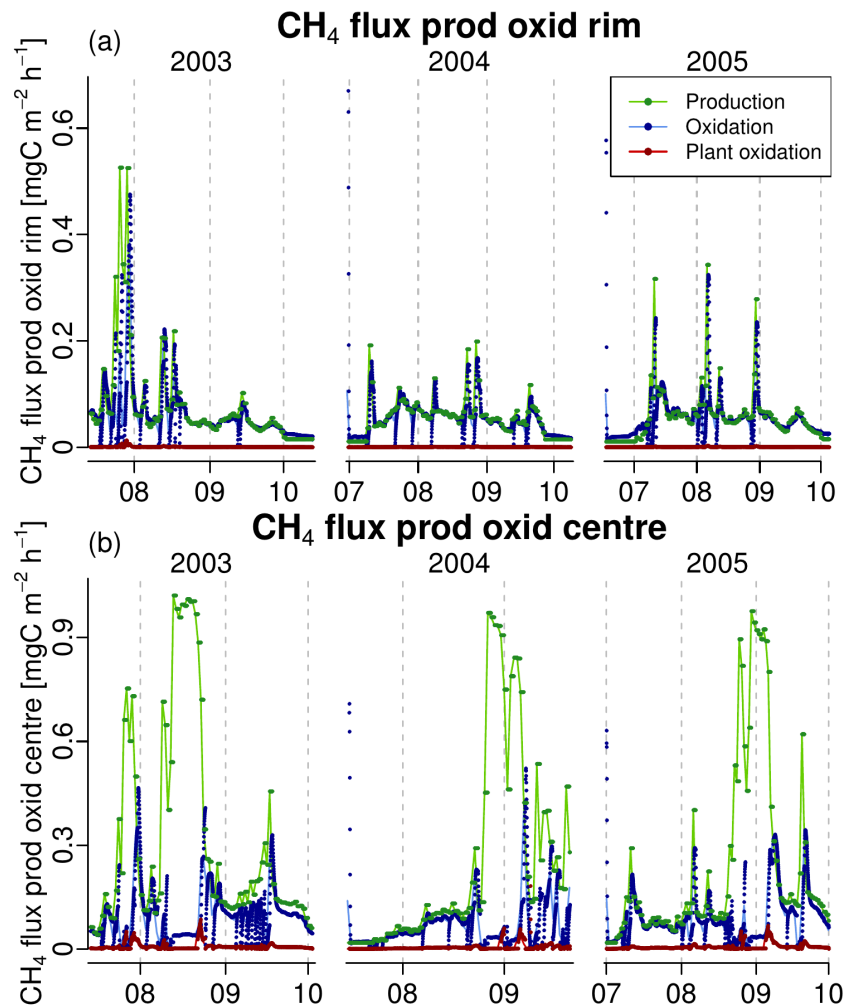
Figure 3.5: Modelled methane amounts that get produced and oxidised at the **(a)** rim and **(b)** centre as hourly data (points) and daily means (lines), split into the different processes. X axes and dashed lines indicate the first day of the respective month of the year. Please note the cutouts in between the different years. Only the summer periods are shown, which means less than 5 cm of snow are on the ground. Please note the different scales. The maxima of the hourly values are 0.670 **(a)** and 1.02 **(b)** mgC m^{-2} h^{-1}.

3.1.5 Parameter sensitivity study

Results of the parameter sensitivity study are summarised in Table 3.2 and indicate that just one of the chosen parameters, fracCh4Anox, has a major influence on

Table 3.2: Methane emission sensitivity towards key parameter settings.

Parameter	Lower range	Upper range
fracCh4Anox	-11.966	12.035
fracO2forOx+fracO2forPh	-1.358	1.305
KmO2	-1.741	2.107
snowThresh	0.549	-0.090
resistRoot	0.024	0.195
thickExoderm	0.204	0.032
rootLength	0.024	0.195
rootDiam	0.024	0.195
tillerNumberMax	0.024	0.195
dominanceCarexAquatilis	-0.151	0.344

Change in the cumulative methane emissions over the modelled time period in %, when the parameter was modified by $\pm\,10\,\%$ compared to its default setting.

the cumulative methane emissions when varied within a $10\,\%$ range. FracCh4Anox represents the fraction of methane produced under anoxic conditions compared to the total decomposition flux. For two more parameters, fracO2forOx+fracO2forPh and KmO2, the net effect was still larger than $1\,\%$. FracO2forOx+fracO2forPh influences the available amount of oxygen for the methane oxidation, whereas KmO2 influences the oxidation as the Michaelis–Menten constant for oxygen. For all remaining parameters, only negligible effects on the cumulative methane emissions were found.

3.1.6   Comparison to chamber measurements

Although the number of available field data is small and from a different year than the meteorological forcing data, the field measurements and model results are of the same order of magnitude (Fig. 3.6). Observations and model results show higher centre values compared to the rim, but the model seems to underestimate occasional uptake events. For the rim, the model gives methane
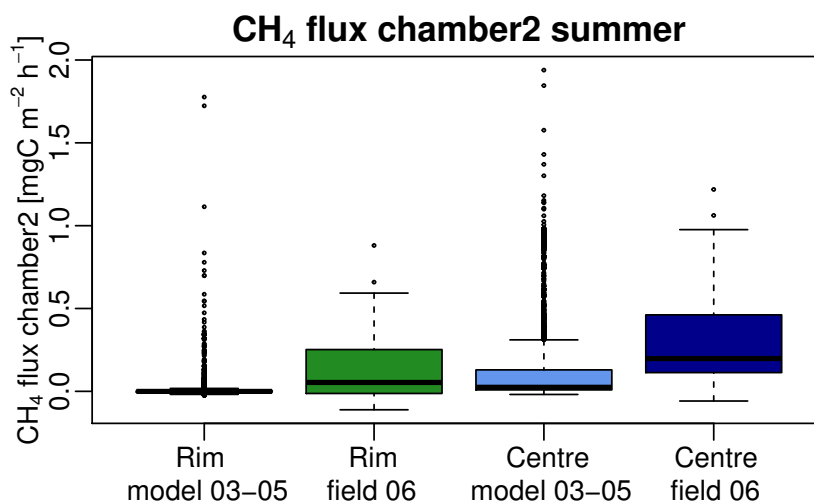
Figure 3.6: Modelled methane flux out of the soil at the rim and centre compared to chamber measurements. Modelled values are only from the summer periods 2003 to 2005, which means less than 5 cm of snow are on the ground. Field measurements took place on 39 days from July to September 2006. Because of the wide spread of high modelled values, to as high as $86.8\,\mathrm{mgC\,m^{-2}\,h^{-1}}$, a portion of $0.347\,\%$ modelled values was cut to provide a reasonable picture. The minimum of the modelled values is $-0.0237\,\mathrm{mgC\,m^{-2}\,h^{-1}}$.

fluxes to the atmosphere of between -0.0237 and $39.3\,\mathrm{mgC\,m^{-2}\,h^{-1}}$, with a mean of $0.0267\,\mathrm{mgC\,m^{-2}\,h^{-1}}$, while the available field measurement values range from -0.111 to $0.881\,\mathrm{mgC\,m^{-2}\,h^{-1}}$, with a mean of $0.154\,\mathrm{mgC\,m^{-2}\,h^{-1}}$. For the centre, the model gives values between -0.0189 and $86.8\,\mathrm{mgC\,m^{-2}\,h^{-1}}$, with a mean of $0.231\,\mathrm{mgC\,m^{-2}\,h^{-1}}$, while the available field measurement values range from -0.0584 to $1.22\,\mathrm{mgC\,m^{-2}\,h^{-1}}$, with a mean of $0.327\,\mathrm{mgC\,m^{-2}\,h^{-1}}$. Besides higher mean values, the extremes are thus lower for the field measurements. This is due to the observation period excluding spring time, when the model calculates the highest emissions in the form of spring bursts.

One should also take into account that JSBACH is a global model; therefore, it requires input parameters from global fields. Furthermore, other modules of JSBACH, like the hydrology or the carbon decomposition, are adjusted for global

applications. Therefore, JSBACH integrates processes over much larger grid cell areas than what chamber measurements may represent. Hydrological conditions and other processes are highly variable in polygonal tundra environments and are of crucial importance for methane processes. Still, they may not be represented with the required detail by the model, so that the modelled conditions are the same as those at the measurement site. Thus, it is obvious that with coarser and different hydrological conditions, the modelled methane emissions per square metre for a 0.5 ° grid cell cannot be identical to the point measurements of chambers. Particularly, the low soil moisture in the hydrological conditions of the model may explain the lower mean modelled methane emissions compared to what is reported by chamber data.

3.1.7   Comparison to eddy measurements

Eddy covariance data had the best available data coverage of field measurements (light grey areas in Fig. 3.7). Overall model results are of the same order of magnitude as observations, but there are also seasonal shifts between model results and measurements. This is due to a mismatch between the real soil conditions at the measurement site and the modelled soil climate and hydrology that cannot be expected to be the same as those in the field. The range of available measurements in the modelled period is 0.0233 to $4.59\,\mathrm{mgC\,m^{-2}\,h^{-1}}$, with a mean of $0.609\,\mathrm{mgC\,m^{-2}\,h^{-1}}$. The range of modelled summer methane emissions in this time frame is -0.023 to $30.4\,\mathrm{mgC\,m^{-2}\,h^{-1}}$, with a mean of $0.0813\,\mathrm{mgC\,m^{-2}\,h^{-1}}$. If less than 5 cm of snow are on the ground, this is defined as summer time. Besides lower means, the model shows a wider range of values.

For this comparison, the same constraints hold like for the comparison to chamber data. The modelled fluxes differ from field measurements because of differences in thermal or hydrological conditions. Critical are periods where observations show substantial methane emissions while at the same time model results show only minor emissions, e.g. in autumn 2003 or spring 2004. During these periods, modelled soil temperature values below 0 ℃ and snow cover result in modelled methane
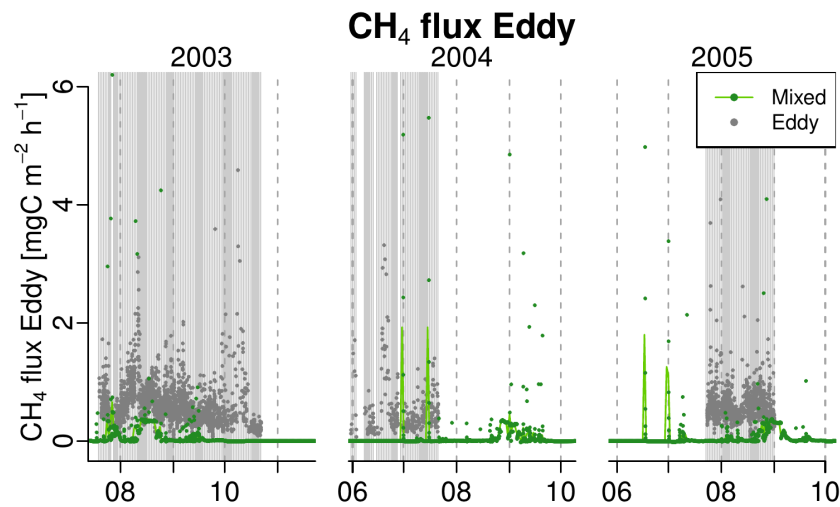
Figure 3.7: Modelled methane flux out of the soil in a mixed approach of 65 % rim plus 35 % centre as hourly data (points) and daily means (lines) compared to hourly eddy covariance measurements. Light grey background indicates measurement data coverage. X axes and dashed lines indicate the first day of the respective month of the year. Please note the cutouts in between the different years. Because of the wide spread of high modelled hourly values, to as high as $30.4 \, \mathrm{mgC \, m^{-2} \, h^{-1}}$, a portion of $0.0507 \, \%$ modelled hourly values was cut to provide a reasonable picture. The minimum of the modelled hourly values is $-0.0235 \, \mathrm{mgC \, m^{-2} \, h^{-1}}$.

fluxes of virtually zero, while in reality soils might be warmer and gas diffusion through snow might be possible (see Sect. 4.1.2).

Still, Fig. 3.7 also shows some patterns that are present in both model results and observations, e.g. periods with increasing fluxes that are followed by a sudden decline in the fluxes in a cyclic manner during a single season. These patterns are linked to the changing soil moisture content. Unfortunately only the first season is covered well by field measurements, while the second misses the later part, and the third covers just a part within. The model shows the largest methane emissions during spring upon snow thaw for both rim and centre in the form of bursts. There is still little evidence in field measurements of the occurrence and magnitude of spring bursts, and to the knowledge of the author, no published data on this effect

exist for Samoylov. In Sect. 4.1.3, the evidence of spring bursts in other northern wetland areas is briefly reviewed to evaluate the representativeness of these events in the model results.

For additional results concerning modelled oxygen uptake, such as the mixed daily sum, seasonally split and cumulative sums as well as transport process split, see Appendix A.2.

3.2   Regional future climate experiments

For the regional future climate experiments, an enhanced model version has been used (Sect. 2.2) with the simulation set-up of Sect. 2.4.2 and forcing data named in Sect. 2.4.3.

To compare the methane fluxes to the carbon dioxide emissions from the soil and to the combined soil respiration fluxes, several different units have been used. All are per m^2 and per time period, but they differ in the quantity that is measured in g or kg. The used quantities are carbon [C] or carbon dioxide [CO_2], but also carbon dioxide equivalent [CO_2e]. There are four possibilities to calculate the carbon dioxide equivalent of methane, for a time horizon of either 100 or 20 years and without or with carbon cycle – climate feedback ([CO_2e100a], [CO_2e100aF], [CO_2e20a] and [CO_2e20aF]). They correspond to global warming potentials of 28, 34, 84 and 86. These units will be used in this section.

For the comparison of the methane process fluxes to each other, the following short names have been used: Prod (methane production), Oxid (bulk soil methane oxidation), Plox (rhizospheric methane oxidation), Plant (plant transport), Ebul (ebullition), Diff (diffusion) and Snow (diffusion through snow). AllTrans denotes the combination of all transport processes (Plant, Ebul, Diff and Snow) together, thus the final flux to the atmosphere. SnowS refers to the diffusion through snow in spring, SnowA to it in autumn.

3.2.1   Modelled gross soil respiration fluxes

For the regional simulations, the modelled gross soil respiration fluxes for the whole
area have been calculated as cumulative sums (Table B.1). Four different datasets
are thus available, one for the historic period from 1951 to 2004 and three for the
future period from 2005 to 2099, represented by the scenarios RCP 2.6, RCP 4.5
and RCP 8.5. Because no preindustrial dataset is available, the historic dataset

Table 3.3: Increase compared to the historic period of the soil respiration fluxes.

$[\mathrm{kgCx\,m^{-2}\,y\,a^{-1}}]$		RCP 2.6	RCP 4.5	RCP 8.5
		$2005 - 2099$	$2005 - 2099$	$2005 - 2099$
	$[Cx] \setminus [y\,a]$	95 a	95 a	95 a
ΔCH_4	[%]	15.7	22.8	31.2
ΔCO_2	[%]	32.7	38.7	52.7
$\Delta(CO_2+CH_4)$	[%]	32.5	38.6	52.6
ΔCH_4	[C]	0.019	0.028	0.038
ΔCO_2	[C]	4.684	5.551	7.563
$\Delta(CO_2+CH_4)$	[C]	4.704	5.579	7.601
ΔCH_4	$[CO_2e100a]$	0.718	1.046	1.431
ΔCH_4	$[CO_2e100aF]$	0.871	1.270	1.738
ΔCH_4	$[CO_2e20a]$	2.153	3.138	4.294
ΔCH_4	$[CO_2e20aF]$	2.204	3.213	4.397
ΔCO_2	$[CO_2]$	17.165	20.340	27.711
$\Delta(CO_2+CH_4)$	$[CO_2e100a]$	17.883	21.386	29.143
$\Delta(CO_2+CH_4)$	$[CO_2e100aF]$	18.036	21.610	29.450
$\Delta(CO_2+CH_4)$	$[CO_2e20a]$	19.318	23.478	32.006
$\Delta(CO_2+CH_4)$	$[CO_2e20aF]$	19.369	23.553	32.108

Increase compared to the historic period of the modelled gross soil respiration fluxes for
three future scenarios in %, rounded to one decimal place, as well as rounded to three
decimal places and in units of kg of Cx, denoted in the second column, per m^2 and per
95 years, denoted also in the third row. An F means that feedback was considered.

has been used as basis of comparison for the RCP scenarios. However, the carbon balance is not in equilibrium in the historic period, but neither are the RCP scenarios in the future period. Moreover, the carbon balance in the model determines not only the carbon dioxide but also the methane emissions from the soil substantially. To still allow a comparison, the data have been aggregated per time period or scenario and for the whole study area.

The increase of the gross soil respiration fluxes in the RCP scenarios compared to the historic period is presented in Table 3.3. The emission of methane increases by 31 % in RCP 8.5 compared to the historic period, while the one of carbon dioxide shows an increase of 53 % in this comparison. In terms of the amount of emitted soil carbon, methane accounts for 0.7 to 0.8 % of the soil respiration fluxes and for 0.4 to 0.5 % of the increase compared to the historic period of these fluxes (Table B.2). This situation changes, if the global warming potential of methane is

Table 3.4: Changes of the methane budget.

$[\mathrm{gCH_4\,m^{-2}\,y\,a^{-1}}]$	Hist	RCP 2.6	RCP 4.5	RCP 8.5
	$1951-2004$	$2005-2099$	$2005-2099$	$2005-2099$
$[\mathrm{y\,a}]$	54 a	95 a	95 a	95 a
Prod	95.72	194.90	207.12	221.91
Oxid	1.98	4.12	4.47	5.24
Plox	0.70	1.46	1.60	1.86
Plant	51.32	95.03	101.02	106.04
Ebul	35.56	79.90	84.85	91.78
Diff	0.02	0.05	0.06	0.06
Snow	6.16	14.37	15.16	16.97
AllTrans	93.07	189.36	201.09	214.85

The changes of the modelled methane budget expressed as cumulative sums for the historical period and three future scenarios, rounded to two decimal places. The units are g of CH_4 per m^2 and per y years, denoted in the third row. For the meaning of the short names, see Sect. 3.2.

also taken into account. Then, depending on the representation and the scenario, the share of methane raises to about 4 to 14 % in the increase compared to the historic period of the gross soil respiration fluxes.

In the same way, also the modelled methane process fluxes to the atmosphere have been processed and analysed. Budgets of these fluxes for the whole area as cumulative sums are given in Table 3.4. To enable an easy comparison of the dimensions of the processes, their share in the budget of the production flux is shown in Table B.3. The biggest share of the overall methane emissions has the plant transport with ebullition being the second most important transport process. The diffusion through snow during winter time delivers the third most share to the overall transport flux. Though there are slight deviations in the numbers, this pattern is present in all time periods or scenarios.

The percentage increase of the methane process budgets in the RCP scenarios compared to the historic period is provided in Table B.4. While plant transport only shows an increase of 17 % in RCP 8.5 compared to the historic period, the methane production increases by 32 %. The other processes all increase by about 47 to 57 % in this perspective. Regarding the absolute changes of the transport processes in the RCP scenarios compared to the historic period, ebullition shows the biggest increase, but plant transport keeps the second and diffusion through snow the third rank (Table 3.4).

3.2.2 Spatial distribution of the modelled soil respiration

The spatial distribution of the soil respiration fluxes indicates big differences among the grid cells and with changing time. The extrema of the fluxes in the grid cells for a mean year of 10 years periods are summarised in Table 3.5. The values for the carbon dioxide emissions and the combined soil respiration fluxes vary between the grid cells 2- to 4-fold, beginning with more than 2-fold in the historic period and ending with 3- to 4-fold in RCP 8.5 (Table B.5).

Table 3.5: Summary of the grid cell soil respiration fluxes.

[gC m^{-2} a^{-1}]	Hist	Curr	RCP 2.6	RCP 4.5	RCP 8.5
	1951 – 1960	1995 – 2004	2090 – 2099	2090 – 2099	2090 – 2099
CH$_4$	0 – 3	0 – 3	0 – 4	0 – 4	0 – 5
CO$_2$	78 – 178	90 – 219	100 – 267	101 – 300	113 – 409
CO$_2$+CH$_4$	79 – 180	92 – 220	102 – 269	103 – 302	115 – 411

Summary of the modelled grid cell soil respiration fluxes for a mean year of 10 years periods of the historic, the current and three future scenarios, rounded to integer. The units are g of C per m^2 and per year.

The analysis of the change in time respectively future scenario shows, that already the smallest modelled grid cell values of the carbon dioxide emission as well as of the combined soil respiration flux increase by 46 % for RCP 8.5 compared to the historic period (Table B.6). However, the highest modelled grid cell values show increases of 129 % in this comparison for carbon dioxide emissions as well as for the combined soil respiration flux (Table B.7). The maximum value of the methane emissions in this perspective increases by 87 %.

The methane flux out of the soil shows a gradient from high to low values from northwest via east to south (Fig. 3.8). This corresponds to the pattern of the modelled landscape: Where soil depth and root depth are high, also high values of methane fluxes have been calculated (compare Fig. 3.10). Furthermore, the more inundated area per grid cell, the more methane fluxes can be seen (compare Fig. 3.11). Relatively little influence on the overall methane flux can be determined for C3 grasses (compare Fig. 3.10). But the emissions are systematically higher in the low altitude wetland areas, namely the Lena River Delta and the riparian areas, than in the upland areas (compare Fig. 2.9 and 2.12).

The carbon dioxide emission from the soil, in contrast, is relatively evenly distributed, with a low emission region in the northeast (Fig. 3.9). This region is the lowest lying delta region (compare Fig. 2.9) and thus both harsh and wet. Con-

CH$_4$ flux to atmosphere -- Mean year sum
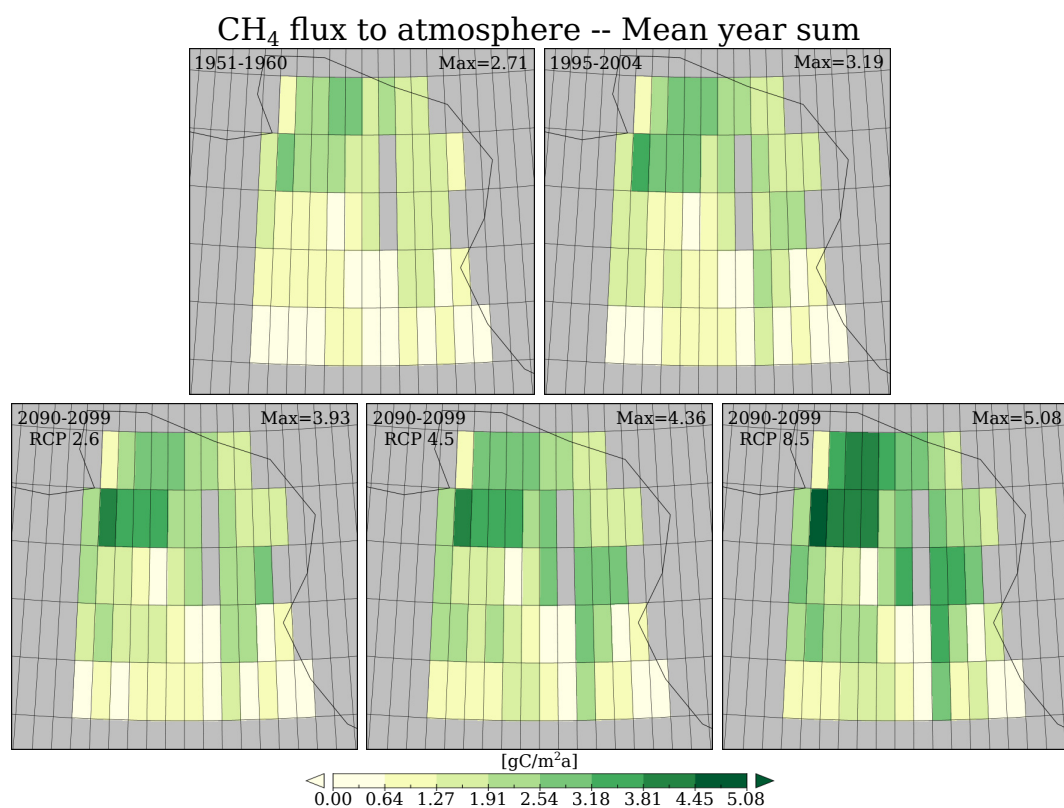
Figure 3.8: Modelled methane flux to the atmosphere as mean year sum over 10 years periods in gC m^{-2} a^{-1}. Please note the details at the top of every subfigure.

CO$_2$ flux to atmosphere -- Mean year sum
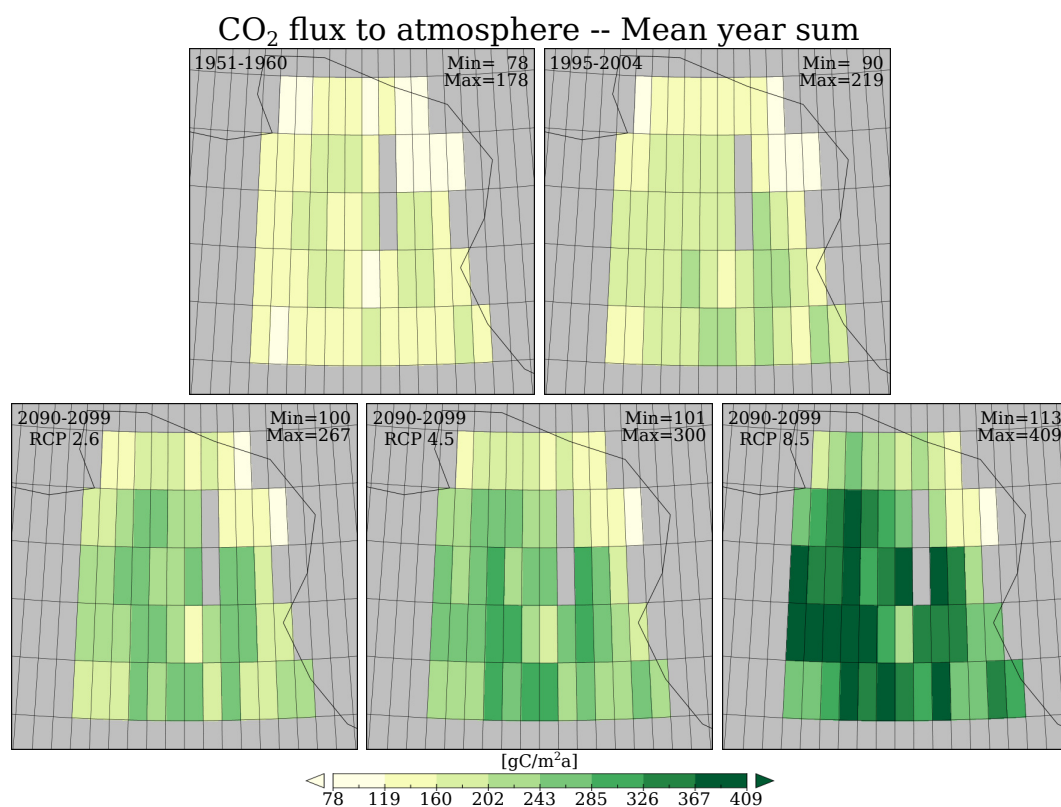
Figure 3.9: Modelled carbon dioxide flux from the soil to the atmosphere as mean year sum over 10 years periods in gC m^{-2} a^{-1}. Please note the details at the top of every subfigure.

sequently, relatively little carbon dioxide emission from the soil can be seen there. In general, the more inundated area per grid cell, the less carbon dioxide emission from the soil has been calculated (compare Fig. 3.11). The carbon dioxide emission from the soil is higher in the tundra regions (compare Fig. 2.12). But the parameters that influence the methane flux (compare Fig. 3.10) have less influence on the carbon dioxide emission from the soil.

Considering the combined soil respiration flux, the pattern is almost identical to the one for carbon dioxide emission from the soil alone, simply due to the proportions between carbon dioxide and methane emissions (Fig. B.1). In general,
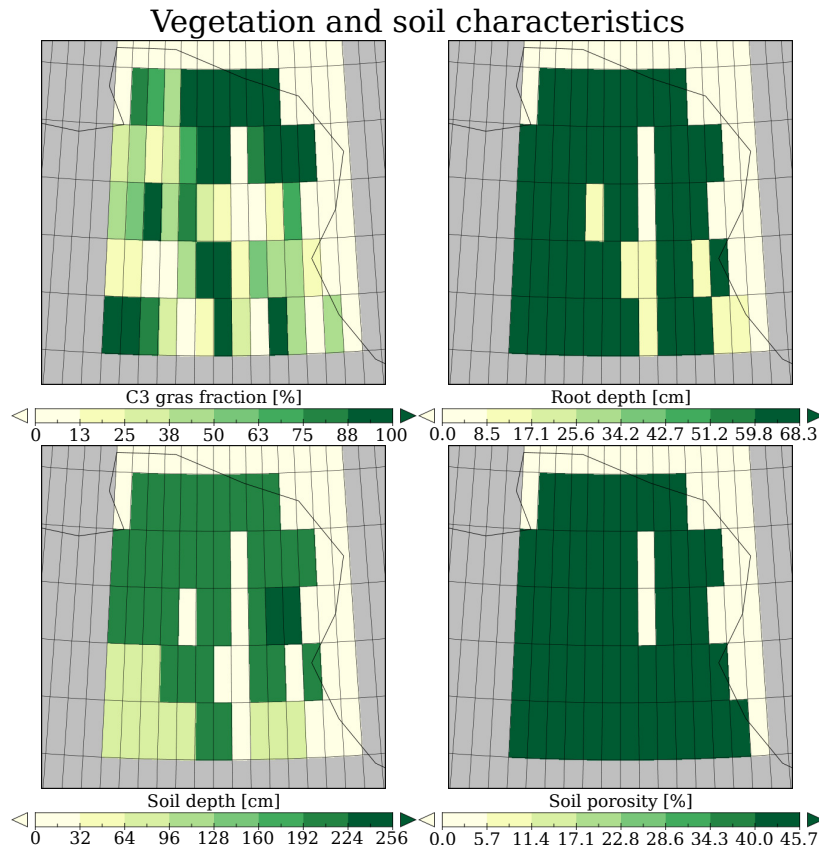
Figure 3.10: Input data for vegetation and soil characteristics: the fraction of C3 grasses in %, root and soil depth in cm and soil porosity in %.
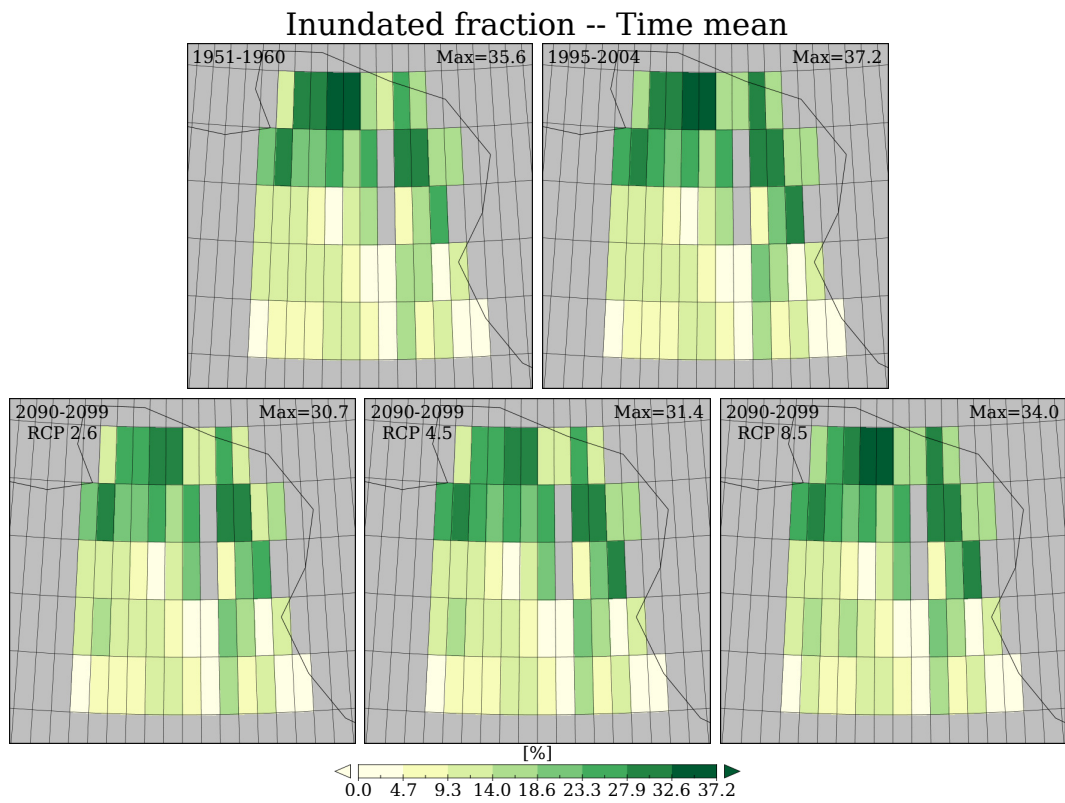
Figure 3.11: Modelled inundated fraction as mean over 10 years periods in %. Please note the details at the top of every subfigure.
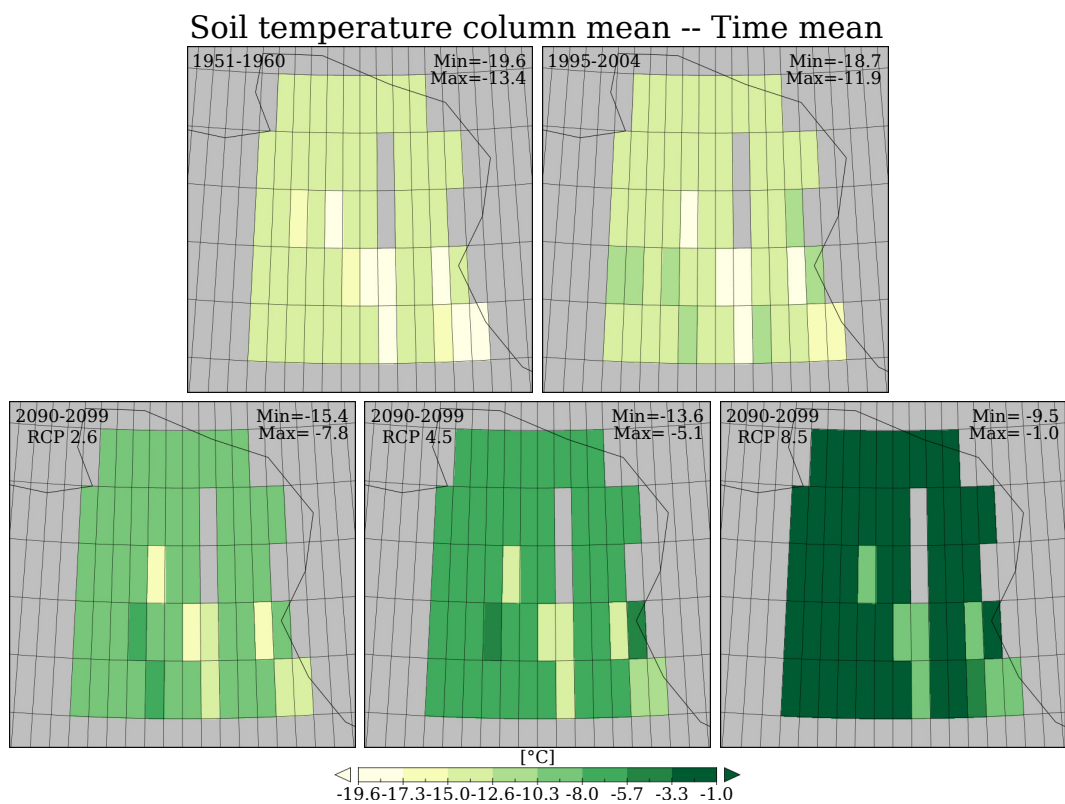
Figure 3.12: Modelled soil temperature as mean over the soil column and over 10 years periods in °C. Please note the details at the top of every subfigure.

the higher the soil temperatures, the more soil respiration is calculated. This holds also true for regional differences, not only for the time development (compare Fig. 3.12, Fig. B.2 and B.3).

The analysis of the change with time respectively future scenario shows, that the later respectively warmer the scenario, the more important become the riparian regions in the south relative to the delta for the methane flux out of the soil (Fig. 3.8). For the carbon dioxide emission from the soil (Fig. 3.9) as well as for the combined soil respiration flux (Fig. B.1), the later respectively warmer the scenario, the more shifts the area of the highest emissions from the central region and the southeast to the west.

To summarise, while the methane flux seems like playing only a minor role compared to the carbon dioxide emissions from the soil (Fig. 3.13), taking the much higher global warming potential of methane into account, the effect of increased methane emissions is with up to 14 % of that of increased carbon dioxide emissions from the soil not at all minor (Table B.2).
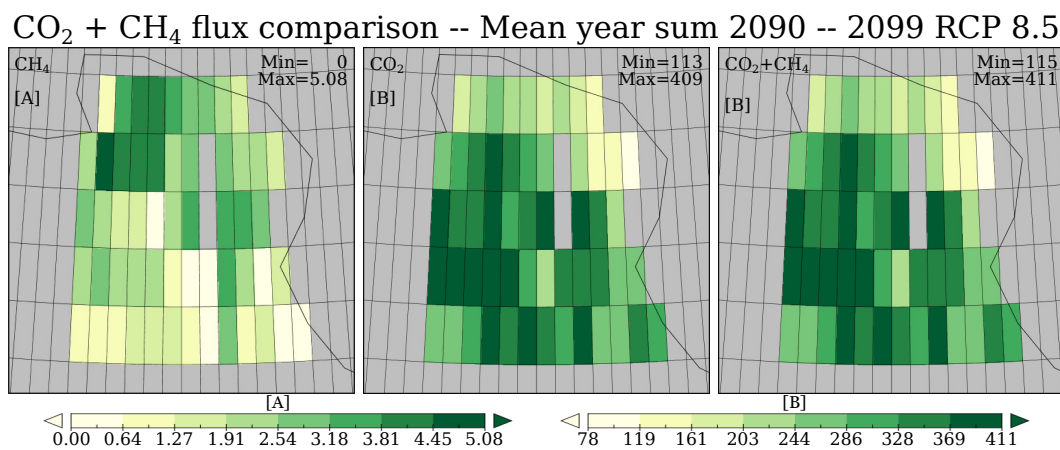
Figure 3.13: Modelled soil respiration fluxes as mean year sum for $2090-2099$ under RCP 8.5 in g of C per m^2 and per year. Please note the different scales [**A**] and [**B**] and the details at the top of every subfigure.

3.2.3 Spatial distribution of the modelled methane fluxes

The spatial distribution of the methane fluxes indicates differences but also similarities among the grid cells, depending on the process as well as with changing time. The maxima of the fluxes in the grid cells for a mean year of 10 years periods are summarised in Table 3.6 for the different methane fluxes.

Table 3.6: Maxima of the grid cell methane process fluxes.

	Hist 1951 – 1960	Curr 1995 – 2004	RCP 2.6 2090 – 2099	RCP 4.5 2090 – 2099	RCP 8.5 2090 – 2099
Prod	3768	4355	5376	5962	6983
Oxid	108	125	131	157	240
Plox	39	46	48	57	87
Plant	2954	3356	2974	3295	4089
Ebul	2100	2627	3314	3769	4445
Diff	1	2	2	3	3
Snow	302	255	377	334	561
AllTrans	3623	4262	5256	5821	6788

Maxima of the modelled grid cell methane process fluxes for a mean year of 10 years periods of the historic, the current and three future scenarios in $mgCH_4 \, m^{-2} \, a^{-1}$, rounded to integer. The minima are always zero. For the meaning of the short names, see Sect. 3.2.

The analysis of the change in time respectively future scenario shows, that the highest modelled grid cell values increase by 85 % for RCP 8.5 compared to the historic period for the methane production (Table B.8). For the diffusion through snow, it is almost the same (86 %). In this comparison, the increase reaches 122 % for the bulk soil oxidation, as well as similar values for the rhizospheric oxidation (121 %) and the diffusion flux (123 %). However, in this perspective, the plant transport only shows an increase of 38 %, while the maximum value of the ebullition increases by 112 %.

The methane production shows almost the same pattern like the overall methane emissions. This is also true for the diffusion through snow, but the riparian areas are less important for that process (compare Fig. 3.14 and B.7 to Fig. 3.8). The diffusion and the ebullition both show high flux values where few C3 grass grows, but the influence is higher for the ebullition than for the diffusion (compare Fig. 3.16 and B.6 to Fig. 3.10). Also, both of these processes show high values in the riparian areas but not in the Lena River Delta itself (compare Fig. 2.12).

The bulk soil oxidation, the rhizospheric oxidation and the plant transport show high flux values in the Lena River Delta (compare Fig. 3.15, B.4 and B.5 to Fig. 2.9), with the highest values in the western part of the delta. In contrast, only very low flux values have been calculated for these processes in the uplands. But the
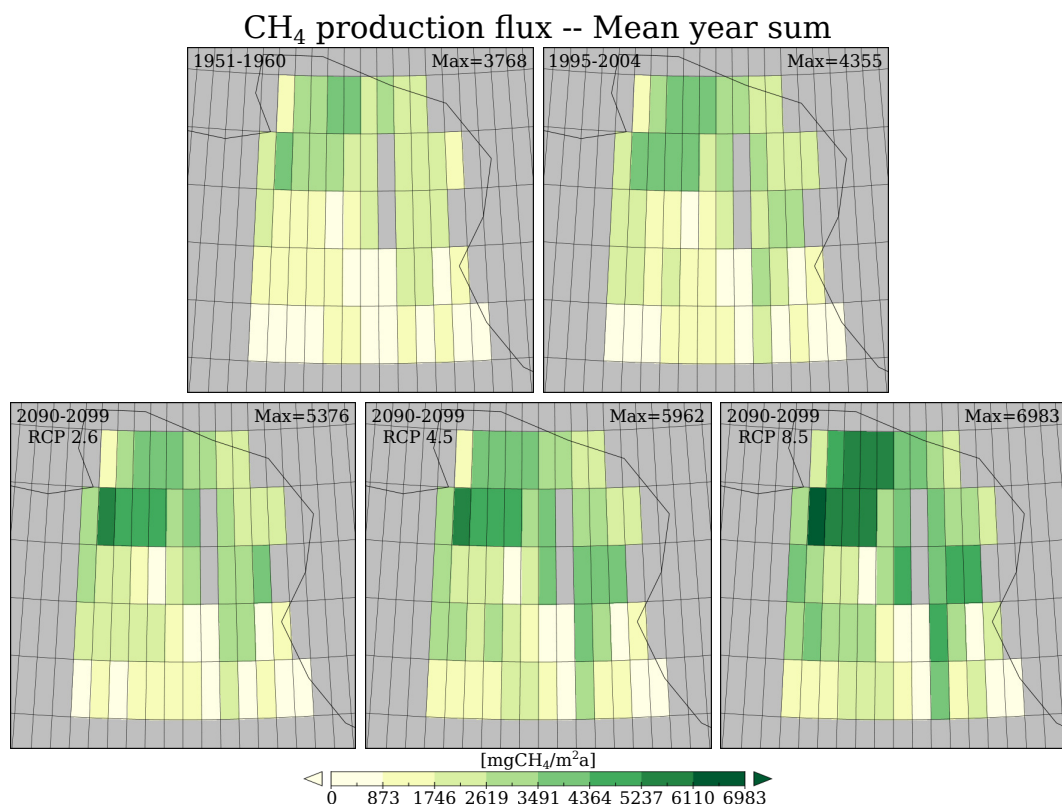
Figure 3.14: Modelled methane production flux as mean year sum over 10 years periods in mgCH$_4$ m^{-2} a^{-1}. Please note the details at the top of every subfigure.

CH$_4$ plant transport flux to atmosphere -- Mean year sum

Figure 3.15: Modelled methane plant transport flux to the atmosphere as mean year sum over 10 years periods in mgCH$_4$ m^{-2} a^{-1}. Please note the details at the top of every subfigure.

CH$_4$ diffusion flux to atmosphere -- Mean year sum

Figure 3.16: Modelled methane diffusion flux to the atmosphere as mean year sum over 10 years periods in mgCH$_4$ m^{-2} a^{-1}. Please note the details at the top of every subfigure.

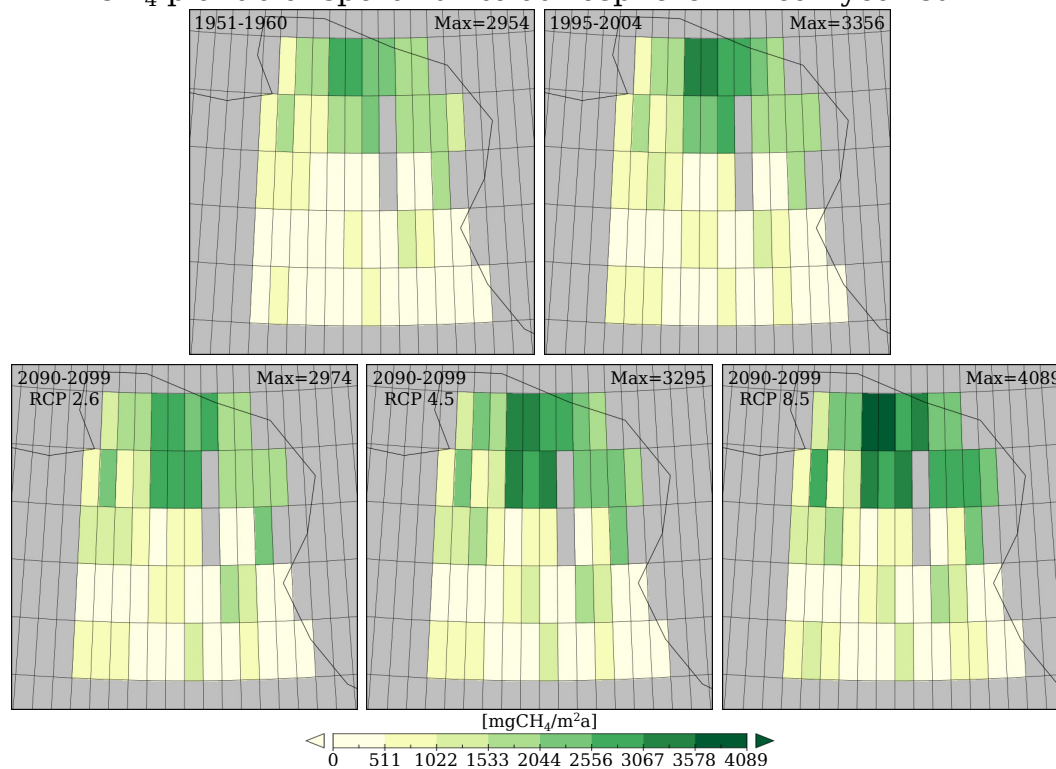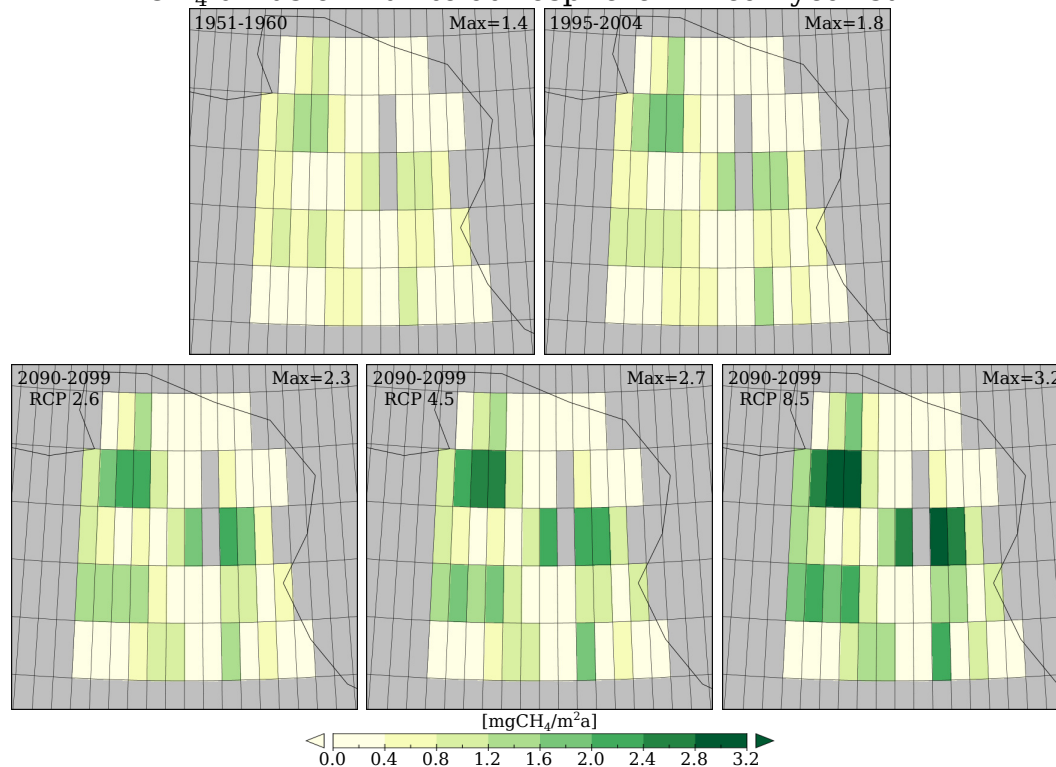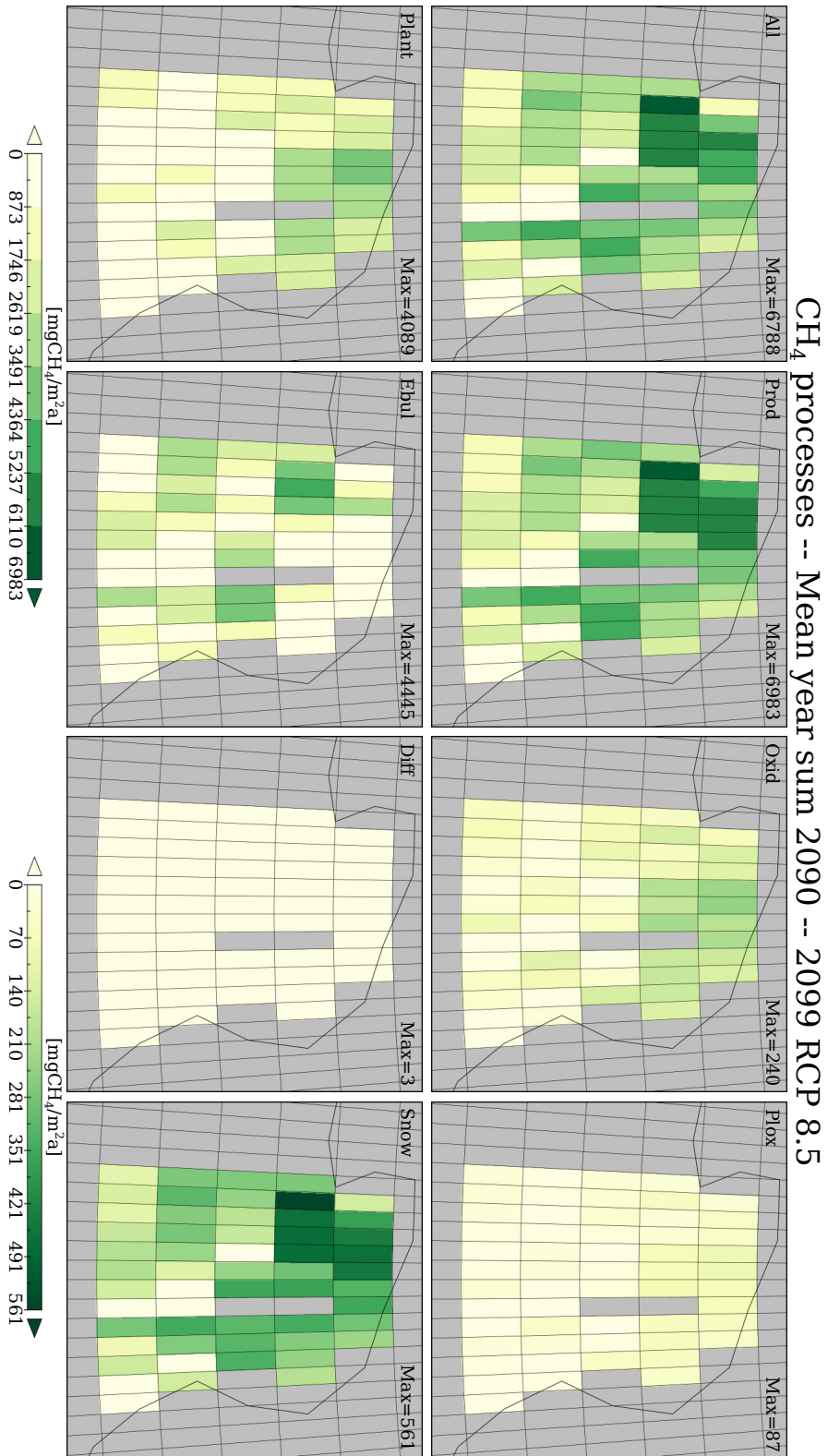Figure 3.17: Modelled methane process fluxes as mean year sum for $2090 - 2099$ under RCP 8.5 in mgCH$_4$ m^{-2} a^{-1}. Please note the two different scales for the left and the right half of the subfigures and the details at the top of every subfigure.

values are higher, where there are high soil depths and a lot of C3 grasses (compare Fig. 3.10). Furthermore, higher flux values can be found for these processes in regions with more inundated area per grid cell (compare Fig. 3.11). For the rhizospheric oxidation and the plant transport, the riparian areas have a little more importance than for the bulk soil oxidation (compare Fig. 2.12). In general, the higher the soil temperatures, the more methane emissions are calculated. This holds also true for regional differences, not only for the time development (compare Fig. 3.12).

The analysis of the change with time respectively future scenario shows, that the later respectively warmer the scenario, the more important become the riparian regions in the south relative to the delta for the methane production as well as for the diffusion through snow (Fig. 3.14 and B.7). But this is less pronounced for the diffusion through snow than for the production. For the plant transport, the bulk soil oxidation and the rhizospheric oxidation, the later respectively warmer the scenario, the higher become the values in the delta (Fig. 3.15, B.4 and B.5). In contrast, there is just a little increase in the uplands. Finally, the later respectively warmer the scenario, the higher the emissions via diffusion and ebullition (Fig. 3.16 and B.6).

To summarise, the main contributions to the overall methane emissions are the plant transport and ebullition fluxes, with another small contribution of diffusion through snow (Fig. 3.17). The regions of high methane production are primarily the western part of the Lena River Delta, but the rest of the delta, too, as well as the riparian areas. The least methane production has been calculated in the upland areas. Under the given conditions, diffusion plays only a minor role. The bulk soil oxidation is more pronounced than the rhizospheric oxidation. Both as well as the plant transport mainly take place in the delta, whereas ebullition and diffusion are low especially there but high in the riparian areas. The riparian areas also play a great role, next to the delta itself, mainly for the production and the diffusion through snow.

3.2.4   Development of the modelled fluxes with time

The modelled soil respiration fluxes field means of the yearly sums increase in the historic period as well as in all future scenarios (Fig. 3.18). However, there are also large deviations year by year from this general trend. A summary of the time series of the soil respiration fluxes is given in Table B.9.

Figure 3.18: Modelled soil respiration fluxes as field means of the yearly sums for the historic (1951 – 2004) and the three RCP scenarios (2005 – 2099) in $gC\,m^{-2}\,a^{-1}$. The straight lines show the respective linear regressions.

The annual increase, thus the increase factor a in a regression $y(t) = a \cdot t + b$ with t in years, of the soil respiration fluxes varies a lot between the fluxes and within the different periods or scenarios (Table B.10). It's pattern in time and scenario shows for both species as well as for their combination a decrease to about a half for RCP 2.6 compared to the historic period, an about 20 % increase for RCP 4.5 and an almost doubling in RCP 8.5 (Table B.11).

The interannual variability of the total soil respiration fluxes, thus their deviations from the linear trend, is not significantly influenced by methane (Table B.12). Methane deviates from the linear trend by -208 to 181 $mgC\,m^{-2}\,a^{-1}$ in the historic period, but by -323 to 290 $mgC\,m^{-2}\,a^{-1}$ in the RCP scenarios (-305 to 290, -305 to

273 and -323 to 274 mgC m^{-2} a^{-1} in RCP 2.6, RCP 4.5 and RCP 8.5). There is some variation between the different periods and scenarios. Compared to the spread in the historic period, methane shows an increase of about a half in all scenarios (Table B.13). On the other hand, the spread of the carbon dioxide emission from the soil as well as of the soil respiration flux gets almost doubled in RCP 8.5 and more than doubled in RCP 2.6 and RCP 4.5.

Also the methane process fluxes field means of the yearly sums increase in the historic period as well as in all future scenarios (Fig. 3.19). But the year by year deviations from this general trend are not as large as for the soil respiration fluxes. Still, the dimension of the values, their trend as well as their deviations from the trend greatly depends on the single process. A summary of the time series of the methane process fluxes is given in Table B.14.

The annual increase of the methane process fluxes has an even more diverse picture, if comparing the different processes and the different periods or scenarios (Table B.15). The greatest annual increase (production in RCP 8.5) is 4 dimensions higher than the smallest one (diffusion in RCP 2.6). Also the pattern in time and scenario varies a lot between the processes (Table B.16). The annual increase might be decreased by 72 % (plant transport in RCP 2.6), it might be increased 10-fold (diffusion through snow in RCP 8.5) or something in between these extremes.

The interannual variability of the methane process fluxes varies more than the one of the soil respiration fluxes, if comparing the different processes (Table B.17). While differences in the variations are in general not very pronounced among the scenarios, compared to the spread in the historic period, there is a general increase that is just relatively evenly distributed among the scenarios (Table B.18). Still, the increase in the deviations varies between 15 % (diffusion through snow in RCP 4.5) and 174 % (bulk soil oxidation in RCP 8.5).
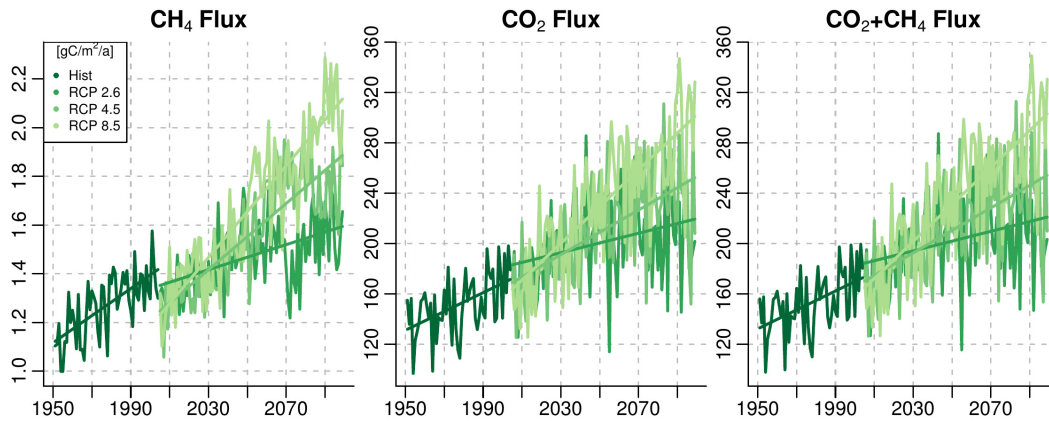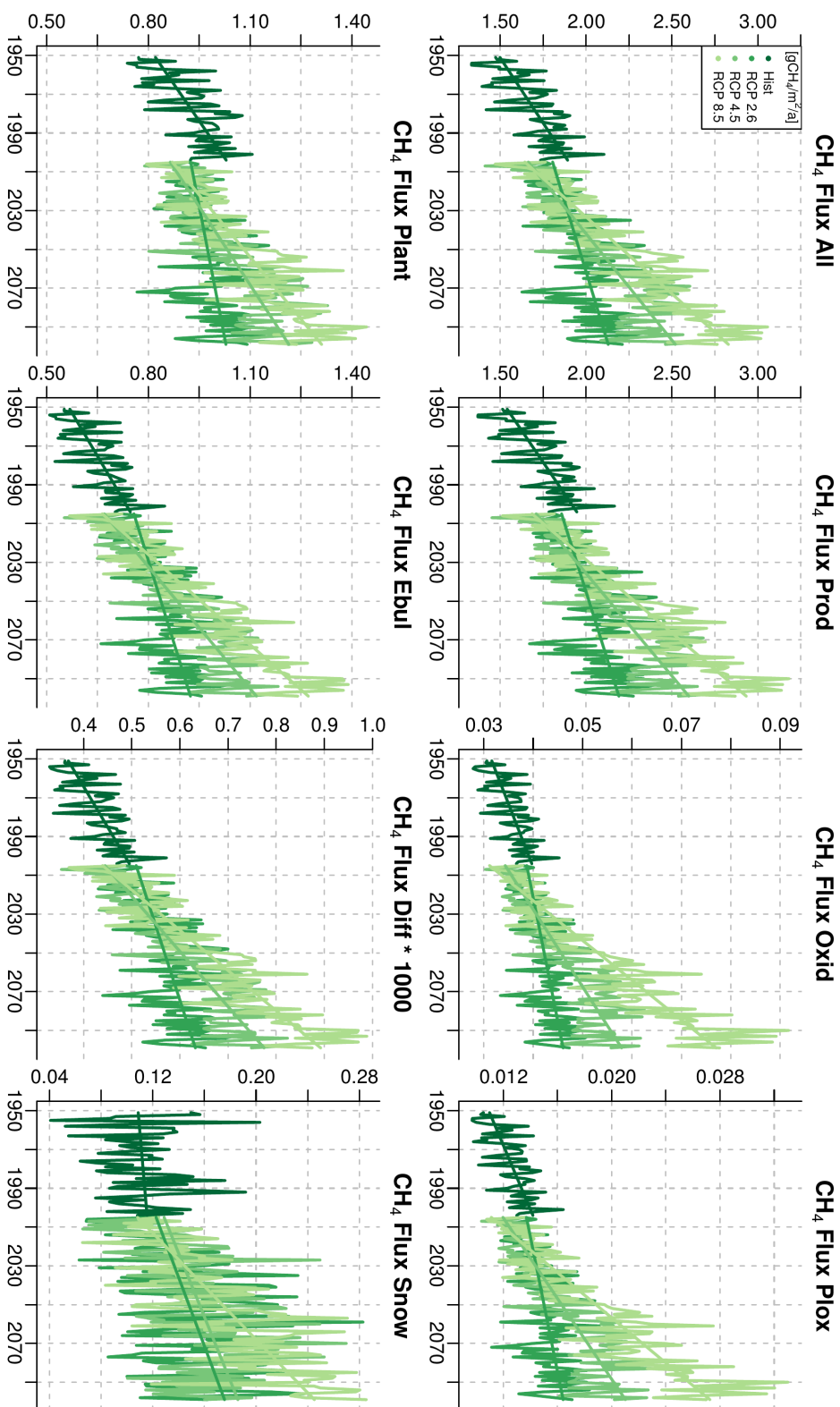
Figure 3.19: Modelled methane process fluxes as field means of the yearly sums for the historic (1951 − 2004) and the three RCP scenarios (2005 − 2099) in gCH₄ m⁻² a⁻¹. The straight lines show the respective linear regressions.

In general, no matter if the total soil respiration fluxes or single methane process fluxes are considered, all show increased deviations from their more or less increasing trends for all future scenarios, compared to the spread of the fluxes in the historic period. Despite the obviously very complex interactions with various
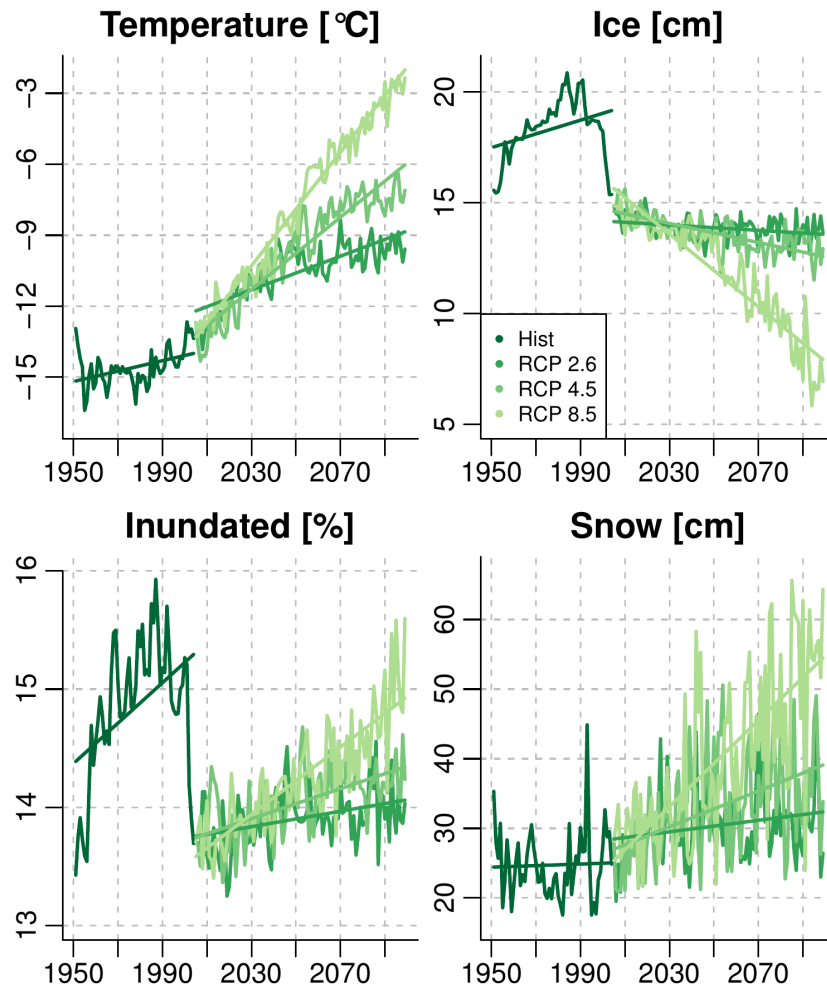
Figure 3.20: Modelled physical variables as field means of the yearly means for the historic (1951 – 2004) and the three RCP scenarios (2005 – 2099): Soil temperature as mean over the soil column, soil ice content as sum over the soil column, inundated fraction of the grid cell and snow depth of the grid cell. The used units are given in the title of every subfigure. The straight lines show the respective linear regressions.

influencing environmental factors within the modelled area, still it may be allowed to refer this behaviour to some physical variables' behaviour in the course of the different periods and scenarios (Fig. 3.20).

Moreover, these modelled physical variables, on which the soil respiration fluxes depend, already show interesting behaviour in the historic period. Around the year 1960, the inundated fraction increases quickly. On the other hand, around the year 2000, not only the inundated fraction but also the soil ice content decrease even more pronounced. This follows a large variation in snow depth and soil temperature. Despite these data are aggregated from single grid cells to the whole model domain and from hourly to yearly values, a comparison to equally treated forcing data (Fig. B.8) reveals the evidence of non-linear effects of the variability in the forcing data on the physical variables. However, this does not translate one to one to the soil respiration fluxes. Still, the inundated fraction and the soil ice content continue at the low level, that they reached at the end of the historic period, also at the beginning of the future scenarios. Thus, the soil respiration fluxes in the future scenarios start at a level, that is influenced by the decrease in the physical variables at the end of the historic period.

3.2.5   Development of the seasonal cycle of the fluxes

Table 3.7: Maxima of the hourly soil respiration fluxes for a mean year.

$[\mathrm{gC\,m^{-2}\,d^{-1}}]$	Hist	Curr	RCP 2.6	RCP 4.5	RCP 8.5
	$1951-1960$	$1995-2004$	$2090-2099$	$2090-2099$	$2090-2099$
CH_4	0.013	0.014	0.014	0.015	0.016
CO_2	1.658	1.968	1.880	2.075	2.379
CO_2+CH_4	1.670	1.981	1.892	2.089	2.395

Maxima of the modelled hourly soil respiration fluxes field means for a mean year of 10 years periods of the historic, the current and three future scenarios, rounded to three decimal places. The units are g of C per m^2 and per day.

In general, the maxima of the modelled hourly soil respiration fluxes field means for a mean year of 10 years periods increase with time respectively increasing RCP scenario (Table 3.7). But in RCP 2.6, they all decrease a bit compared to the maxima of the current period. The difference between the change of the maxima of the hourly methane fluxes and that of the carbon dioxide emissions from the soil as well as of the soil respiration fluxes is a generally by about a third lower increase for methane (Table B.19).

The timing of the yearly maxima of the soil respiration fluxes also varies with the time period or scenario (Table B.20). In RCP 2.6, the methane flux reaches its maximum 38 days earlier than the carbon dioxide emission from the soil (Table B.21), despite in the other time periods and scenarios, the shift is much smaller (8 to 11 days). The soil respiration flux reaches its maximum at the same day as the carbon dioxide emission from the soil alone.

Table 3.8: Maxima of the hourly methane process fluxes for a mean year.

	Hist	Curr	RCP 2.6	RCP 4.5	RCP 8.5
	$1951 - 1960$	$1995 - 2004$	$2090 - 2099$	$2090 - 2099$	$2090 - 2099$
Prod	17.263	19.316	18.957	20.298	22.777
Oxid	0.393	0.458	0.461	0.532	0.783
Plox	0.148	0.175	0.176	0.206	0.294
Plant	9.935	10.938	9.933	10.365	11.180
Ebul	6.804	7.763	8.553	9.305	10.565
Diff	0.005	0.005	0.006	0.007	0.008
SnowS	2.004	2.225	2.489	2.599	3.590
SnowA	2.418	1.895	3.743	2.533	3.852
AllTrans	16.743	18.707	18.349	19.586	21.748

Maxima of the modelled hourly methane process fluxes field means for a mean year of 10 years periods of the historic, the current and three future scenarios in $mgCH_4 \, m^{-2} \, d^{-1}$, rounded to three decimal places. For the meaning of the short names, see Sect. 3.2.

Table 3.9: Start dates of the main emission seasons of the hourly soil respiration
           fluxes for a mean year.

	Hist	Curr	RCP 2.6	RCP 4.5	RCP 8.5
	1951 − 1960	1995 − 2004	2090 − 2099	2090 − 2099	2090 − 2099
CH_4	11.05.	03.05.	23.04.	17.04.	07.04.
CO_2	22.05.	10.05.	19.04.	15.04.	28.03.
CO_2+CH_4	22.05.	10.05.	19.04.	15.04.	28.03.

Start dates of the main emission seasons of the modelled hourly soil respiration fluxes
field means for a mean year of 10 years periods of the historic, the current and three
future scenarios. As indicator of the timing of the main emission seasons 5 % of the
maximum in the historic period was used.

On the other hand, while the methane flux reaches its maximum in the current
period and in the RCP scenarios at most a bit earlier than in the historic period (3
to 7 days), the carbon dioxide emission from the soil as well as the soil respiration
flux reach their maxima in the current period and in RCP 2.6 much later (13 to
39 days) but in RCP 4.5 and RCP 8.5 a bit earlier (2 to 5 days) (Table B.22).

Table 3.10: End dates of the main emission seasons of the hourly soil respiration
            fluxes for a mean year.

	Hist	Curr	RCP 2.6	RCP 4.5	RCP 8.5
	1951 − 1960	1995 − 2004	2090 − 2099	2090 − 2099	2090 − 2099
CH_4	28.10.	03.11.	09.11.	14.11.	27.11.
CO_2	29.10.	05.11.	14.11.	01.12.	29.12.
CO_2+CH_4	29.10.	05.11.	14.11.	01.12.	29.12.

End dates of the main emission seasons of the modelled hourly soil respiration fluxes
field means for a mean year of 10 years periods of the historic, the current and three
future scenarios. As indicator of the timing of the main emission seasons 5 % of the
maximum in the historic period was used.

The maxima of the modelled hourly methane process fluxes show a more diverse picture than the hourly soil respiration fluxes, if comparing the different processes and the different periods or scenarios (Table 3.8). The diffusion through snow in autumn is the only process, that has a reduced maximum compared to the historic period, namely in the current period. All other processes increase in all periods or scenarios compared to the historic period, but their behaviour is not uniform (Table B.29). The higher the scenario, the higher is the increase, despite again for the diffusion through snow in autumn, which reaches a much smaller maximum in RCP 4.5 than in the other two scenarios. In the current period, the production, the plant transport and the combined flux to the atmosphere have higher increases of their maxima than in RCP 2.6, the plant transport even higher than in RCP 4.5.

Table 3.11: Start dates of the main emission seasons of the hourly methane process fluxes for a mean year.

	Hist	Curr	RCP 2.6	RCP 4.5	RCP 8.5
	1951 – 1960	1995 – 2004	2090 – 2099	2090 – 2099	2090 – 2099
Prod	11.05.	04.05.	24.04.	18.04.	07.04.
Oxid	02.06.	26.05.	17.05.	14.05.	08.05.
Plox	04.06.	29.05.	18.05.	17.05.	16.05.
Plant	02.06.	26.05.	17.05.	15.05.	15.05.
Ebul	01.06.	23.05.	14.05.	12.05.	11.05.
Diff	02.06.	25.05.	15.05.	12.05.	11.05.
SnowS	12.04.	08.04.	26.03.	19.03.	02.02.
SnowA	20.09.	01.10.	26.09.	10.10.	15.10.
AllTrans	11.05.	03.05.	23.04.	17.04.	07.04.

Start dates of the main emission seasons of the modelled hourly methane process fluxes field means for a mean year of 10 years periods of the historic, the current and three future scenarios. As indicator of the timing of the main emission seasons 5 % of the maximum in the historic period was used. For the meaning of the short names, see Sect. 3.2.

Table 3.12: End dates of the main emission seasons of the hourly methane process
           fluxes for a mean year.

	Hist $1951-1960$	Curr $1995-2004$	RCP 2.6 $2090-2099$	RCP 4.5 $2090-2099$	RCP 8.5 $2090-2099$
Prod	28.10.	02.11.	08.11.	13.11.	27.11.
Oxid	16.10.	21.10.	27.10.	30.10.	11.11.
Plox	09.10.	15.10.	17.10.	24.10.	27.10.
Plant	12.10.	18.10.	18.10.	26.10.	28.10.
Ebul	11.10.	18.10.	18.10.	26.10.	29.10.
Diff	09.10.	15.10.	17.10.	25.10.	29.10.
SnowS	10.06.	05.06.	31.05.	30.05.	28.05.
SnowA	17.11.	22.11.	08.12.	23.12.	27.01.
AllTrans	28.10.	03.11.	09.11.	14.11.	27.11.

End dates of the main emission seasons of the modelled hourly methane process fluxes
field means for a mean year of 10 years periods of the historic, the current and three
future scenarios. As indicator of the timing of the main emission seasons 5 % of the
maximum in the historic period was used. For the meaning of the short names, see
Sect. 3.2.

Also, the timing of the yearly maxima of the methane process fluxes varies with
the time period or scenario and among the different processes (Table B.30). Es-
pecially in RCP 2.6, the plant transport and the two oxidation processes reach
their maxima about 1 week earlier than the methane production (Table B.31). In
contrast in RCP 8.5, the maxima of the two oxidation processes are reached 18
days earlier than the one of the methane production.

On the other hand, while all methane processes despite the diffusion through snow
in autumn reach their maxima earlier in the other time periods or scenarios than
in the historic period, they reach it later in RCP 8.5, despite the diffusion through
snow in spring (Table B.32). Still, the shift of the maxima depends very much on
the process as well as on the time period and scenario.

To sum up the behaviour of the maxima, despite for the diffusion through snow, all methane process fluxes reach their maximum earlier in the current period as well as in RCP 2.6 and RCP 4.5 but later in RCP 8.5 than in the historic period. The spring time maximum of the diffusion through snow is in all later periods or scenarios earlier, the autumn time maximum of it later than in the historic period.

As indicator of the timing and length of the main emission seasons of the different fluxes, 5 % of the particular fluxes maximum in the historic period have been used. In general, all soil respiration and all methane process fluxes have an earlier start and a later end date than in the historic period (Tables 3.9 to 3.12). The only exception is the diffusion through snow, whose spring emission period ends earlier and whose autumn emission period starts later than in the historic period (Tables B.34 and B.36).

With the definition of the start and end date of the main emission season, also statements about the length of this period are possible to give. The methane flux has a longer emission season than the carbon dioxide emission from the soil or the soil respiration flux in the historic and current period but a shorter one in the RCP scenarios (Table 3.13). But all soil respiration fluxes' main emission seasons increase with later periods or increased RCP scenarios.

Table 3.13: Length of the main emission seasons of the hourly soil respiration fluxes for a mean year.

	Hist	Curr	RCP 2.6	RCP 4.5	RCP 8.5
	$1951 - 1960$	$1995 - 2004$	$2090 - 2099$	$2090 - 2099$	$2090 - 2099$
CH_4	170	184	200	211	234
CO_2	160	179	209	230	276
$CO_2 + CH_4$	160	179	209	230	276

Length of the main emission seasons of the modelled hourly soil respiration fluxes field means for a mean year of 10 years periods of the historic, the current and three future scenarios.

Table 3.14: Length of the main emission seasons of the hourly methane process
          fluxes for a mean year.

	Hist	Curr	RCP 2.6	RCP 4.5	RCP 8.5
	1951 – 1960	1995 – 2004	2090 – 2099	2090 – 2099	2090 – 2099
Prod	170	182	198	209	234
Oxid	136	148	163	169	187
Plox	127	139	152	160	164
Plant	132	145	154	164	166
Ebul	132	148	157	167	171
Diff	129	143	155	166	171
SnowS	59	58	66	72	116
SnowA	58	52	73	74	104
Snow	117	110	139	146	220
AllTrans	170	184	200	211	234

Length of the main emission seasons of the modelled hourly methane process fluxes field
means for a mean year of 10 years periods of the historic, the current and three future
scenarios. For the meaning of the short names, see Sect. 3.2.

Also, all methane process fluxes show a broadening of their main emission season,
when comparing later periods or scenarios to the historic period (Table 3.14). Only
the diffusion through snow also shows a shift in its two main emission seasons, to
earlier dates in spring and to later ones in autumn. Moreover, all main emission
seasons are increasing with later periods and increasing RCP scenarios, but the one
of the diffusion through snow also shows a slight decrease in length only in RCP 2.6.

For a more detailed analysis, the reader is also referred to the Tables B.23 to
B.28 and Tables B.33 to B.38.

All these changes in the seasonal patterns of the soil respiration fluxes, e.g. the
broadening of the season, the earlier emission increase in spring, the overall higher
emissions and the later decline of the emissions in autumn, when comparing later

periods or increasing scenarios, can also be seen in Fig. 3.21. The seasonal pattern of carbon dioxide emission from the soil is not that smooth like the one of methane. And the influence of methane in the combined soil respiration fluxes is only visible via higher values, so that it does not change the overall picture. For a visualisation of the seasonal start and end of the soil respiration fluxes, the reader is also referred to Fig. B.9.

Similarly, the changes in the seasonal patterns of the methane process fluxes, again the broadening of the season, the earlier emission increase in spring, the overall higher emissions and the later decline of the emissions in autumn, when comparing later periods or increasing scenarios, can be seen in Fig. 3.22. The methane production shows the same pattern like the overall methane flux out of the soil. For the plant transport, the ebullition and the diffusion, it is similar. Also, the two oxidation processes show that pattern, despite that they also show a much bigger in-
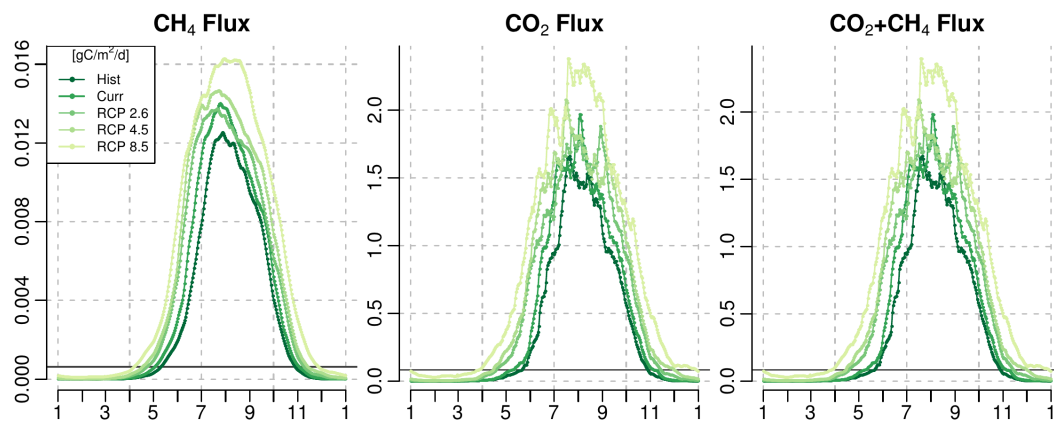

Figure 3.21: Modelled soil respiration fluxes field means as hourly data (points) and daily means (lines) for a mean year of the historic (1951–1960), the current (1995–2004) and the three RCP scenarios (2090–2099) in $gC\,m^{-2}\,d^{-1}$. X axes indicate the first day of the respective month of the year. The solid line is 5 % of the maximum in the historic period as indicator of the timing of the main emission seasons.
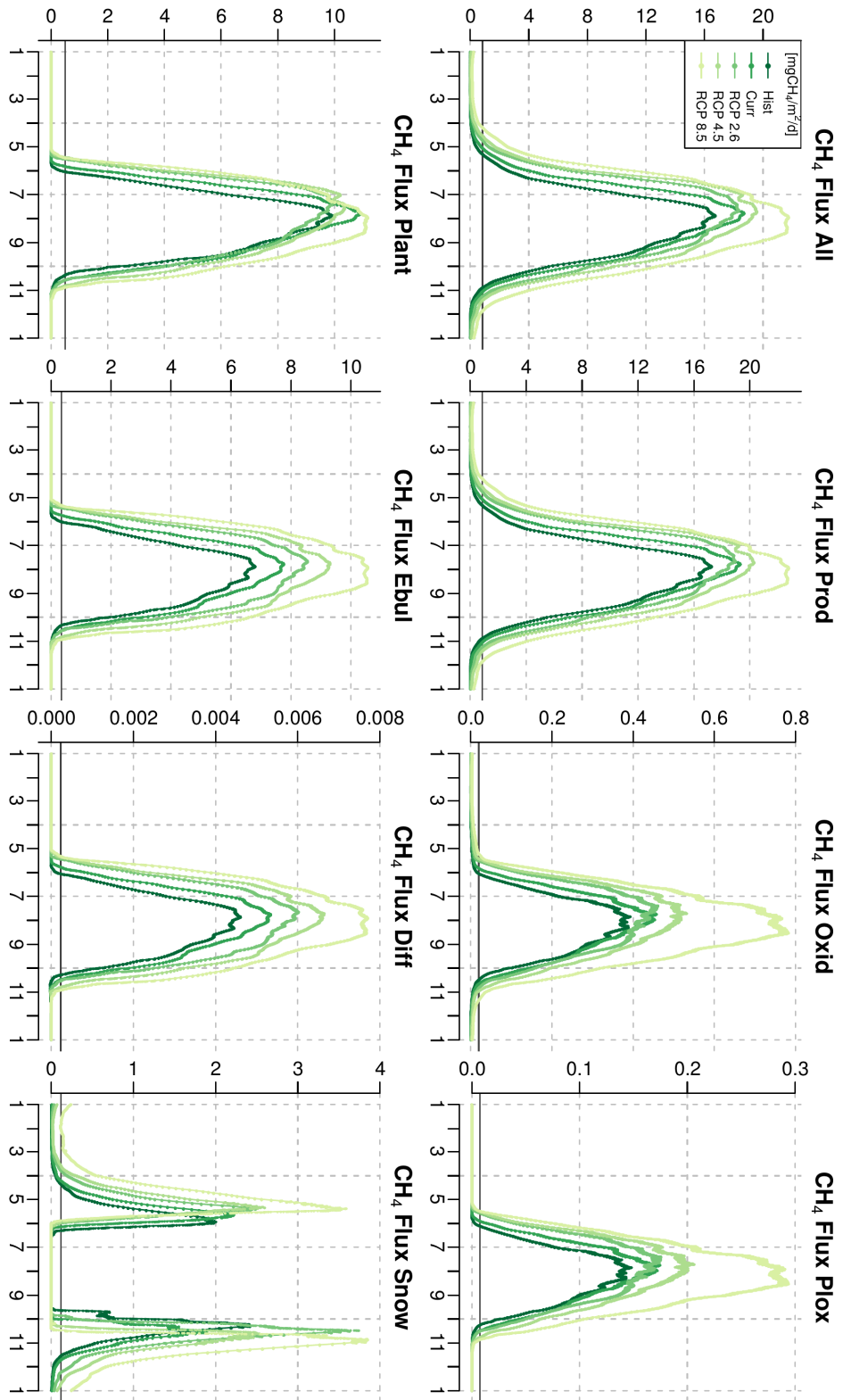
Figure 3.22: Modelled methane process fluxes field means as hourly data (points) and daily means (lines) for a mean year of the historic (1951 − 1960), the current (1995 − 2004) and the three RCP scenarios (2090 − 2099) in mgCH$_4$ m^{-2} d^{-1}. X axes indicate the first day of the respective month of the year. The solid line is 5% of the maximum in the historic period as indicator of the timing of the main emission seasons.

crease in RCP 8.5. The diffusion through snow shows, despite the broadening of both of its main seasons, additionally a shift in time to earlier dates for spring and to later ones for autumn. Also, it increases during the low emission period in winter time, too. For a visualisation of the seasonal start and end of the methane process fluxes, the reader is also referred to Fig. B.10.

The changing seasonal behaviour of the soil respiration fluxes, despite integrated over several years and multiple grid cells, can still be related to the changing seasonal behaviour of some physical variables (Fig. 3.23). There is clearly an overall warming of the soil. Also less cold winter temperatures lead to a decreasing temperature amplitude, from more than 17 to less than 10 K. The soil warms earlier and stays warmer longer in the year. Consequently, less ice is in the soil. In RCP 8.5, there is even no ice in summer. Also, there is earlier thawing as well as later refreezing in winter. And the inundation happens earlier in spring but the drying in summer starts earlier in RCP 2.6 and RCP 4.5. In RCP 8.5, there is no drying before winter. Less area is inundated in the middle and last part of the summer for RCP 2.6 and RCP 4.5, but more for RCP 8.5, but much less in winter for RCP 8.5. The snow melt also happens earlier in spring and the snow accumulation starts later in autumn.
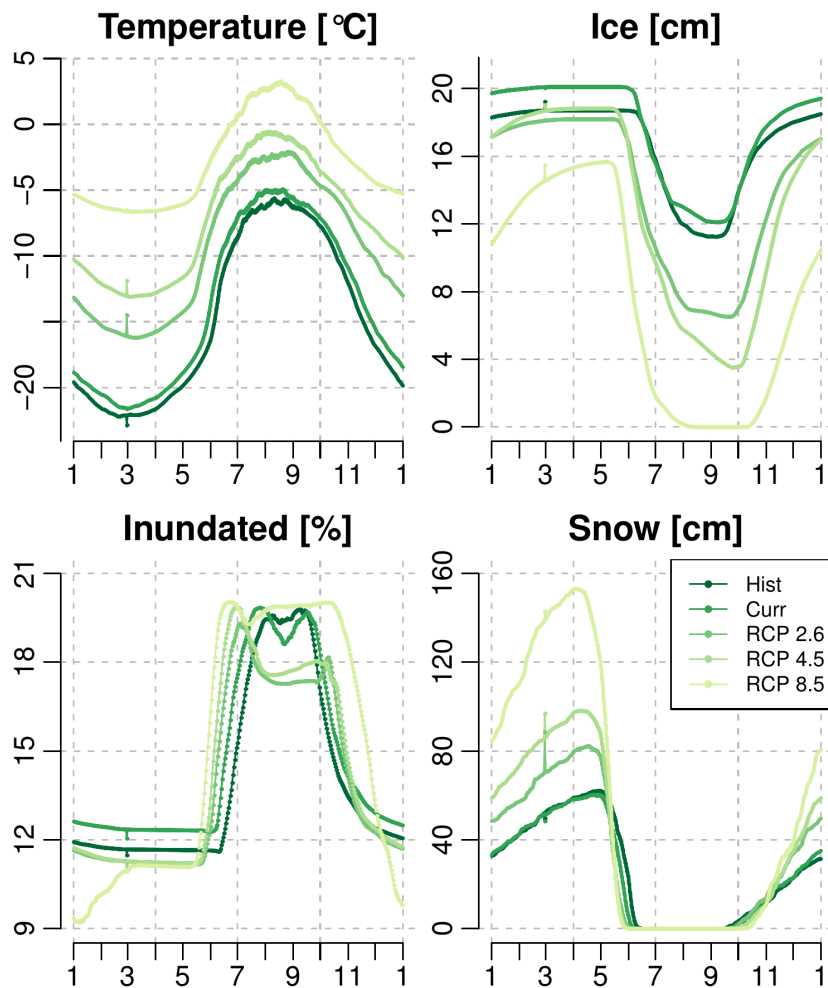
Figure 3.23: Modelled physical variables field means as hourly data (points) and daily
means (lines) for a mean year of the historic (1951 – 1960), the current
(1995 – 2004) and the three RCP scenarios (2090 – 2099): Soil temperature
as mean over the soil column, soil ice content as sum over the soil column,
inundated fraction of the grid cell and snow depth of the grid cell. The
used units are given in the title of every subfigure. X axes indicate the first
day of the respective month of the year.

Chapter 4

Discussion

Within this work, two different versions of the presented methane module and the enveloping JSBACH model have been applied. The regional future climate experiments use further developed versions compared to the site-level study.

4.1 Site-level study

4.1.1 General discussion about this study

The newly developed methane module for the JSBACH land surface scheme that was used in this study is itself completely integrated into the larger framework of the JSBACH model. Therefore, sensitivity tests can only be conducted using the full model and a clean separation between the existing structure and new components is not always possible. The interpretation and discussion of all findings should therefore consider that the functioning of the new methane module is to a large extent dependent on, and in many aspects limited by, the performance of the JSBACH model as a whole.

The presented methane module determines methane production, oxidation and transport as well as transport and use of oxygen in the soil. All of these key processes are heavily dependent on soil moisture status as well as the quality and quantity of carbon in different soil pools. Both of these aspects, i.e. soil hydrology

and carbon decomposition, are handled by existing JSBACH modules which were not modified in the context of the presented study. With an exclusive focus on simulating processes at site-level scale, it may even be possible to upgrade these modules and add some features that would be relevant for the methane processes. However, since the scope was to provide a methane extension for JSBACH that can be applied globally, certain limitations regarding the representation of site-level observations need to be taken into account. This situation is even aggravated due to the use of parameter settings from global fields, i.e. with a coarse spatial resolution that aggregates conditions over larger areas and thus naturally cannot provide the exact details for the field site where the reference fluxes were measured. Such systematic deviations in modelling framework and parameter configurations will generate systematic differences between model output and site-level measurements. Accordingly, modelled hydrological conditions and amounts of decomposed carbon need to be considered when comparing modelled methane emissions to the site-level observations and interpreting the spatiotemporal differences.

As mentioned above, the JSBACH hydrology module has been designed for global applications and is not capable of capturing conditions in complex landscapes such as polygonal tundra. Therefore, for the Samoylov site, which was used for this site-level analysis, the modelled soil climate and hydrology systematically deviate from those found in the field (Beer, 2016). It was still chosen to work at this site, because a highly valuable interdisciplinary dataset could be provided to evaluate different facets of the model output. To adapt the model to represent the complex hydrology, a mixed approach of combining two different model runs was applied. This approximation implies a very simplified representation of the real hydrological conditions and cannot fully offset all site-level differences between model simulations and observational datasets. Accordingly, systematic biases need to be considered when interpreting the findings. However, through this approach, the paramount importance of realistic hydrologic boundary conditions for simulations of the methane balance could be demonstrated. In many aspects, details in the behaviour of the methane processes are tightly linked to the spatiotemporal

variation of hydrological conditions; therefore, biases in hydrology are directly projected onto the methane processes.

Still, the author believes that the comparison of methane simulations against selected site-level measurements is an important first step to evaluating the overall performance of the new module. It is obvious that the limitations of the observational database employed herein, i.e. using just one single observation site and focusing on the growing season alone, cannot allow for a comprehensive assessment of the newly implemented algorithms. Accordingly, the limited amount of available field measurements from chamber and eddy-covariance-based fluxes requires a careful interpretation when compared to model results, particularly regarding the evaluation of JSBACH as a process-based global biosphere model. For the Arctic domain, methane emissions during shoulder and winter seasons have been shown to add considerably to the full annual budget, an aspect that cannot be evaluated based on the given database. Moreover, the question of temporal and spatial representativeness is complicated by the discontinuous nature of the methane fluxes (e.g. Tokida et al., 2007a; Jackowicz-Korczyński et al., 2010; Tagesson et al., 2012). To overcome these limitations, in follow-up studies the author plans to conduct model evaluations based on longer-term flux measurements, covering full annual cycles for multiple Arctic sites.

Even though eddy-covariance-based fluxes are regarded as the most reliable reference data source for longer-term site-level model evaluation, the influence of microsite variability in the area surrounding the tower clearly poses a challenge here. Particularly with respect to methane fluxes, pronounced variability in the distribution of soil organic matter and water content may lead to a mosaic of different source strengths. For the Samoylov domain, which is characterised by polygonal structures, the apparent differences between wet (centre) and moist (rim) areas were mimicked through the execution of two model runs with different settings. Still, the footprint composition of the eddy covariance tower might not match the mixed approach of 65 % rim and 35 % centre used for modelling (Sachs

et al., 2010). Even though this mixture generally captures the composition of the larger area surrounding the tower, particularly when footprints are smaller during daytime, the reduced field of view of the sensors might focus on areas that are wetter or drier than the average. The concept of combining two separate model runs has to be regarded as an approximation to cope with the hydrological constraints of a global model on the one hand and the complex landscape on the other.

The model application for remote permafrost areas may also be limited by the availability of long-term and complete observations of meteorological data to be used as model forcing. Forcing data and methane fluxes are required for the same time period, which optimally lasts over 1 or more entire years. When going towards regional to global applications, this new module might be additionally compared to regional or global atmospheric inversion results (e.g. Bousquet et al., 2011; Berchet et al., 2015) or data-driven upscaling of eddy-covariance- or chamber-based observations (e.g. Christensen et al., 1995; Marushchak et al., 2016).

Within the methane module presented in this work, the discretisation as well as the pore volume are variable. This requires that the time step of calculation and the diffusion coefficients must fit to the thicknesses of the soil layers. If not set up properly, instabilities like oscillations or unrealistic behaviour like negative concentrations may occur. However, because the new methane module has been designed to be flexible in this respect, adjustments can easily be made in case numerical problems arise.

4.1.2   Discussion about specific assumptions

A parameter sensitivity study (Sect. 3.1.5) showed that the uncertainty of the resulting overall methane emissions scales linearly only for one parameter with the uncertainty of that parameter. This parameter represents the amount of methane produced under anoxic conditions compared to the total anoxic decomposition flux of carbon dioxide and methane combined $\left(\frac{[CH_4]}{[CO_2]+[CH_4]} \right)$. Based on the stoichiometry of the methanogenesis chemical reaction equation and based on labor-

atory and field data (Segers, 1998), this parameter was chosen to be 0.5 in Eq. 2.2. In other models, this parameter is used as an effective parameter and has been tuned to match ultimate methane and carbon dioxide emissions from soil to the atmosphere in the absence of an explicit representation of oxygen and hence methanotrophy (Wania et al., 2010).

Regarding the assumptions concerning fluxes during winter time or plant transport, according to recent findings (Zona et al., 2016; Marushchak et al., 2016), the settings chosen within the context of this work might be oversimplifying the actual processes in the field. The implemented mechanism that prevents gas exchange with the atmosphere once the snow cover reaches a depth of 5 cm is a very crude approximation of the snow cover influence. It resulted from biases in the modelled hydrological conditions in winter, where freezing of relatively dry soils led to oxic soil conditions that facilitated methane transport into the soil. The next iteration of the model development will include a more sophisticated, process-based representation of methane diffusion through snow. This upgrade, however, needs to be coupled to a major restructuring of several model components and thus cannot be reconciled with the model version presented within the context of this study.

The implementation of the plant transport follows a mechanistic approach, but its definition is limited by the availability of observational evidence on e.g. diffusion velocities. Therefore, the parameter settings used in this study are subject to high uncertainty. The value for the diffusion coefficient in the exodermis was chosen to be 80 % of the diffusion coefficient in water (C. Knoblauch, personal communication, 2014). The subsequent gas transport within the aerenchyma is assumed to be as quick as diffusion in air. With this set-up, the effective barrier of the root exodermis will limit the plant transport efficiency and therefore act as a dominant control for this emission pathway. The thickness of this barrier has a large influence on plant transport as well; i.e. a thinner root exodermis would lead to increased plant transport. While this parameter is relatively easy to define, the cumulative surface area of all gas transporting roots in the soil column is difficult to constrain.

Considering the basic assumption made that plant transport is slower than diffusion in water, the general patterns of flux processes and soil moisture for rim and centre conditions appear plausible. Regarding the quantitative flux rates, however, the fraction of the total flux emitted through plant transport in the model tends to be too low. With larger root surface leading to increased plant transport, this setting could therefore be used as a tuning parameter to improve this issue. However, the oxygen available to consume methane also plays another modulating role, particularly for plant transport. Accordingly, new observational evidence would certainly improve the associated uncertainties; therefore, this issue is subject to ongoing investigations. With the new methane module, designed to be flexible regarding these kinds of settings, parameter adjustments with respect to newer findings can easily be implemented.

The contribution of labile root exudates to methane production and emission has been largely neglected in existing model implementations and is also not considered in this model configuration. This is also an understudied process in field experiments and can only be estimated indirectly. The rate of root exudates is linked to the nutrient availability in soils, with more root exudates present for plants located in nutrient-poor wetland soils (Koelbener et al., 2010). The wetland soils in Arctic tundra are known to be nitrogen-limited (Melle et al., 2015; Gurevitch et al., 2006). The plant growth in the polygonal lowland tundra of Indigirka, Russia, is co-limited by nitrogen and phosphorus, and only about $5\,\%$ of the total nitrogen soil content is active in the biological fraction (Beerman et al., 2015). The presence of vascular plants in Arctic wetlands supports the production of highly labile low molecular weight carbon compounds which can promote methane emissions through their methanogenic decomposition (Ström et al., 2012).

Indirect evidence of the role of root exudates in methane production in polygonal ponds and water-saturated soils in Samoylov is presented by Knoblauch et al. (2015). These authors found almost 4-fold higher potential methane production rates in vegetated sites compared to the non-vegetated ones, both with the

same carbon and nitrogen soil concentrations. Thus, the contribution to methane emissions from wetland soils in Arctic tundra due to the decomposition of root exudates should be taken into account in models. This will allow the understanding of the role of root exudates under present climate conditions. On the other hand, the potential nutrient mobilisation in soils due to permafrost degradation under climate change (Kuhry et al., 2010) may reduce the role of root exudates in methane emissions. However, the current JSBACH configuration lacks of a full soil nutrient cycle, and the assimilation of nutrients by plant roots, as well as the contribution of root exudates to the total methane emissions, cannot be modelled at this point.

4.1.3 Comparison to published data

In Samoylov, the minimum of modelled daily sums of methane emissions during summer is smaller and the maximum much higher for rim and centre compared to measurements published by Kutzbach et al. (2004). However, these observations do not include spring bursts with very short but also very high emissions or even dry phases with small uptake. Moreover, such high modelled emissions are rather rare, and the general level of modelled values is lower than in observations (Fig. 3.7). Thus, the mean of the measurements is 3 times as high for the rim and 3.5 times as high for the centre compared to the modelled daily sums in summer (Table 4.1).

Table 4.1: Summary of daily methane flux.

	Min	Mean	Max
Rim	-0.690	1.34	208
Centre	-0.208	8.21	385
Mixed	-0.521	2.90	135

Modelled daily methane flux out of the soil for the summer periods 2003 to 2005 for the rim, centre and a mixed approach of 65 % rim plus 35 % centre in $mgCH_4\,m^{-2}\,d^{-1}$, rounded to three non-zero digits. Summer means less than 5 cm of snow are on the ground. Please note the different unit here.

Table 4.2: Summary of hourly methane flux.

	Min	Mean	Max
Rim	-0.0237	0.0267	39.3
Centre	-0.0189	0.2310	86.8
Mixed	-0.0235	0.0813	30.4

Modelled hourly methane flux out of the soil for the summer periods 2003 to 2005 for the rim, centre and a mixed approach of 65 % rim plus 35 % centre in $mgC\,m^{-2}\,h^{-1}$, rounded to three non-zero digits. Summer means less than 5 cm of snow are on the ground.

When comparing the model results at Samoylov to published results from other high-latitude regions, reasonable agreement is found. The modelling results are about 40 to 60 % lower than measurements for BOREAS, Canada, and Abisko, Sweden, (Wania et al., 2010). The Lena River Delta region is much colder and drier compared to these sites, suggesting that lower flux rates are indeed reasonable. Furthermore, the Samoylov site is characterised by mineral soils containing substantially lower organic carbon as a substrate for methane production than the organic soils at the BOREAS site and the mire in Abisko. Compared to measurements done by Desyatkin et al. (2009) on a thermokarst terrain at the Lena River near Yakutsk, the mean results are well within the measurement range when comparing the rim to the drier sites, the centre to the wetter sites, and the mixed approach to the entire ecosystem (Table 4.2). However, climate and environmental conditions in this study were very different from those observed in Samoylov; thus, this comparison can only be regarded as a rough guideline. Nakano et al. (2000) measured methane fluxes at Tiksi near the mouth of the Lena River. While the mean value at the rim is 4.5 times as high as the mean measurements in Tiksi, the mean at the centre is 5.5 times as high as the modelled mean value (Table 4.1). The modelled minimum is lower for the centre but comparable for the rim.

The large methane spring bursts simulated by the model at both the rim and centre may represent the release of methane that has been accumulated during winter in the topsoil below the snow layer. To the knowledge of the author, there

is no observational reference of spring bursts measured in Samoylov. However, evidence of these events have been presented for other wetland areas using chambers and eddy covariance measurements, e.g. in northern Sweden (Jammet et al., 2015; Friborg et al., 1997), in Finland (Hargreaves et al., 2001), in northern Japan (Tokida et al., 2007b) and in Northeast China (Song et al., 2012). These studies suggest the presence of spring thaw emissions of methane that occur sporadically over short periods in the form of bursts. The magnitude of the spring bursts can exceed the mean summer fluxes by a factor of 2 to 3. Although spring emissions can account for a large share of the total annual fluxes, their occurrence, duration and magnitude are still uncertain. To adequately characterise the spring bursts in Samoylov, it is necessary to perform dedicated field measurements during the spring thaw period. These results will then help to evaluate the representativeness of the modelled spring bursts. In future model iterations, the spring bursts will also be evaluated for larger spatial scales.

In Zona et al. (2009), several measurements of methane emissions from the Arctic tundra are presented. Despite the modelled mean values being located towards the lower end, the modelled minimum, mean and maximum values fit well within the given range. Bartlett et al. (1992) measured methane fluxes near Bethel in the Yukon–Kuskokwim Delta, Alaska. The provided values for upland tundra compare well to the modelled mean and minimum values. However, the modelled maximum fluxes are higher than the measurement values for upland tundra, but still well within the range of measured values for wet meadow, which has higher moisture contents than upland tundra. In fact, the highest values are calculated if soil moisture is highest, so despite being more on the lower end of this waterlogged landscape type's emissions, they also fit well therein. In summary, the variability of results of this pan-Arctic survey indicates that methane budgets within all these places are influenced by different conditions in terms of climate, hydrology and carbon pools. Accordingly, the good agreement of the modelled values with these references confirms that the results are within a plausible range at the greater picture, but a detailed evaluation cannot be performed without in-depth analysis of the site-level conditions.

4.1.4   Suggested improvements

Regarding the general structure of the JSBACH model, other parts of the land
surface scheme require advancements before its application with the methane mod-
ule at a global scale and over long time periods can be suggested. For example,
soil organic matter should be represented as vertically resolved (Braakhekke et
al., 2011, 2014; Koven et al., 2015; Beer, 2016), with different soil carbon pools
and a moisture-dependent decomposition. Furthermore, the site hydrology should
include soil moisture contents above field capacity and standing water above the
surface (Stacke and Hagemann, 2012). The author is also aware, however, that
it is not the best approach to calculate an empirical water table depth follow-
ing Stieglitz et al. (1997) under unsaturated soil water conditions. Together with
the water table depth, the soil moisture content itself is of great importance to
the presented methane module. Still, with this model version, the importance
of different processes, their interplay and the influence of climatic or hydrologic
drivers can be studied at site level, which is a major step forward. Furthermore,
this process-based implementation can be applied at other sites or with another
hydrology, and still, the methane-related processes will only depend on the soil
conditions.

In order to improve the hydrological scheme of the current model version, it would
be desirable to use other approaches like TOPMODEL (e.g. Kleinen et al., 2012)
that would allow one to represent the fraction of the inundated area in a model
grid cell based on the topography profile. This would provide a modelled wetland
extent and a representation of the water table depth in saturated soils, especially
for large-scale applications. This step has been considered and will be included
in future model iterations. Despite being a complex process model, the interplay
of the processes is consistent. Thus, the influence of climate and hydrology on
methane fluxes can be studied in detail. Knowing the dominating processes and
environmental conditions provides useful information about the complex behaviour
of the methane dynamics in permafrost soils. To summarise, a lot of information
can be gained from using this model that may all help understand the complex

network of drivers, influencing factors and constraints that govern the methane balance in periglacial landscapes.

4.2   Regional future climate experiments

4.2.1   General discussion about this study

To predict future methane fluxes at the larger area of the Lena River Delta, regional future climate experiments have been carried out. These experiments were also done in order to show the applicability of the further developed land surface scheme JSBACH, including the enhanced methane module, to a wider range of input parameter constellations as well as their combined performance as another step towards the global application. Still, and even more for this model version, the statement holds true, that all interpretation and discussion of findings about or with the new methane module should consider its tight integration and undeniable dependence, if not limitation, on the concepts and possibilities of the framework of the JSBACH model. In the context of the uncertainty of model parameters, the overall values of methane compared to carbon dioxide emissions from the soil may be looked at with care.

The altered JSBACH version includes changes in the hydrological scheme and in the carbon decomposition. The methane module incorporates an additional transport process, the diffusion of gases through snow. The order of the transport processes has been adjusted, as well as the methane production and the plant transport. Like the processes of the previous methane module, also the updated ones are highly dependent on the soil moisture regime, the soil temperature and the carbon decomposition.

Because of special properties of the new TOPMODEL hydrology, it influences the methane emissions differently than the old hydrology did. Not the changing soil moisture in the soil column may change the behaviour of the methane-related processes, but rather the changing size of the inundated area of a grid cell in prin-

ciple determines the share between oxic and anoxic decomposition processes, thus methane or carbon dioxide production. If an area of a grid cell is inundated, the relative moisture content of the ice-free pores is always and over the whole column 95 % and methane can be produced in the whole column. If, on the other hand, an area of a grid cell is not inundated, the whole column is seen as oxic and no methane will be produced at all.

The fixed setting of 95 % pore moisture has also the consequence, that the physical conditions of JSBACH that are used by the methane module are not coupled anymore among each other. The inundated fraction, the fixed pore moisture content and consequently also the soil moisture content do not have a connection or feedback to the soil temperature and the soil ice content. One can only understand this setting in the light of the difficulties of modelling complex hydrologies. While the old hydrology caused large problems like discussed earlier in the context of the site-level study, integrating the TOPMODEL approach into JSBACH solved these problems but also induced new ones. TOPMODEL is not a process-based model for the soil moisture status. Still, it has the advantage of providing inundated areas, although to the cost of less process-based, more decoupled soil physics. It is clear, that this is an issue that should be addressed as soon as possible. A process-based methane module can only show its full qualities, if the underlying soil physics is at least not contradicting itself but at the best also process-based.

Another consequence of the fixed pore moisture is, that the former distinction between an oxic stratum above the current water table, a currently anoxic stratum below the current water and a permanently anoxic stratum below the minimal water table as well as its consequences for carbon decomposition is not valid anymore. Moreover, only mineral soil is considered and such complex landscape features like a polygonal microstructure cannot be represented with this model.

Despite these shortcomings, the new hydrological scheme is still of great benefit for the effectiveness of the methane processes, because it allows for soil conditions,

that are much closer to the real situation in the environment under consideration, than what was possible with the previous model version's hydrology. Of course, it would be best, to enable a combination of both, a description of the vertically explicit soil moisture distribution and at the same time a model of the spatial distribution of the inundated area. Even further, soil moisture contents above field capacity and the height of the water table above the surface, thus standing water, could be beneficial for the methane processes if they would be available via a process-based model part.

The spin-up procedure, despite summing up to 10 900 years of model spin-up, only uses input data from the years 1951 to 1980, because no preindustrial dataset was available. Still, the carbon pools are in equilibrium after that, starting with year 1951, and the results can be analysed from thereon. Thus, despite the model results do not contain preindustrial information, still the historic period from 1951 to 2004 can serve as basis of comparison for the RCP scenarios in the future period from 2005 to 2099.

In the historic period, the input data show signs of an unusual moist phase starting around the year 1960 and ending with an unusual drop to drier conditions around the year 2000. This translates into unusual wet years starting around 1960 and ending around 2000 in the model as well. The time frame of this dataset is not long enough to identify a proper mean case. But it can be seen, that the deviations from the trend within this time horizon are quite large, larger for the modelled physical soil conditions than for the climate input even. This of course also translates into variations in the soil respiration fluxes. Particularly, the methane emissions vary substantially, after the wetter phase changed into the drier phase in the end of the historic period. This is logical, because only in the inundated fraction of a grid cell, the methane module is active in this model version and can thus produce methane. The subsequent future period with the three RCP scenarios thus takes over at a relatively low level of both, inundation and methane emissions.

The used input data for the RCP scenarios were harmonised with the historic dataset. However, the restart procedure that has been applied for the model is currently under review. According to ongoing investigations, it would be necessary, to equilibrate the model again after the restart during about 7 years, to overcome possibly induced steps directly after the restart. Still, these steps, if they could be shown, were much smaller than the here presented variations in the model hydrology 5 years before the restart. On the other hand, it has been found, that this JSBACH version has not undergone the virtual mandatory restart reproducibility exercises. So, it might also be possible, that if these tests would have been done properly, this issue would not have risen at all. Anyway, by using either the whole data of the future period aggregated or by even using only the last 10 years, this issue may not influence the results presented here in a relevant quantity.

4.2.2   Discussion about specific assumptions

The author is aware, that it was not ideal to have set the fraction of anoxic decomposed carbon that becomes methane to 0.1. However, the JSBACH framework was updated and the interplay of the new hydrology and carbon decomposition with the methane processes was taken care of in a global framework. Thus, it was agreed at first, to keep this parameter for this study at that value, but to discuss this practice here. While a value of 0.5 was used as a process-based choice in a process-based methane module that was depending on a not very suitable hydrology and a relatively coarse carbon decomposition before, the new value has been used in order to balance the further developed hydrology and the more detailed carbon decomposition with the methane processes. The result of the interplay of these processes was too much methane compared to carbon dioxide emission from the soil. So, the easiest way for the global approach seemed to be to down-regulate artificially the methane production by changing this parameter. However, in the regional approach in ongoing investigations, it could be shown, that the main reason for too high methane emissions was the too high inundated fraction instead of an unbalance between methane and carbon dioxide in the anoxic carbon decomposition.

However, if instead of as a tuning parameter, this fraction would have been used as the process-based parameter with its original value, much more produced methane would have been to be expected. Of course, the overall emissions in respect of emitted carbon would not have changed, but in respect of carbon dioxide equivalent, it would have had an effect. In the site-level study, the parameter sensitivity study showed, that the overall methane emissions varied more than linearly with the variation of this parameter ($\pm 12\,\%$ methane, if $\pm 10\,\%$ fracCh4Anox; see Table 3.2). If this behaviour would be extrapolated from the tested $10\,\%$ change (0.45 and 0.55 instead of 0.5) in the previous model version to a change from 0.1 to 0.5 in the new model version, which would be a parameter value change of $500\,\%$, than the methane emissions could be expected to be about 5 times more or 6 times as much as presented here. However, in this argumentation, one should keep in mind, that not this parameter alone is responsible for the amount of produced methane. If set back to the original value, at the same time, it would be mandatory to adjust the parameters of the TOPMODEL module in such a way, that the inundated area fits the values found by measurements. Then, like ongoing investigations show, the original values of 0.5 works fine again. But this may also point to the speculation, that the inundated area, that was calculated with this model version for the Lena River Delta, may be overestimated 6 times, despite the fact, that the model was said to be adjusted to global applications.

On the other hand, this parameter is only for the division between methane and carbon dioxide from the decomposed soil carbon. It is not the overall division between the corresponding emission fluxes of the two gases, because there are two oxidation pathways in between, that may reduce the emitted methane further. Thus, if Knoblauch et al. (2015) find lower values for the overall remaining methane fraction in their measurements, this difference in meaning should be taken into account. Still, with using this parameter as tuning parameter in order to compensate too high methane emission because of an overestimated inundated fraction in a global set-up, maybe it can be understood, why this was done. However, the better way would have been, to correct the inundated fraction directly,

which would have reduced the amount of produced methane automatically, and thus the original value of 0.5 could have been restored. Ongoing investigations are doing exactly this.

The newly integrated soil carbon module YASSO provides the decomposed soil carbon only in two category values instead of three over depth. This already leads to a change in the methane production. But additionally, for calculating the decomposed soil carbon, YASSO does not take soil temperature or moisture into account. Instead, it uses 15 day means of air temperature and precipitation. The advantage of YASSO is, that it calculates the anoxic carbon decomposition in the inundated fraction on a grid cell in a more sophisticated way. This was also the reason for integrating it into JSBACH, despite the former carbon decomposition already used soil temperature and moisture. But the drawback is now, that YASSO does not see permafrost conditions. This is not ideal, because in summer, air temperatures rise in every year above $0\,°C$. Thus, the carbon of the whole soil column can be decomposed, no matter if it is actually frozen or not. If the aim is to model methane in permafrost regions and if YASSO delivers the carbon for the methane production, this has definitively to be addressed.

The order of the transport processes proved to have an influence on their share of the total methane emissions with the new model version, despite none was found with the previous one. This might well be due to the hydrological shortcomings in the old model version, that was that dry that ebullition might not have been able to take advantage of it being the first process in place. However, ebullition as a physical based process will remove all excess methane from the soil pores and leave nothing for plant transport, if it is allowed to take place before it. Thus, plant transport should be allowed before ebullition takes place. Even more advanced would be solutions to allow for parallel execution of all relevant transport processes, but ideas how to balance the processes among each other still need to be found.

On the other hand, under the given soil moisture conditions, diffusion only plays a minor role, which is also different from the situation for the site-level study. There, drier conditions allowed diffusion to take a substantial share of the total emissions. Under wet conditions, this is not the case, and the new model version only takes such wet conditions into account. Thus, improvements of the hydrology should be in the direction of enabling detailed soil moisture profiles again, because soil moisture is critical for all methane processes and imbalances might easily arise from ignoring that.

The updated hydrology showed some shortcomings of the plant transport, that were enhanced in the new model version. Now, a more realistic description is used in the sense that the root surface is now coupled to the soil depth. But still, the surface area of the root surface of gas transporting plants is highly uncertain. On the other hand, the newly introduced physical restriction of the plant transport at least takes care for unrealistic high values. Still, freezing of the soil and staying frozen over a particular time span kills plant roots and should thus reduce the available root surface again. This is another suggestion for further improvements. Moreover, the plant transport until now will be stopped as soon as at least 5 cm of snow is on the ground. Of course then, diffusion through snow comes into play. But it would be better, to couple this switch to the vegetation height in respect to the snow height. Then of course, the vegetation height would need to be not just the vegetation height of a grid cell, but the height of the gas transporting plants would be needed to know instead of the overall vegetation height. Furthermore, the concept, that lead to the decision to follow the 5 cm rule, was, that drifting snow would crinkle the culms anyway, so that plant transport would be prohibited by that.

The newly introduced diffusion through snow until now uses the diffusion coefficients calculated from the soil temperature and pressure in the first soil layer. It would be much better to use the diffusion coefficients instead, that are calculated from temperature and pressure in the middle of the snow. But those were not

available yet. Furthermore, when calculating the pressure in the soil, the snow in turn should be accounted for. These improvements have to be done as soon as possible, to assure a representation of the diffusion through snow that is similarly based on physics and as process-based as the other methane processes of the presented module.

4.2.3   Comparison to published data

The regional future climate experiments have been done for an area around the Lena River Delta, spanning from 71 ° to 74 ° N as well as from 123 ° to 130 ° E. Modelling such large regions makes it almost impossible to compare appropriately to measurement data. It would either need a dense network of measurement stations, which is unrealistic for such large and remote regions, or such a big tower like ZOTTO (e.g. Heimann et al., 2014). But even if there was such a facility near Lena River Delta, still, it would not be trivial to compare its data to the model results. Still, there is ongoing work trying to provide top-down estimates for this region. The results will surely be available in near future, but not within the time frame of this study. If in contrast, a lot of site-level studies could be done, in principle it would be possible to compare point measurements with model results, but this has its own difficulties like pointed out before. Still, much more detailed information would be available. However, this does not help for the bigger picture, because the number of site-level studies needed to cover the whole spectrum of possibilities is itself an unknown number. Thus, the maybe best solution would be intermediate towers in a coarse grid.

This study found, that the amount of methane accounts only for less than 1 % of the soil respiration flux in the historic as well as the future period with every tested RCP scenario. Schuur et al. (2015) provided an estimate, that 2.3 % of the total emissions from permafrost soils would be methane, to which the presented results are comparable. Furthermore, compared to the historic period until 2004, this study found, that the methane flux to the atmosphere increases for RCP 2.6 by 16 %, for RCP 4.5 by 23 % and for RCP 8.5 by 31 % until 2099. Koven et al. (2015)

give values of 7% for RCP 4.5 and 35% for RCP 8.5 in the last decade of the 21st century compared to 2010. Again, the results presented here seem comparable to that. In the study presented here, monthly average methane emissions for the current period (1995 – 2004) of 9.01, 17.4, 16.2 and 11.1 mgCH$_4$ m^{-2} d^{-1} for June, July, August and September have been found. These values are a bit lower than the values reported by Sachs et al. (2008) (17.1, 18.3, 20.6 and 18.2 mgCH$_4$ m^{-2} d^{-1} for the same months in 2006) and Wille et al. (2008) (15.7, 22.3 and 15.2 mgCH$_4$ m^{-2} d^{-1} for July, August and September in 2003 to 2004). However, while those data are eddy covariance measurements from a 4 m tower, the here presented values are averages over the whole study region.

Table 4.3: Summary of the seasonal fractionation of the methane emissions.

	Hist 1951 – 2004	RCP 2.6 2005 – 2099	RCP 4.5 2005 – 2099	RCP 8.5 2005 – 2099
Zero	10.0 [2.7 – 24.0]	7.7 [3.0 – 17.1]	7.5 [3.0 – 20.5]	6.8 [1.5 – 21.0]
Cold	14.8 [6.2 – 27.6]	10.4 [2.7 – 19.2]	10.2 [3.2 – 20.3]	9.3 [2.8 – 20.9]
Warm	75.2 [49.2 – 87.2]	81.9 [65.4 – 92.7]	82.3 [61.4 – 92.4]	83.9 [61.0 – 93.8]

Modelled seasonal fractionation of the methane emissions in %, rounded to one non-zero digit. Given are the mean values over the 48 grid cells with non-zero methane emissions (compare Fig. 3.8) and over all years in the respective time frame or scenario with minima and maxima in brackets. Zero means, that the temperature of the first soil layer is between -0.75 and 0.75 °C, while for Cold this temperature is lower and for Warm higher than this range.

The soil physics of the used JSBACH version does not show much time with freezing from the top (Fig. B.11), still there are methane emissions from the soil at times, when the first soil layer is frozen. To investigate the share of the zero curtain and cold season emissions in the modelled annual methane budget, a statistic has been calculated (Table 4.3). This suggests, that in later times or with increasing scenario, the share of the methane emissions during the zero curtain as well as in the cold season gets reduced, in favour of the warm season, as one would expect

under a warming climate. However, compared to measurement data, the share of
the modelled cold season emissions in the annual methane budget is less than a
third of that reported by Zona et al. (2016). For the zero curtain, it is still just
half of the reported value. Although it has to be stated, that Zona et al. (2016)
considered only the zero curtain period in autumn for their given value. And they
measured in Alaska instead of in Siberia, while the measurement time spanned
over 20 months compared to the long time frame of more than 100 modelled years
in the work presented here.

4.2.4 Suggested improvements

The detailed analyses of the soil respiration and methane process fluxes show the
relevance of the methane compared to the carbon dioxide emissions from the soil.
The analysis of their spatial distribution leads to insights into the pattern of re-
gions with favourable conditions for methane emissions. The changes with time
give an impression about the increase of the gas fluxes due to a changing but
predefined climate under the given hydrological scheme, and the analysis of the
seasonal behaviour shows the broadening of the emission season length due to the
same. The potential of the model to show all this is a major step forward to-
wards global process-based methane modelling. For example with the maps, the
relevance of the single processes can be carved out really well, and this is only pos-
sible with a process-based model that describes each of these processes realistically.

All the shown effects and patterns might give an impression about how the meth-
ane emissions might react to continued climate change. However, missing processes
in the model, coarse simplifications or even wrong assumptions may still change
these results. Moreover, developable connections among other model components
that are highly relevant for methane processes also hold the potential to alter the
findings. The focus should therefore not be on the numbers, not even on the
numbers of change, but more on the tendency, the direction and the strength of
the effects or the relation of patterns in the emissions with patterns in natural
landscapes. These can be treated as rather reliable, while the absolute numbers

should be treated as unconfident and e.g. the input still has to be stated to be often speculative, at least with limited confidence.

Other processes and features highly relevant for periglacial landscapes, including cryoturbation, thermokarst, permafrost carbon or peat accumulation, are still missing in this model version. Cryoturbation is the vertical but also horizontal mixing of soil in permafrost areas due to freezing and thawing processes. Thus, organic matter from the topsoil can be transported down into deeper layers, buried and frozen. Only warming climate, thus thawing of these layers, would make this cryoturbated organic matter available for decomposition. Thermokarst denotes the formation, development and drainage of lakes because of thawing ground ice in permafrost areas. These lakes act as heat reservoirs for the area beneath and aside them. They can thus prohibit the freezing by keeping the temperatures longer above $0\,°C$. This will exhibit the organic matter contained in the unfrozen soil parts longer to decomposition, that would have been unavailable when frozen.

Permafrost carbon is soil organic matter, that was frozen in permafrost soils for long time and gets available for decomposition under warming climatic conditions. Thus a feedback might establish, if warming induces thawing, which causes decomposition, which leads to more warming. Peat, finally, is the accumulation of partially decomposed organic matter because of wet hydrological soil conditions, that provide anoxic conditions under which decomposition is slowed down substantially. Peat soils have different characteristics, such as higher porosity, very high contents of organic matter, but also better water holding capacity, higher heat capacity and low nutrient availability. All these properties are of importance for biological life, thus also for methane processes in the end. Consequently, all these processes should be included in models that shall simulate realistic methane emissions also in periglacial landscapes.

What makes models useful, is their ability to disentangle the complexity of interactions that may arise in a network of interconnected processes. Despite known

and understood individual processes, it may not be possible without models to overlook their interplay in the whole network. Moreover, still there might be details in the individual processes, that have been overlooked, ignored or remained unknown, but that are crucial for the ecosystem to function correctly. Thus, the resulting simulation may diverge even more from an approximation of the truth and thus show, what is important to look at next. Consequently, this knowledge about the deviations can be used to investigate the reasons for them occurring and find details to consider as critically important.

In the case of process-based modelling of the methane balance in periglacial landscapes, some of the connections and interactions of the single processes are for example the several methane transport processes that all use the same source of methane in the soil and happen in parallel if the conditions allow for it. What determines, which process will transport which share of the available methane? And if the processes differ in their allowance of methane oxidation, how does this influence the share of emitted methane per process? In the end, how will the overall methane emissions be influenced by changes that do not consider just one single process? These kind of questions should be able to be addressed with the presented model. Still it is known that other single processes that are linked to methane processes, or even just properties of already modelled processes, are not or not well represented in the current model version. Thus, by finding possibilities for comparisons to field measurements and by implementing additional processes and features, it should be possible to point out the important missing parts or the spots of mismatch for the gain of improved process understanding. When using the provided model as it is, still the interactions in the network of the implemented processes can be studied in detail. The overall emissions can be compared under varying conditions or split into their individual processes' share. With the production, two oxidation processes, four methane and three oxygen transport processes, this is already quite complex. Several main driving factors, like soil moisture and ice content, soil temperature, snow cover, inundated fraction, water table position and the amount of decomposed carbon, increase this complexity greatly.

With the new model version, the relevance of the methane fluxes compared to the carbon dioxide emissions from the soil could be shown. The patterns of regions with favourable conditions for methane emissions as well as the increase of the gas fluxes and the broadening of the emission season length due to a changing climate could be demonstrated. Furthermore, this implementation can be applied in other regions, without the need to change its structure or model code. Relevant parameters are available via a namelist and can thus easily be modified. Still, the interplay of the methane processes among each other and with their environmental driving processes, like hydrology or carbon decomposition, is consistent. But it is a complex process model with various possibilities to apply and to improve. The influence of the climate, the hydrology and grid cell specific conditions on the soil respiration and the methane process fluxes can be studied with this model version also for larger regions. The gained knowledge about the overall behaviour of the complex methane dynamics in permafrost soils enables also a better understanding of the most likely changes in a warming world. Summarising, to apply this model provides a lot of possibilities to learn about the complex network of drivers, influencing factors and constraints that govern the methane balance in periglacial landscapes also at regional scales and in a warming world. It can thus be coupled to an atmospheric model in future research projects to study the contribution of methane to the carbon cycle – climate feedback mechanisms.

Chapter 5

Summary, conclusions and outlook

5.1 Regional patterns and future projections

The aim of this work was to gain insights into the complex behaviour and various interactions of the methane-related processes in the soil with an additional focus on periglacial landscapes. The differences between the several methane-related processes, their seasonal differences as well as differences between the rim and centre microsites have been shown in a site-level study (Sect. 3.1). The complex flux patterns that each of the different methane processes exhibits, where each process follows its own drivers, were described in detail. The annual budget of the methane emissions calculated within this study is $262 \, \mathrm{mgC \, m^{-2} \, a^{-1}}$ in a mixed approach of 65% rim plus 35% centre, where on the rim a value of $86.3 \, \mathrm{mgC \, m^{-2} \, a^{-1}}$ and at the centre a value of $587 \, \mathrm{mgC \, m^{-2} \, a^{-1}}$ have been calculated. Within this set-up, ebullition is dominating under wet environmental conditions, while diffusion is more prominent under moist conditions. On the other hand, transport through plants is high, when there are a lot of plants growing that are able to transport gases. Consequently, the most influential environmental drivers for the methane emissions are the soil moisture and the soil temperature, the plant growth, physical characteristics like the gas-saturation of the soil water as well as the ice

content of the soil. In a comparison with field measurements, sufficiently good agreements could be demonstrated, despite the module not having been adjusted to site-specific processes or features.

While the regional future climate experiments (Sect. 3.2) showed the applicability of the updated land surface scheme JSBACH, including the enhanced methane module, for a large region in periglacial landscapes, also the differences between the fluxes of soil respiration and methane processes in overall amount, spacial distribution, temporal development and seasonal behaviour have been demonstrated. In the analysis of the regional future climate experiments, various features of the involved processes have been shown. Their correspondence to features of the modelled landscape and the used input of the methane module appears to be promising and realistic.

The regional future climate experiments suggested, that the share of methane in the soil respiration fluxes is about 0.7 to 0.8 % in terms of the amount of emitted soil carbon. However, if the global warming potential of methane is taken into account, depending on the used future scenario and the representation of methane in the change of the soil respiration fluxes, its share in the increase compared to the historic period raises to 4 to 14 %. Furthermore, the seasonal cycle of the methane fluxes shows its maximum in July, earlier than the one of the carbon dioxide emissions from the soil in a mean year of 1995 to 2004, but later than it in a mean year of 1951 to 1960. The start of the main emission season appears to be in the beginning of May, while the end seems to lie in the end of October or in the beginning of November. Despite start and end of the main emission season have been calculated to be earlier for the methane fluxes than for the carbon dioxide emissions from the soil, the season length seems to be also longer for methane than for carbon dioxide. On the other hand, the year to year variations of the methane emissions appear to be quite large, e.g. for 1951 to 2004, deviations from the linear trend of -208 to 181 mgC m^{-2} a^{-1} have been calculated, compared to an annual increase of only 5.46 mgC m^{-2} a^{-1}.

Finally, the calculated consequences of climate change on the methane emissions have been illustrated e.g. for the period of 2005 to 2099 under RCP 8.5 compared to the period of 1951 to 2004. An overall increase of up to 31.2 % has been demonstrated as well as about 70.9 % higher annual increase of the methane emissions. Compared to a mean year of 1995 to 2004, in a mean year of 2090 to 2099 under RCP 8.5, the start of the main emission season appears to be about one month earlier. Likewise, the end of it has been calculated to take place about one month later. Thus, the length of the main emission season seems to increase by 50 days in that scenario.

5.2 Model development

In the course of this work, a more detailed and consistent process-based methane module for a land surface scheme which is also reliable in permafrost ecosystems has been developed. Based on previous work by Wania et al. (2010) and Walter and Heimann (2000), the JSBACH land surface scheme of the MPI-ESM global Earth system model has been enhanced for this purpose. The new methane module of JSBACH-methane represents methane production, oxidation and transport. Methane transport has been represented via ebullition, diffusion and plant transport. Oxygen can be transported via diffusion through soil pores and plant tissue (aerenchyma). Two methane oxidation pathways are explicitly described: one takes the amount of soil oxygen into account and the other explicitly uses oxygen that is available via roots (rhizospheric oxidation).

In the updated version, JSBACH additionally includes the horizontal hydrology module TOPMODEL and the soil carbon module YASSO. The methane module of JSBACH-methane has been incorporated into this version and subsequently further developed by changes in methane-related hydrological conditions, in the methane production, the order of the transport processes and in the plant transport. A new transport pathway, the diffusion of gases through snow, has been added.

The module in this work is also highly integrated with permafrost and wetland processes, e.g. changing pore space in the soil because of freezing and thawing or changing water table depths due to changing soil water content. Also the changes in the methane module work consistently and process-based together with each other and with the updated JSBACH version, so that a detailed, consistent and process-based methane module for a land surface scheme for global applications could be provided with this model version. All methane-related processes therein respond to different environmental conditions in their specific ways. They increase or decrease according to their requirements with e.g. changing soil moisture, temperature, ice content, inundated area or snow cover.

5.3 Relevance of models for permafrost research

Such a methane-advanced land surface scheme can be used to estimate the global methane land fluxes, including for periglacial landscapes. These regions are rich in soil carbon (Hugelius et al., 2014) and show good conditions for methane production (Schneider et al., 2009). However, they are often remote and rather hard to investigate. Thus, process-based modelling can contribute to understanding the role of methane emissions as long as widespread and long-term measurements remain scarce. In addition, the role of methane for future permafrost carbon feedbacks to climate change can be studied. Coupling such a land surface scheme to atmosphere, ocean and ice schemes in an Earth system model will provide the basis for studying methane-related feedback mechanisms to climate change.

Many questions like the ones posed within Sect. 1.6 can be answered with this model. Like demonstrated in Chapter 3, the variety of topics that can be addressed is large. With the model version that was used for the site-level study, it is possible, to discriminate the single methane process fluxes between the soil layers. And, on the other end of the scale, with the version that was used for the regional future climate experiments, area related effects can be studied, that are relevant on scales of several hundreds of kilometres.

The answers to the questions posed within Sect. 1.6 could be provided. In fact, there is a large variety of answered questions. Still, the topics to further investigate with this model are numerous. However, with a further improved hydrology, including e.g. the combined description of vertical and horizontal soil moisture distribution, water-saturated soil conditions and standing water, as well as advanced enhancements in the description of the plant transport and the diffusion through snow, this methane including land surface scheme will gain even more reliability. Additionally, if missing processes that feature periglacial landscapes, like thermokarst, cryoturbation, peat accumulation or the role of permafrost carbon would be integrated, the carbon balance in cold regions can be studied in greater detail and with a better understanding concerning the permafrost – carbon feedback.

Appendix A

Site-level study − add. results

A.1 Modelled physical conditions

A.1.1 Modelled relative soil moisture content

The modelled soil moisture content changes seasonally very much. However, because the soil water content is restricted to field capacity, there is also a limit for the soil moisture content at field capacity. At the rim (Fig. A.1a), the soil moisture increases in the upper soil part in spring but decreases with the ongoing thawing season. In contrast, at the centre (Fig. A.1b), soil moisture increases only slowly in spring, but this increase is ongoing until almost the end of the thawing season. This is due to the larger amount of ice in the soil, which thaws slowly. On the other hand, the higher input of water to the centre than to the rim as soon as there is runoff created at the rim is a continuous additional supply of soil moisture to the centre later in the thawing season. With this, the rim is more moist than the centre in the beginning of the thawing season but drier in the middle and at the end of it (Fig. A.1c). Just in the deeper layers, the rim has a little bit more liquid water during the whole thawing season. In winter, however, the amount of liquid water is negligible both at the rim and at the centre. Thus, differences may only be seen in the timing of changes due to thawing or freezing, which both happen earlier at the rim than at the centre. Consequently, they result in earlier wetting of the rim's soil during spring as well as earlier drying of it during freezing.
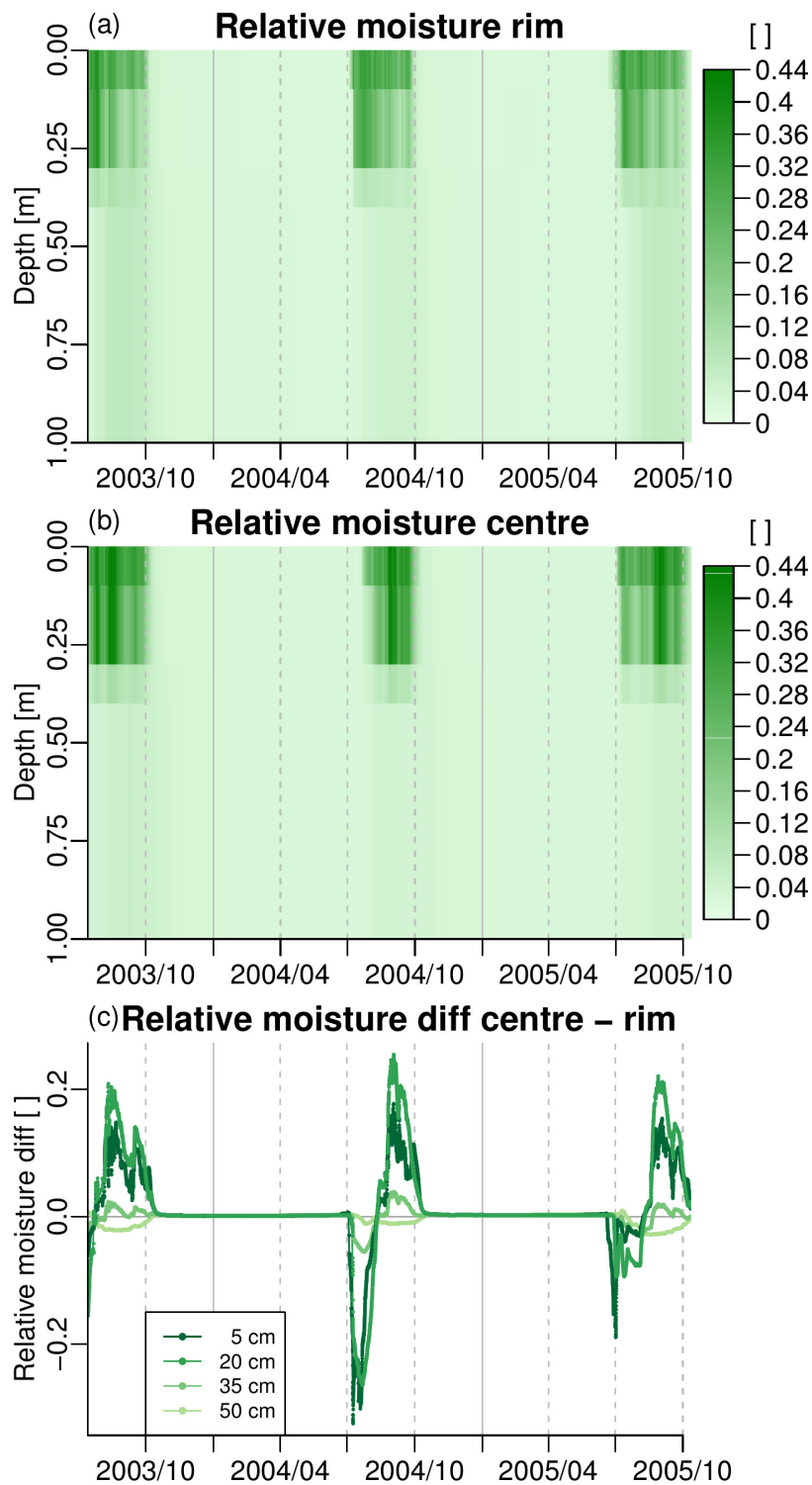
Figure A.1: Modelled relative soil moisture content of the uppermost metre at the **(a)** rim and **(b)** centre as well as **(c)** the difference centre minus rim in several depths as hourly data (points) and daily means (lines). Solid lines indicate 1 January; dashed lines indicate 1 April, 1 July and 1 October of the respective year. The scale maximum for **(a)** and **(b)** is the field capacity, ceiled to two digits.

A.1.2 Modelled relative soil ice content

The modelled soil ice content, in contrast, is almost always higher at the centre than at the rim. Only during freezing in autumn is there a short period when there is more ice in the uppermost soil part at the rim than at the centre. During the thawing season, there is generally very little ice in the upper part of the rim's soil (Fig. A.2a), while at the centre, small amounts of ice may also occur in this period (Fig. A.2b). Both rim and centre show substantial amounts of ice in depths below 30 cm, even during the summer. Furthermore, during spring, while the uppermost part of the soil at the centre is already thawed, an accumulation of new ice takes place right below, which thaws shortly after. In general, the upper soil part gets its ice thawed and frozen more slowly and later at the centre than at the rim because there is more ice at the centre. Below 30 cm depth, the difference in ice content between rim and centre increases in summer (Fig. A.2c). However, this levels off during freezing until it reestablishes at a lower level in winter. In winter, the soil part with the least amount of ice is not on top, but between 10 and 30 cm both at rim and centre.

A.1.3 Modelled soil temperature

The modelled soil temperatures show deeper thawing and higher temperatures during the thawing season at the rim compared to the centre (Fig. A.3a). In addition, rim temperatures reach lower values in winter. Moreover, the thawing season starts earlier and ends later for the rim than for the centre (Fig. A.3b). These effects are due to the generally drier soil at the rim compared to the centre. Water dampens the amplitude of the temperature change, and, in addition, the phase change takes up energy. While the warming to $0\,℃$ occurs quickly, the phase change takes time and the soil can only warm further after the phase change is completed. During freezing, the reverse occurs. The cooling then is faster and to lower temperatures at the rim compared to the centre. In general, deeper layers react more slowly and are dampened compared to layers close to the surface. At the rim as well as at the centre, there are short periods with temperatures below $0\,℃$
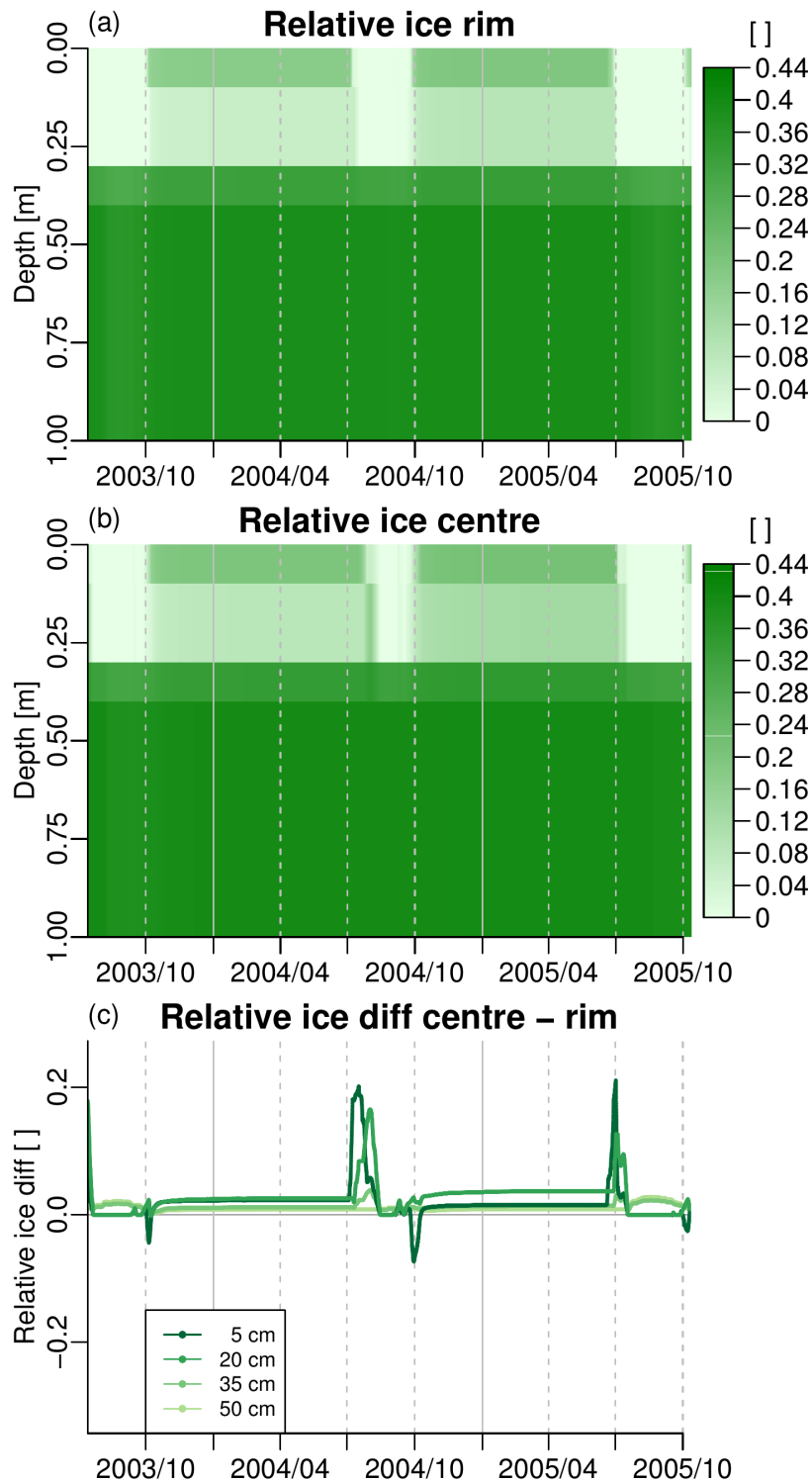
Figure A.2: Modelled relative soil ice content of the uppermost metre at the **(a)** rim and **(b)** centre as well as **(c)** the difference centre minus rim at several depths as hourly data (points) and daily means (lines). Solid lines indicate 1 January; dashed lines indicate 1 April, 1 July and 1 October of the respective year. The scale maximum for **(a)** and **(b)** is the field capacity, ceiled to two digits. The scale for **(c)** is the same as for the difference of the modelled relative soil moisture content.
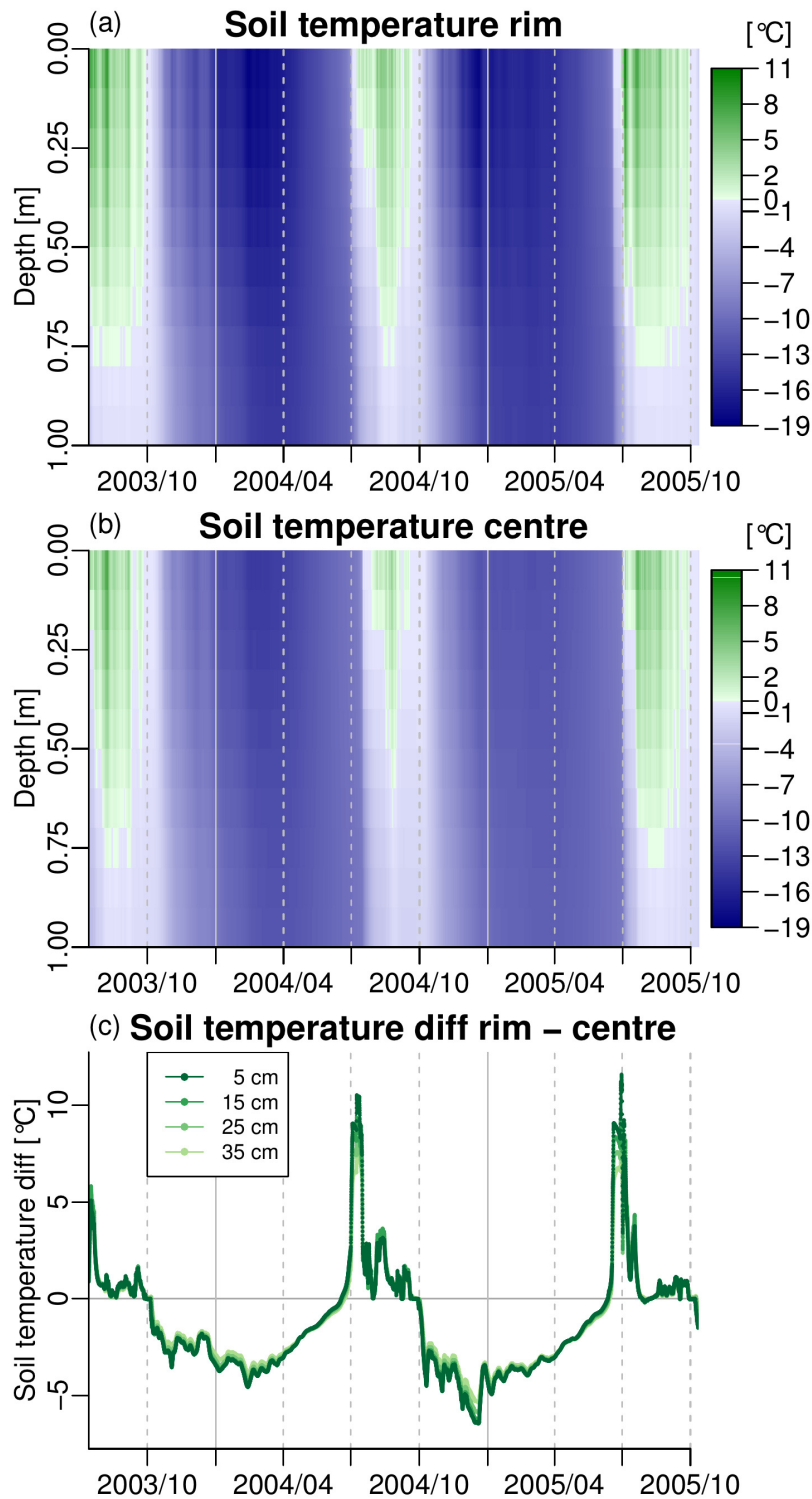
Figure A.3: Modelled soil temperature of the uppermost metre at the **(a)** rim and **(b)** centre as well as **(c)** the difference rim minus centre at several depths as hourly data (points) and daily means (lines). Solid lines indicate 1 January; dashed lines indicate 1 April, 1 July and 1 October of the respective year.

even during summer. The highest temperature differences occur during early spring when there is more ice in the ground at the centre than at the rim. Thus, the rim can reach the zero curtain easier (Fig. A.3c).

A.2 Modelled oxygen uptake

A.2.1 Mixed daily sum

O$_2$ flux mixed daily sum
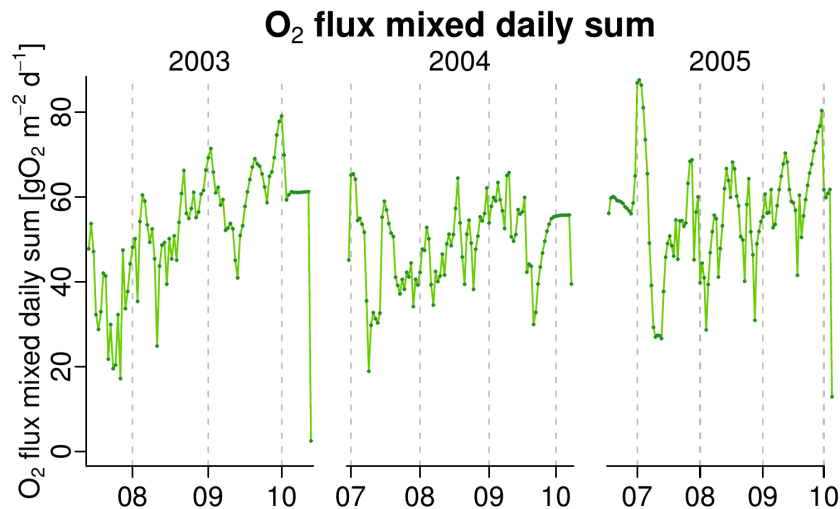
Figure A.4: Modelled oxygen flux into the soil in a mixed approach of 65 % rim plus 35 % centre as the daily sum. X axes and dashed lines indicate the first day of the respective month of the year. Please note the cutouts in between the different years. Only the summer periods are shown, which means less than 5 cm of snow are on the ground. The range of the modelled values for the whole study period is -0.00184 to 87.6 gO$_2$ m^{-2} d^{-1}.

The overall pattern of oxygen uptake shows big portions during the early and late thawing season, with a reduced uptake during the mid season (Fig. A.4). This is the most moist part of the season, and water effectively reduces oxygen diffusion into the soil. There is also some daily variation in the amount of uptake during the thawing season that is connected to the soil moisture content. The wetter the soil, the less oxygen can enter. Because there is high uptake at the beginning and

the end of the thawing season, the overall transport of oxygen is more similar for the rim and the centre, in contrast to methane, where the centre dominates. In winter, no uptake takes place because snow hinders the exchange.
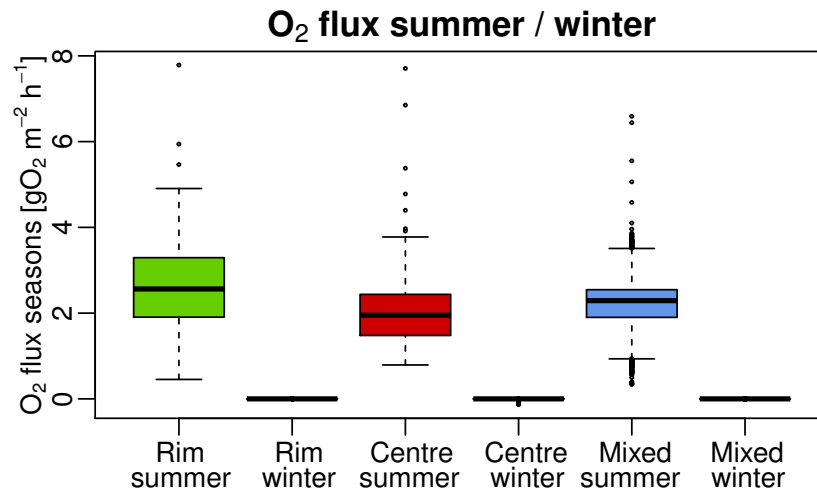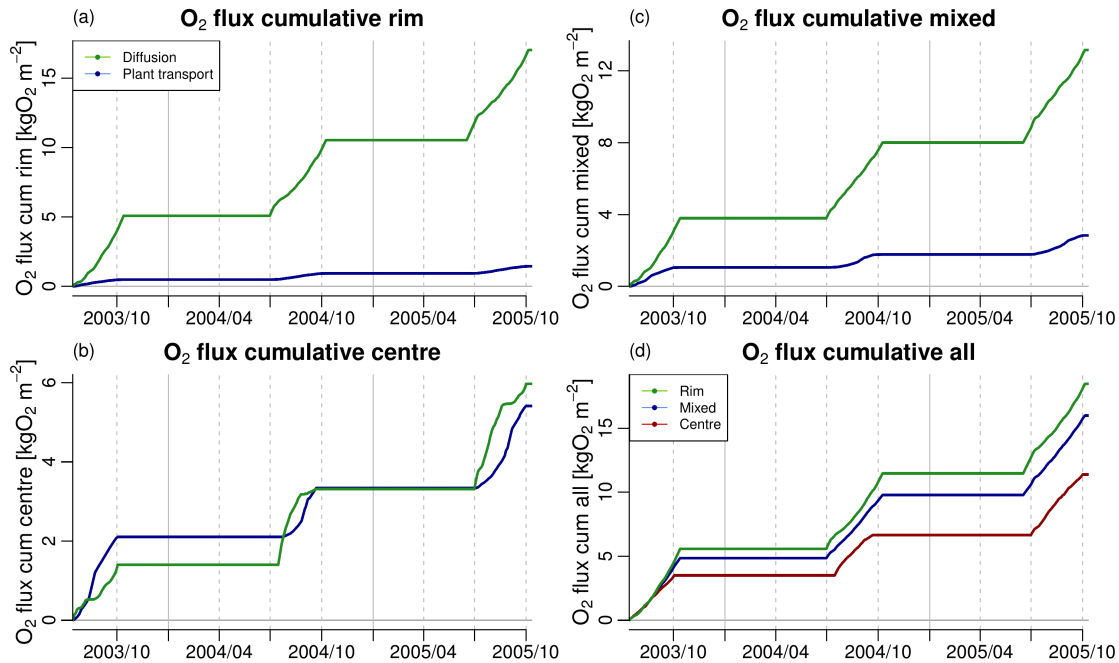
A.2.2 Split into summer and winter flux

Figure A.5: Modelled oxygen flux into the soil at the rim, the centre and a mixed approach of 65 % rim plus 35 % centre, split into summer and winter. Summer means less than 5 cm of snow are on the ground; winter is the remainder. Because of the wide spread of values, to as high as $16.3\,\mathrm{gO_2\,m^{-2}\,h^{-1}}$, a portion of 0.0118 % values was cut to provide a reasonable picture. The minimum of the values is $-0.136\,\mathrm{gO_2\,m^{-2}\,h^{-1}}$.

The modelled oxygen uptake at the rim and at the centre is different for the different seasons (Fig. A.5). In summer, the uptake is purely positive and higher for the rim than for the centre. Also, the spread of uptake is larger for the rim than for the centre. This is again due to the drier conditions that allow more diffusion through air, which is quicker and can thus lead to higher uptake compared to diffusion in water or via plants under the wetter conditions at the centre. In winter, the uptake is zero, following the assumption that snow hinders the exchange. In the mixed approach, the overall mean uptake is about $2.21\,\mathrm{gO_2\,m^{-2}\,h^{-1}}$.

A.2.3   Cumulative sums of oxygen

Figure A.6: Modelled oxygen flux into the soil at **(a)** the rim, **(b)** the centre, **(c)** a mixed approach of 65 % rim plus 35 % centre, split into the different transport processes, and at **(d)** the rim, the centre and a mixed approach of 65 % rim plus 35 % centre combined, as a cumulative sum of hourly data (points) and the daily means (lines). Solid lines indicate 1 January; dashed lines indicate 1 April, 1 July and 1 October of the respective year. Please note the different scales. Table A.1 gives the maximal values.

At the rim, diffusion delivers a much larger portion of oxygen than plant transport (Fig. A.6a). At the centre, both processes provide almost the same amount of oxygen (Fig. A.6b). There are no such pronounced bursts during spring like for methane. While plant transport is smaller than diffusion for both, rim and centre, the difference is much bigger at the rim. At the centre, there is more plant transport but less diffusion than at the rim. Diffusion at the rim and plant transport at the centre are increasing towards the end of the thawing season. In contrast, diffusion at the centre and plant transport at the rim show decreasing contributions towards the end of the thawing season.

In the mixed approach, rim and centre add to a relatively uniform increase in oxygen flux by diffusion over the whole thawing season. For plant transport, the mid season increase is highest, with smaller contributions at the beginning and the end of the thawing season (Fig. A.6c). This results from the different timings of high soil moisture content at the rim and at the centre that compensate each other in case of the diffusion. Furthermore, the wetter the soil, the more plant transport relative to diffusion should occur, because the more water, the more diffusion is slowed down. If, moreover, these conditions occur towards the end of the growing season, which is the case at the centre, the effect is bigger than if this happens in spring, which is the case at the rim. Still, diffusion accounts for a larger proportion of uptake than plant transport because plant transport was defined as being slower than diffusion in water, while diffusion in air is rather quick. It might still be that the plant transport is too low compared to the total uptake because the root surface might have been chosen too small, like the results for the methane emissions suggest. In total, the rim accounts for more oxygen uptake than the centre (Fig. A.6d), but the difference is not as high as for the methane emissions. While the late season is slightly more important at the rim, it is the early season for the centre.

Table A.1: Maximal cumulative oxygen uptake.

	Rim	Centre	Mixed
Diffusion	17.0	5.97	13.2
Plant transport	1.45	5.41	2.84
All	18.5	11.4	16.0

Maximal values of the cumulative sums of modelled oxygen uptake over the modelled time period for rim, centre and a mixed approach of 65 % rim plus 35 % centre for the different transport processes and combined in $kgO_2\,m^{-2}$, rounded to three non-zero digits.

When comparing rim and centre total uptake, diffusion gets reduced to about a third at the centre compared to the rim, and plant transport gets almost 4 times as high (Table A.1). This results in a reduction to less than two-thirds of the overall uptake at the centre compared to the rim. While at the rim, diffusion is almost 12

times as high as plant transport, they are almost at the same level at the centre. These differences are again due to the differences in soil moisture content. In the mixed approach, diffusion accounts for about 4.5 times the uptake of plant transport. Overall, 16 kg of oxygen are taken up by each square metre in the course of the modelled time period.

A.2.4   Split into the different transport processes

Splitting the overall oxygen uptake into the transport processes shows differences in the amount of their contribution per process, depending on location, but also differences in the pattern (Fig. A.7a). The uptake is split into different portions between the processes that are more equal for the centre (Fig. A.7b), but differ a lot for the rim. There, diffusion is responsible for the majority of the uptake. At the centre, this is only true in the early season and at the freezing. In the mid season, plant transport is much higher than diffusion. While the diffusion part is lower at the centre than at the rim, the opposite is the case for plant transport. In spring, large amounts of oxygen are taken up both at the rim and at the centre. In the late season, some small emissions via diffusion also occur at the centre. In general, the uptake through diffusion is higher when the soil is drier, which is the case for the rim in the late season and for the centre in the early season. While plant transport is more steady at the rim, there are pronounced peaks at the centre when the soil is wettest. In spring, when the soil is wettest at the rim, plants are not yet that far developed that plant transport could increase to similarly high values as at the centre during the respective times with high soil moisture content.
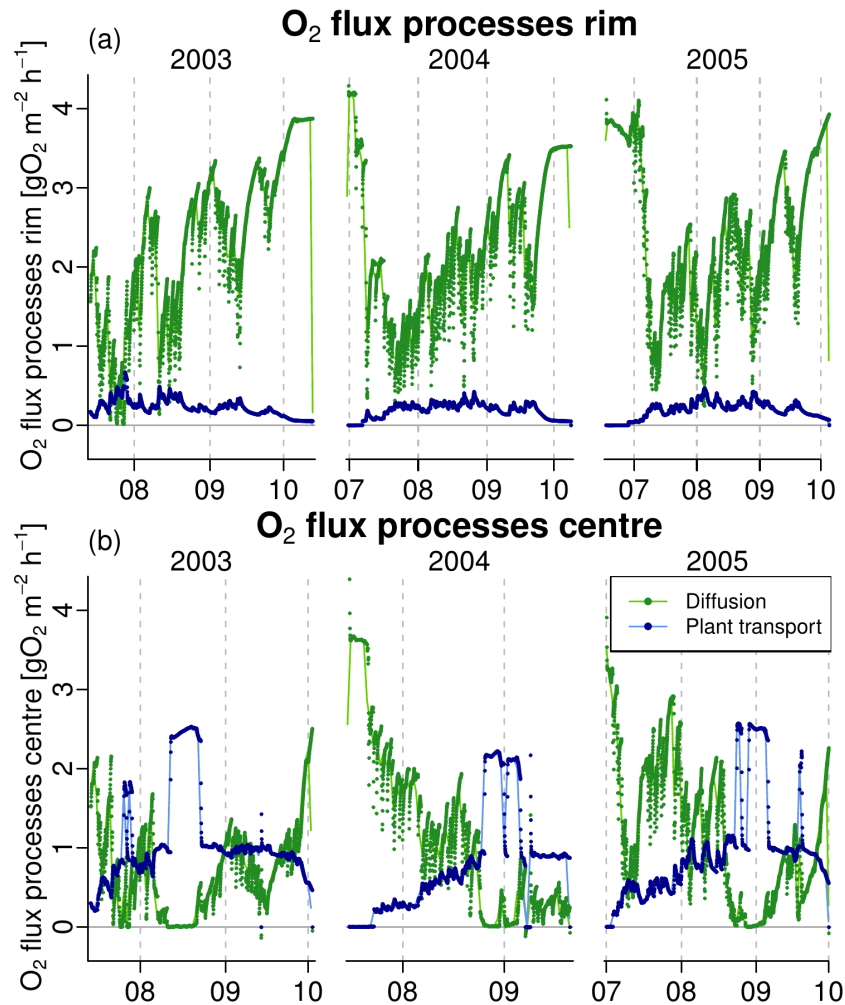
Figure A.7: Modelled oxygen flux into the soil at the **(a)** rim and **(b)** centre as hourly data (points) and daily means (lines), split into the different transport processes. X axes and dashed lines indicate the first day of the respective month of the year. Please note the cutouts in between the different years. Only the summer periods are shown, which means less than 5 cm of snow are on the ground. Because of the wide spread of high hourly values, to as high as 16.3 **(a)** and 14.4 **(b)** $gO_2\,m^{-2}\,h^{-1}$, a portion of 0.0254 % **(a)** and 0.0178 % **(b)** hourly values was cut to provide reasonable pictures. The minima of the hourly values are -0.00185 **(a)** and -0.136 **(b)** $gO_2\,m^{-2}\,h^{-1}$.

Appendix B

Regional future climate experiments – additional results

B.1 Modelled gross soil respiration fluxes

Table B.1: Gross soil respiration fluxes.

[kgC m^{-2} y a^{-1}]	Hist	RCP 2.6	RCP 4.5	RCP 8.5
	$1951 - 2004$	$2005 - 2099$	$2005 - 2099$	$2005 - 2099$
[y a]	$54\,a$	$95\,a$	$95\,a$	$95\,a$
CH$_4$	0.070	0.142	0.151	0.161
CO$_2$	8.150	19.023	19.889	21.901
CO$_2$+CH$_4$	8.220	19.165	20.040	22.062

Cumulative sums of the modelled gross soil respiration fluxes for the historical period and three future scenarios, rounded to three decimal places. The units are kg of C per m^2 and per y years, denoted in the third row.

Table B.2: Share of methane in the gross soil respiration fluxes.

		Hist 1951 – 2004	RCP 2.6 2005 – 2099	RCP 4.5 2005 – 2099	RCP 8.5 2005 – 2099
CH_4	[C]	0.8	0.7	0.8	0.7
ΔCH_4	[C]		0.4	0.5	0.5
ΔCH_4	[CO_2e100a]		4.0	4.9	4.9
ΔCH_4	[CO_2e100aF]		4.8	5.9	5.9
ΔCH_4	[CO_2e20a]		11.1	13.4	13.4
ΔCH_4	[CO_2e20aF]		11.4	13.6	13.7

Share of methane in the modelled gross soil respiration fluxes for the historical period and three future scenarios as well as in the increase compared to the historic period of these fluxes in %, rounded to one decimal place. Shown are the values for the different possibilities of representing methane in the sum.

Table B.3: Share of the processes in the changes of the budget of the methane production flux.

	Hist 1951 – 2004	RCP 2.6 2005 – 2099	RCP 4.5 2005 – 2099	RCP 8.5 2005 – 2099
Oxid	2.06	2.11	2.16	2.36
Plox	0.73	0.75	0.77	0.84
Plant	53.62	48.76	48.77	47.78
Ebul	37.15	41.00	40.97	41.36
Diff	0.02	0.03	0.03	0.03
Snow	6.44	7.37	7.32	7.65
AllTrans	97.23	97.16	97.09	96.82

Share of the processes in the changes of the budget of the modelled methane production flux for the historical period and three future scenarios in %, rounded to two decimal places. For the meaning of the short names, see Sect. 3.2.

Table B.4: Increase compared to the historic period of the methane process fluxes.

	RCP 2.6	RCP 4.5	RCP 8.5
	2005 − 2099	2005 − 2099	2005 − 2099
Prod	15.7	23.0	31.8
Oxid	18.4	28.7	50.7
Plox	19.3	30.4	51.4
Plant	5.3	11.9	17.4
Ebul	27.7	35.6	46.7
Diff	32.1	40.9	53.8
Snow	32.5	39.8	56.5
AllTrans	15.7	22.8	31.2

Increase compared to the historic period of the changes in the budget of the modelled methane process fluxes for three future scenarios in %, rounded to one decimal place. For the meaning of the short names, see Sect. 3.2.

B.2   Spatial distribution of the soil respiration

Table B.5: Spread of the grid cell soil respiration fluxes.

	Hist	Curr	RCP 2.6	RCP 4.5	RCP 8.5
	1951 − 1960	1995 − 2004	2090 − 2099	2090 − 2099	2090 − 2099
CO_2	229	242	265	295	361
CO_2+CH_4	227	241	264	294	357

Spread, thus maxima compared to minima, of the modelled grid cell soil respiration fluxes for a mean year of 10 years periods of the historic, the current and three future scenarios in %, rounded to integer.

Table B.6: Increase compared to the historic period of the minima of the grid cell soil respiration fluxes.

	Curr $1995 - 2004$	RCP 2.6 $2090 - 2099$	RCP 4.5 $2090 - 2099$	RCP 8.5 $2090 - 2099$
CO_2	16.1	29.1	30.4	45.7
CO_2+CH_4	16.0	28.8	30.2	45.6

Increase compared to the historic period of the minima of the modelled grid cell soil respiration fluxes for a mean year of 10 years periods of the current and three future scenarios in %, rounded to one decimal place.

Table B.7: Increase compared to the historic period of the maxima of the grid cell soil respiration fluxes.

	Curr $1995 - 2004$	RCP 2.6 $2090 - 2099$	RCP 4.5 $2090 - 2099$	RCP 8.5 $2090 - 2099$
CH_4	17.6	45.1	60.6	87.3
CO_2	22.7	49.5	68.0	129.1
CO_2+CH_4	22.7	49.7	68.3	128.8

Increase compared to the historic period of the maxima of the modelled grid cell soil respiration fluxes for a mean year of 10 years periods of the current and three future scenarios in %, rounded to one decimal place.
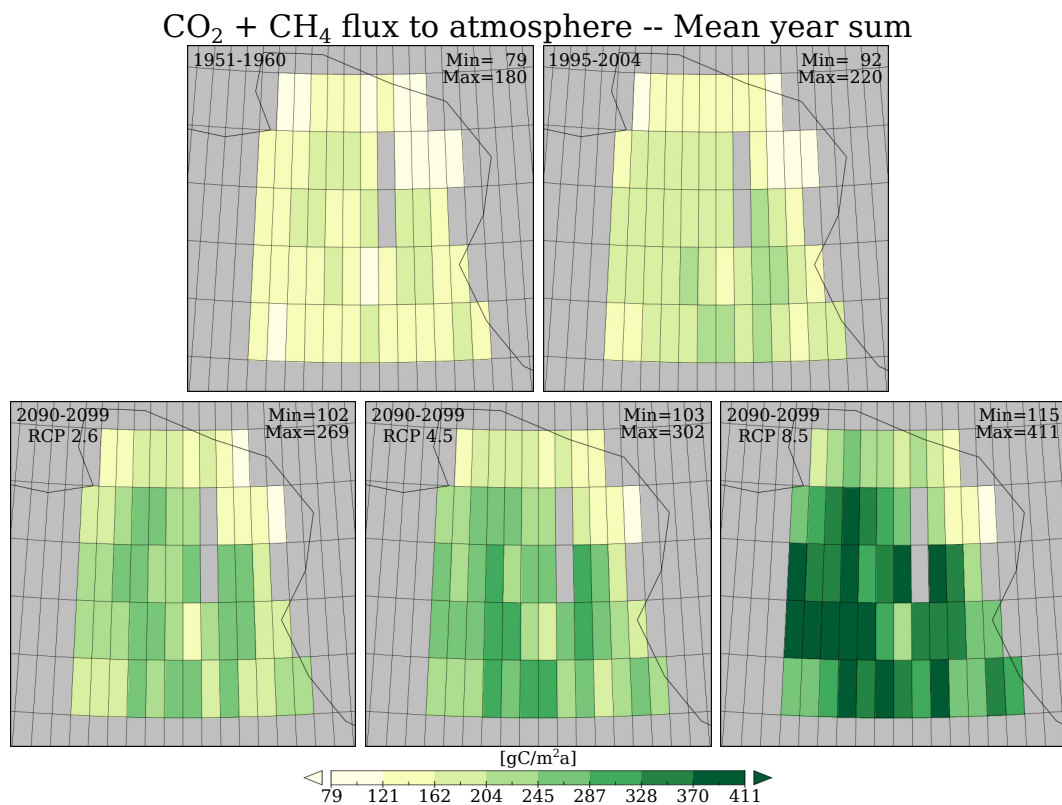
Figure B.1: Modelled soil respiration flux as mean year sum over 10 years periods in gC m^{-2} a^{-1}. Please note the details at the top of every subfigure.

Soil ice content column total -- Time mean
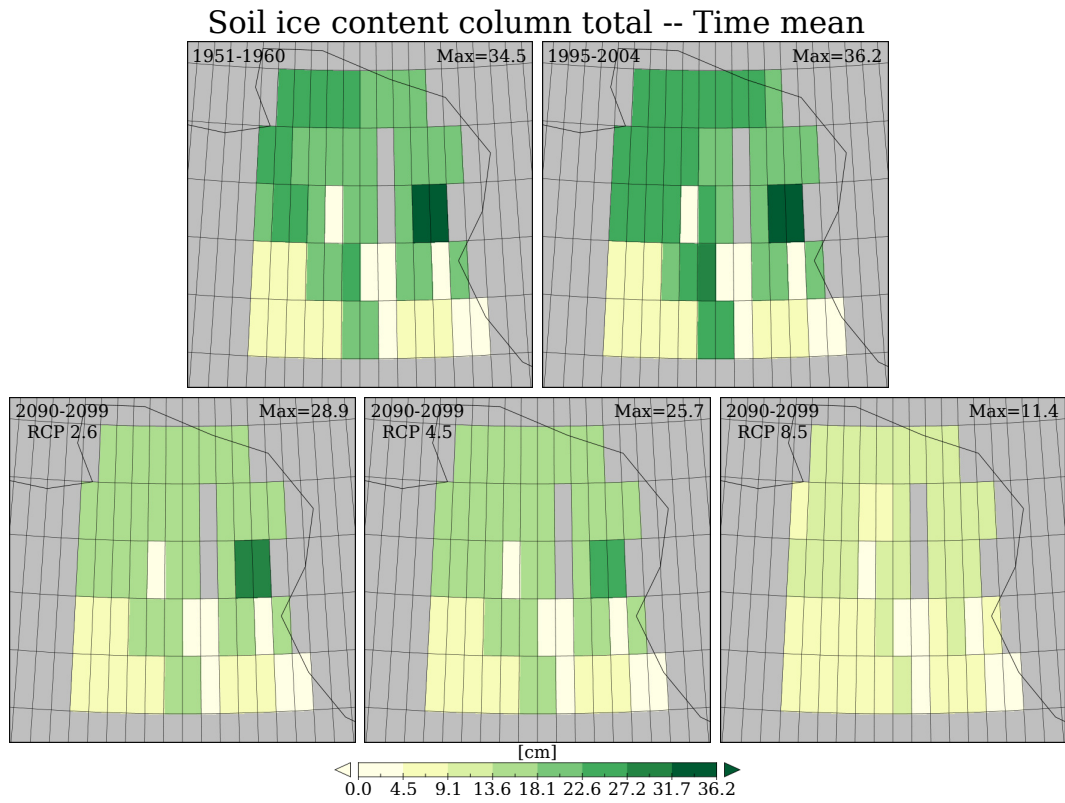
Figure B.2: Modelled soil ice content as sum over the soil column and mean over 10 years periods in cm. Please note the details at the top of every subfigure.
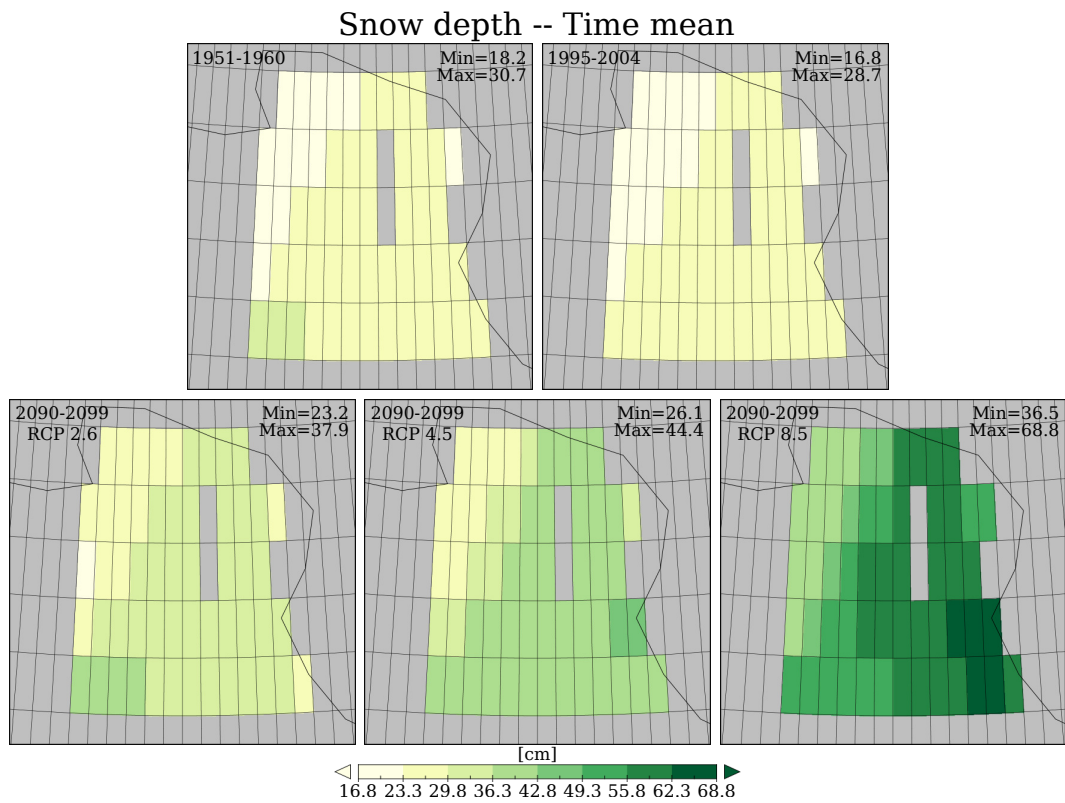
Snow depth -- Time mean

Figure B.3: Modelled snow depth as mean over 10 years periods in cm. Please note the details at the top of every subfigure.

B.3　Spatial distribution of the methane fluxes

Table B.8: Increase compared to the historic period of the maxima of the grid cell
methane process fluxes.

	Curr 1995 – 2004	RCP 2.6 2090 – 2099	RCP 4.5 2090 – 2099	RCP 8.5 2090 – 2099
Prod	15.6	42.7	58.2	85.3
Oxid	15.2	21.0	44.8	121.5
Plox	16.4	20.6	44.6	120.9
Plant	13.6	0.7	11.6	38.4
Ebul	25.1	57.8	79.5	111.6
Diff	26.0	61.9	85.2	122.9
Snow	-15.5	25.1	10.8	86.1
AllTrans	17.6	45.1	60.6	87.3

Increase compared to the historic period of the maxima of the modelled grid cell methane
process fluxes for a mean year of 10 years periods of the current and three future scenarios
in %, rounded to one decimal place. For the meaning of the short names, see Sect. 3.2.

CH₄ oxidation flux -- Mean year sum
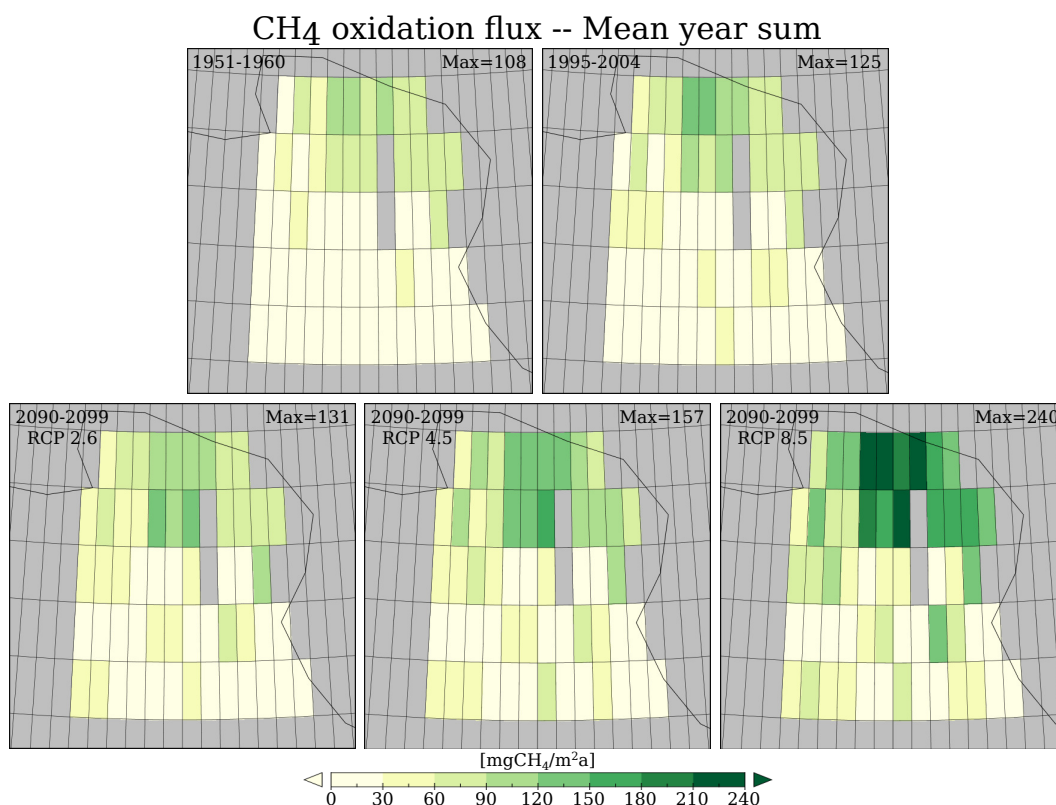
Figure B.4: Modelled bulk soil methane oxidation flux as mean year sum over 10 years periods in mgCH$_4$ m^{-2} a^{-1}. Please note the details at the top of every subfigure.
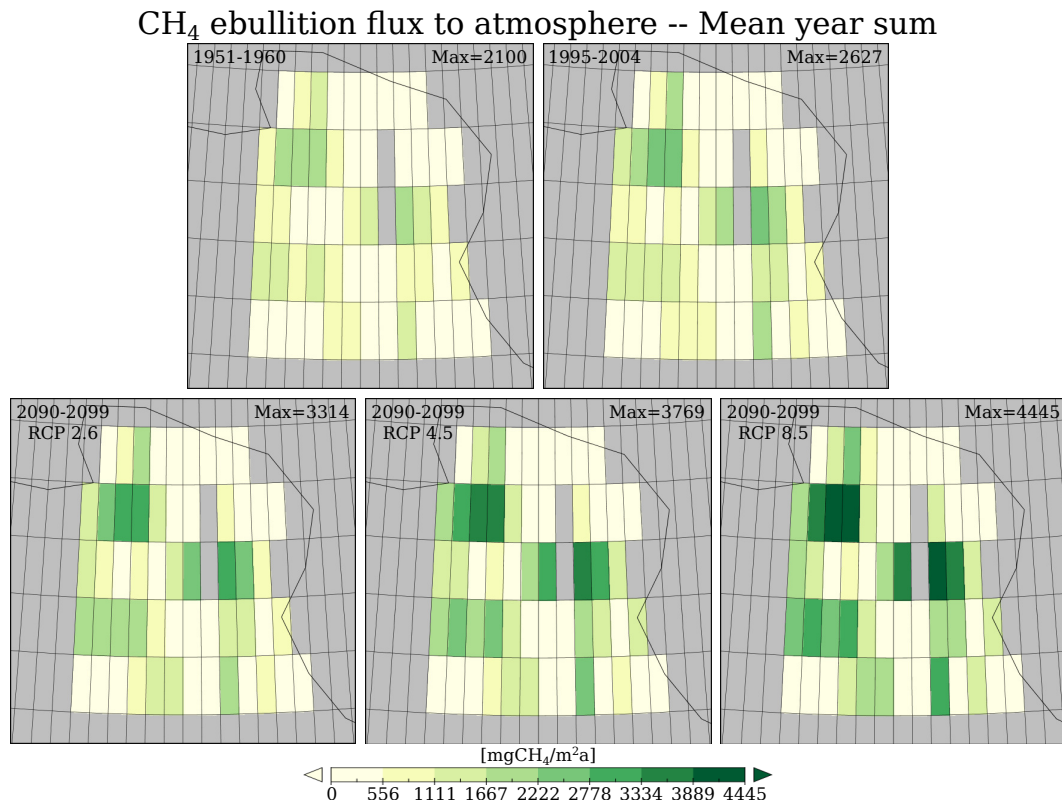
CH₄ plant oxidation flux -- Mean year sum
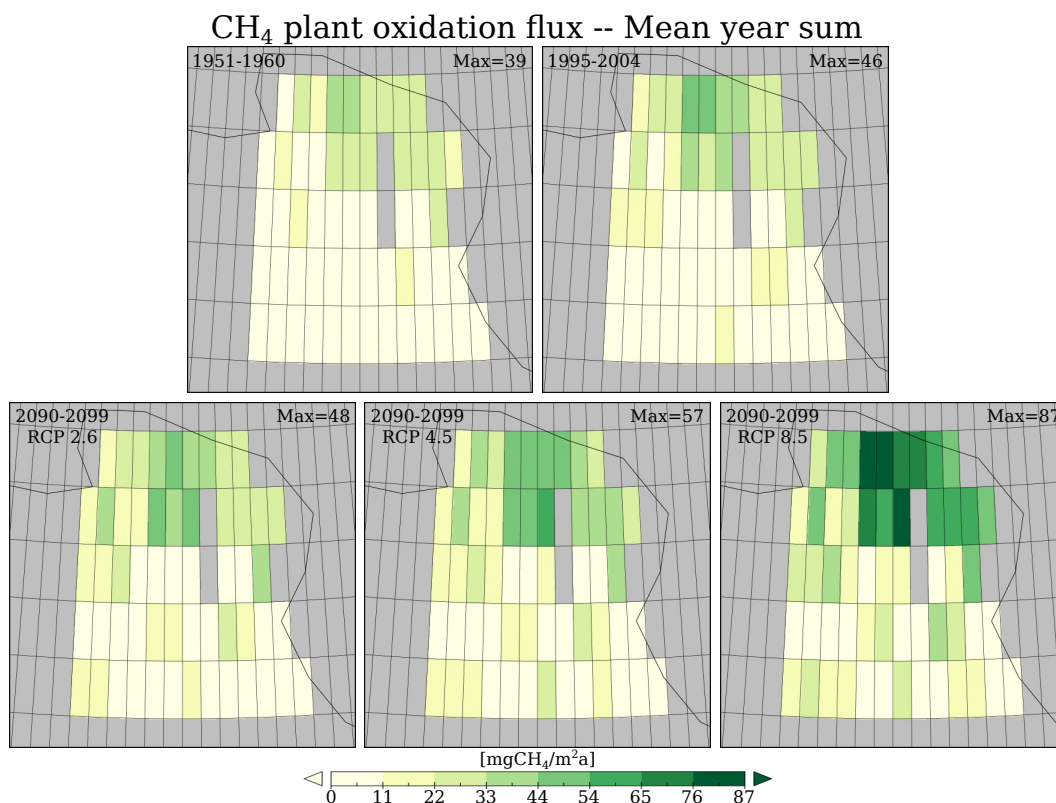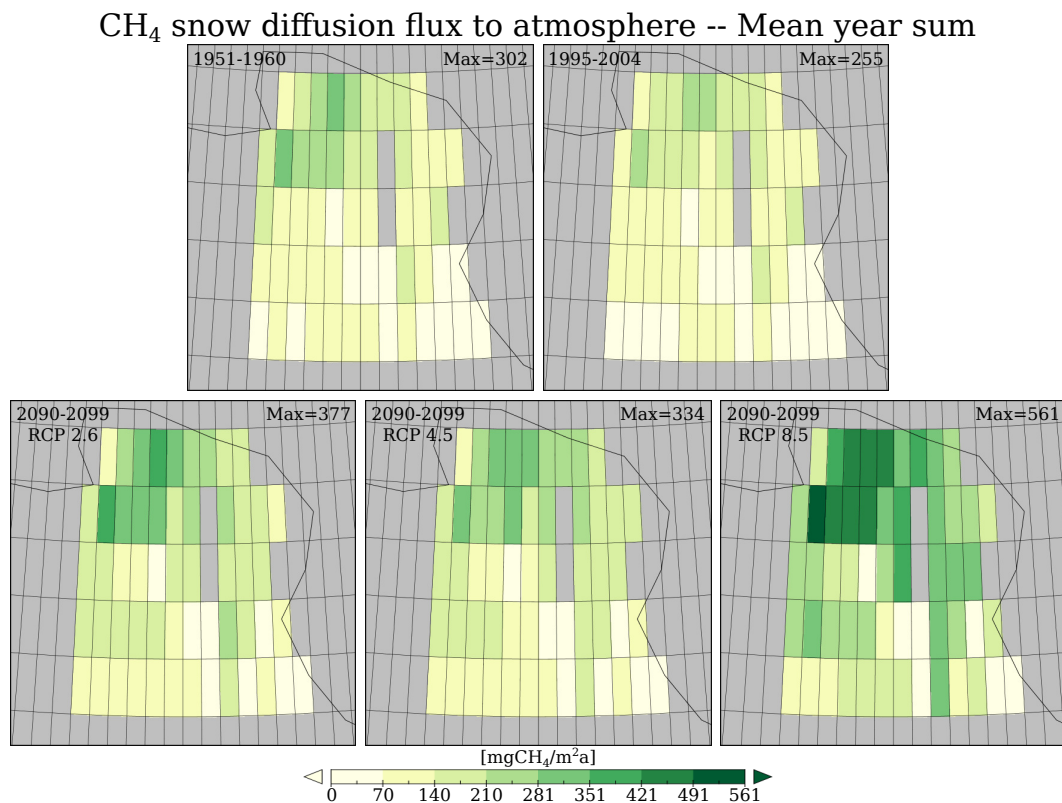

Figure B.5: Modelled rhizospheric methane oxidation flux as mean year sum over 10 years periods in mgCH$_4$ m^{-2} a^{-1}. Please note the details at the top of every subfigure.

CH$_4$ ebullition flux to atmosphere -- Mean year sum

Figure B.6: Modelled methane ebullition flux to the atmosphere as mean year sum over 10 years periods in mgCH$_4$ m^{-2} a^{-1}. Please note the details at the top of every subfigure.

CH$_4$ snow diffusion flux to atmosphere -- Mean year sum

Figure B.7: Modelled methane diffusion through snow flux to the atmosphere as mean year sum over 10 years periods in mgCH$_4$ m^{-2} a^{-1}. Please note the details at the top of every subfigure.

B.4 Development of the soil respiration with time

Table B.9: Summary of the time series of the soil respiration fluxes.

$[\text{gC}\,\text{m}^{-2}\,\text{a}^{-1}]$	Hist	RCP 2.6	RCP 4.5	RCP 8.5
	$1951-2004$	$2005-2099$	$2005-2099$	$2005-2099$
CH_4	$1-\quad 2$	$1-\quad 2$	$1-\quad 2$	$1-\quad 2$
CO_2	$97-198$	$114-286$	$125-311$	$126-347$
CO_2+CH_4	$98-200$	$116-287$	$126-313$	$127-349$

Summary of the time series of the modelled soil respiration fluxes field means of the yearly sums for the historical period and three future scenarios, rounded to integer. The units are g of C per m^2 and per year.

Table B.10: Annual increases of the soil respiration fluxes.

$[\text{mgC}\,\text{m}^{-2}\,\text{a}^{-1}]$	Hist	RCP 2.6	RCP 4.5	RCP 8.5
	$1951-2004$	$2005-2099$	$2005-2099$	$2005-2099$
CH_4	5.46	2.55	6.74	9.34
CO_2	731.66	382.20	877.12	1443.74
CO_2+CH_4	737.12	384.75	883.86	1453.07

Annual increases of the modelled soil respiration fluxes field means of the yearly sums for the historical period and three future scenarios, rounded to two decimal places. It is the increase factor a in a regression $y(t) = a \cdot t + b$ with t in years. The units are mg of C per m^2 and per year.

Table B.11: Increase compared to the historic period of the annual increases of the soil respiration fluxes.

| | RCP 2.6 | RCP 4.5 | RCP 8.5 |
	2005 − 2099	2005 − 2099	2005 − 2099
CH_4	-53.3	23.4	70.9
CO_2	-47.8	19.9	97.3
CO_2+CH_4	-47.8	19.9	97.1

Increase compared to the historic period of the annual increases of the modelled soil respiration fluxes field means of the yearly sums for three future scenarios in %, rounded to one decimal place.

Table B.12: Spread of the deviations from the linear trend of the soil respiration fluxes.

| $[gC\, m^{-2}\, a^{-1}]$ | Hist | RCP 2.6 | RCP 4.5 | RCP 8.5 |
	1951 − 2004	2005 − 2099	2005 − 2099	2005 − 2099
CH_4	-0 − 0	-0 − 0	-0 − 0	-0 − 0
CO_2	-43 − 34	-88 − 88	-98 − 74	-87 − 62
CO_2+CH_4	-43 − 34	-88 − 88	-98 − 74	-87 − 62

Spread, thus minima to maxima, of the deviations from the linear trend of the modelled soil respiration fluxes field means of the yearly sums for the historical period and three future scenarios, rounded to integer. The units are g of C per m^2 and per year.

Table B.13: Increase compared to the historic period of the spread of the deviations from the linear trend of the soil respiration fluxes.

| | RCP 2.6 | RCP 4.5 | RCP 8.5 |
	2005 − 2099	2005 − 2099	2005 − 2099
CH_4	53.2	48.8	53.7
CO_2	129.3	123.1	94.2
CO_2+CH_4	128.8	122.9	93.7

Increase compared to the historic period of the spread of the deviations from the linear trend of the modelled soil respiration fluxes field means of the yearly sums for three future scenarios in %, rounded to one decimal place.
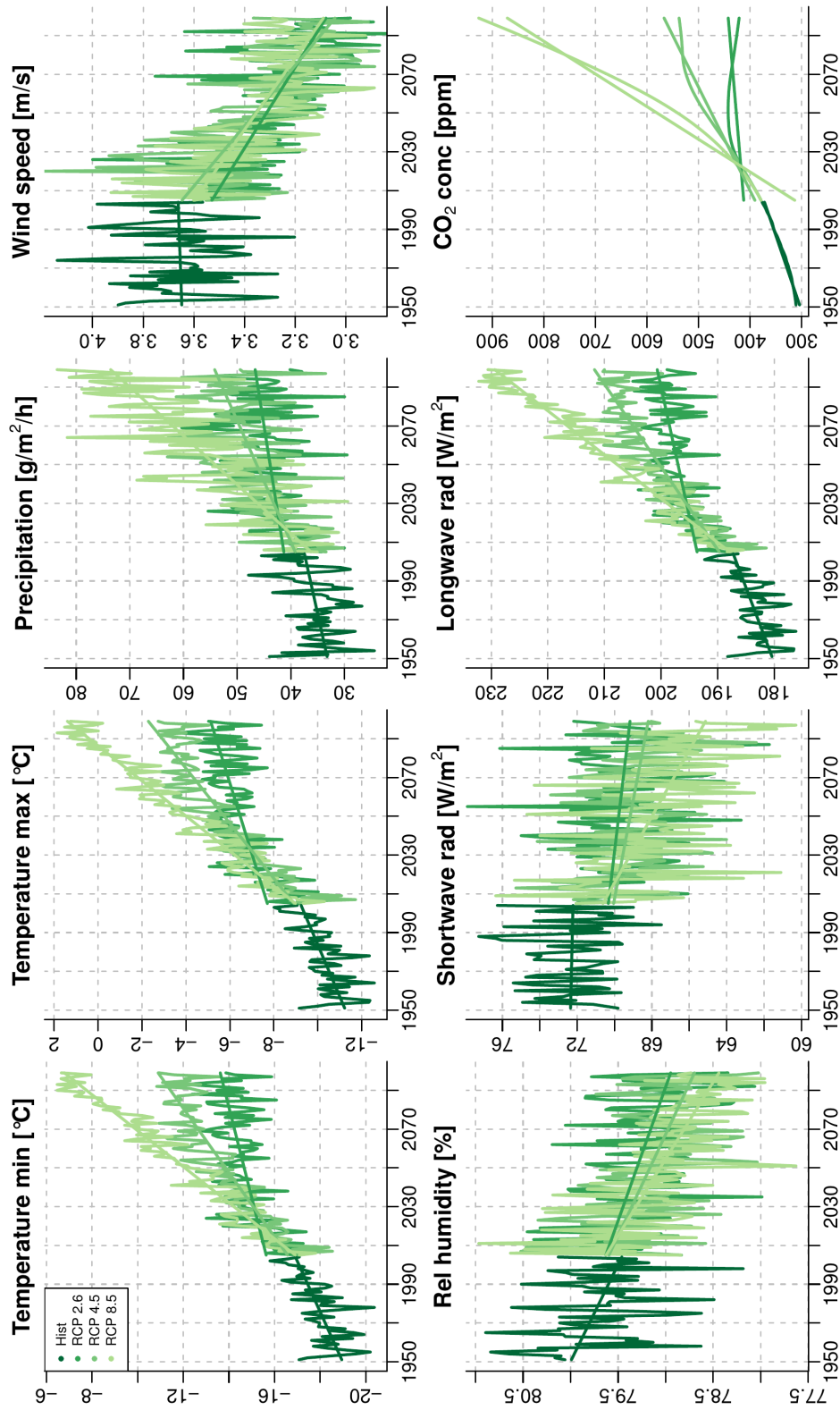
Figure B.8: Climate forcing as field means of the yearly means for the historic (1951 − 2004) and the three RCP scenarios (2005 − 2099): Minimum and maximum temperature in 2 m height, precipitation, wind speed in 10 m height, relative humidity, surface downward short- and long-wave radiation and atmospheric CO_2 concentration. The used units are given in the title of every subfigure. The straight lines show the respective linear regressions.

B.5 Development of the methane fluxes with time

Table B.14: Summary of the time series of the methane process fluxes.

	Hist	RCP 2.6	RCP 4.5	RCP 8.5
	$1951 - 2004$	$2005 - 2099$	$2005 - 2099$	$2005 - 2099$
Prod	$1370 - 2166$	$1671 - 2418$	$1452 - 2741$	$1513 - 3182$
Oxid	$28 - 45$	$33 - 52$	$30 - 63$	$31 - 92$
Plox	$10 - 16$	$11 - 19$	$10 - 23$	$11 - 33$
Plant	$738 - 1107$	$767 - 1155$	$789 - 1329$	$795 - 1443$
Ebul	$509 - 848$	$656 - 1039$	$552 - 1183$	$568 - 1390$
Diff	$0 - 1$	$0 - 1$	$0 - 1$	$0 - 1$
Snow	$41 - 203$	$63 - 283$	$66 - 270$	$66 - 285$
AllTrans	$1333 - 2105$	$1627 - 2347$	$1412 - 2657$	$1471 - 3057$

Summary of the time series of the modelled methane process fluxes field means of the yearly sums for the historical period and three future scenarios in $\mathrm{mgCH_4\,m^{-2}\,a^{-1}}$, rounded to integer. For the meaning of the short names, see Sect. 3.2.

Table B.15: Annual increases of the methane process fluxes.

	Hist	RCP 2.6	RCP 4.5	RCP 8.5
	$1951 - 2004$	$2005 - 2099$	$2005 - 2099$	$2005 - 2099$
Prod	7506.1	3513.4	9348.0	13123.1
Oxid	150.1	77.4	248.0	482.8
Plox	59.3	28.5	95.1	169.9
Plant	3862.7	1094.2	3679.5	4631.2
Ebul	3303.5	1753.8	4719.8	6392.3
Diff	2.3	1.3	3.5	4.8
Snow	127.7	557.8	601.5	1441.5
AllTrans	7296.1	3407.1	9004.3	12469.8

Annual increases of the modelled methane process fluxes field means of the yearly sums for the historical period and three future scenarios in $\mu\mathrm{gCH_4\,m^{-2}\,a^{-1}}$, rounded to one decimal place. It is the increase factor a in a regression $y(t) = a \cdot t + b$ with t in years. For the meaning of the short names, see Sect. 3.2.

Table B.16: Increase compared to the historic period of the annual increases of the methane process fluxes.

| | RCP 2.6 | RCP 4.5 | RCP 8.5 |
	$2005-2099$	$2005-2099$	$2005-2099$
Prod	-53.2	24.5	74.8
Oxid	-48.4	65.3	221.8
Plox	-52.0	60.5	186.5
Plant	-71.7	-4.7	19.9
Ebul	-46.9	42.9	93.5
Diff	-44.8	48.2	103.2
Snow	336.9	371.2	1029.2
AllTrans	-53.3	23.4	70.9

Increase compared to the historic period of the annual increases of the modelled methane process fluxes field means of the yearly sums for three future scenarios in %, rounded to one decimal place. For the meaning of the short names, see Sect. 3.2.

Table B.17: Spread of the deviations from the linear trend of the methane process fluxes.

| | Hist | RCP 2.6 | RCP 4.5 | RCP 8.5 |
	$1951-2004$	$2005-2099$	$2005-2099$	$2005-2099$
Prod	$-286.4-249.8$	$-422.3-401.1$	$-423.7-374.2$	$-451.7-389.4$
Oxid	$-6.4-\ \ 6.2$	$-10.5-\ \ 9.6$	$-11.5-\ \ 9.8$	$-14.8-\ 19.5$
Plox	$-2.6-\ \ 2.5$	$-4.5-\ \ 3.8$	$-4.6-\ \ 4.4$	$-5.9-\ \ 7.5$
Plant	$-136.6-150.6$	$-231.6-183.3$	$-232.6-191.8$	$-230.5-244.7$
Ebul	$-133.4-125.8$	$-214.9-183.4$	$-200.6-153.5$	$-239.6-206.9$
Diff	$0.1-\ \ 0.1$	$-0.2-\ \ 0.1$	$-0.1-\ \ 0.1$	$-0.2-\ \ 0.2$
Snow	$-68.5-\ 93.6$	$-77.4-130.1$	$-78.4-107.5$	$-113.4-\ 87.6$
AllTrans	$-277.6-241.1$	$-407.2-387.6$	$-407.5-364.2$	$-430.9-366.6$

Spread of the deviations from the linear trend of the modelled methane process fluxes field means of the yearly sums for the historical period and three future scenarios in $mgCH_4\,m^{-2}\,a^{-1}$, rounded to one decimal place. For the meaning of the short names, see Sect. 3.2.

Table B.18: Increase compared to the historic period of the spread of the deviations from the linear trend of the methane process fluxes.

| | RCP 2.6 | RCP 4.5 | RCP 8.5 |
	$2005-2099$	$2005-2099$	$2005-2099$
Prod	53.6	48.8	56.9
Oxid	61.0	70.2	174.3
Plox	61.9	75.7	160.7
Plant	44.5	47.8	65.5
Ebul	53.7	36.6	72.2
Diff	60.8	45.1	84.6
Snow	28.0	14.7	24.0
AllTrans	53.2	48.8	53.7

Increase compared to the historic period of the spread of the deviations from the linear trend of the modelled methane process fluxes field means of the yearly sums for three future scenarios in %, rounded to one decimal place. For the meaning of the short names, see Sect. 3.2.

B.6 Development of the seasonal cycle of the soil respiration

Table B.19: Increase compared to the historic period of the maxima of the hourly soil respiration fluxes for a mean year.

	Curr 1995 − 2004	RCP 2.6 2090 − 2099	RCP 4.5 2090 − 2099	RCP 8.5 2090 − 2099
CH_4	11.7	9.6	17.0	29.9
CO_2	18.7	13.4	25.1	43.5
CO_2+CH_4	18.6	13.3	25.1	43.4

Increase compared to the historic period of the maxima of the modelled hourly soil respiration fluxes field means for a mean year of 10 years periods of the current and three future scenarios in %, rounded to one decimal place.

Table B.20: Dates of the maxima of the hourly soil respiration fluxes for a mean year.

	Hist 1951 − 1960	Curr 1995 − 2004	RCP 2.6 2090 − 2099	RCP 4.5 2090 − 2099	RCP 8.5 2090 − 2099
CH_4	29.07.	26.07.	22.07.	24.07.	30.07.
CO_2	21.07.	03.08.	29.08.	16.07.	19.07.
CO_2+CH_4	21.07.	03.08.	29.08.	16.07.	19.07.

Dates of the maxima of the modelled hourly soil respiration fluxes field means for a mean year of 10 years periods of the historic, the current and three future scenarios.

Table B.21: Change compared to carbon dioxide of the dates of the maxima of the hourly soil respiration fluxes for a mean year.

	Hist 1951 − 1960	Curr 1995 − 2004	RCP 2.6 2090 − 2099	RCP 4.5 2090 − 2099	RCP 8.5 2090 − 2099
CH_4	8	-8	-38	8	11
CO_2+CH_4	0	0	0	0	0

Change compared to carbon dioxide of the dates of the maxima of the modelled hourly soil respiration fluxes field means for a mean year of 10 years periods of the historic, the current and three future scenarios in days. Positive values indicate a later maximum.

Table B.22: Change compared to the historic period of the dates of the maxima of the hourly soil respiration fluxes for a mean year.

	Curr 1995 − 2004	RCP 2.6 2090 − 2099	RCP 4.5 2090 − 2099	RCP 8.5 2090 − 2099
CH_4	-3	-7	-5	1
CO_2	13	39	-5	-2
CO_2+CH_4	13	39	-5	-2

Change compared to the historic period of the dates of the maxima of the modelled hourly soil respiration fluxes field means for a mean year of 10 years periods of the current and three future scenarios in days. Positive values indicate a later maximum.

Table B.23: Change compared to carbon dioxide of the start dates of the main emission seasons of the hourly soil respiration fluxes for a mean year.

	Hist 1951 − 1960	Curr 1995 − 2004	RCP 2.6 2090 − 2099	RCP 4.5 2090 − 2099	RCP 8.5 2090 − 2099
CH_4	-11	-7	4	2	10
CO_2+CH_4	0	0	0	0	0

Change compared to carbon dioxide of the start dates of the main emission seasons of the modelled hourly soil respiration fluxes field means for a mean year of 10 years periods of the historic, the current and three future scenarios in days. Positive values indicate a later start.

Table B.24: Change compared to the historic period of the start dates of the main emission seasons of the hourly soil respiration fluxes for a mean year.

	Curr 1995 – 2004	RCP 2.6 2090 – 2099	RCP 4.5 2090 – 2099	RCP 8.5 2090 – 2099
CH_4	-8	-18	-24	-34
CO_2	-12	-33	-37	-55
CO_2+CH_4	-12	-33	-37	-55

Change compared to the historic period of the start dates of the main emission seasons of the modelled hourly soil respiration fluxes field means for a mean year of 10 years periods of the historic, the current and three future scenarios in days. Positive values indicate a later start.

Table B.25: Change compared to carbon dioxide of the end dates of the main emission seasons of the hourly soil respiration fluxes for a mean year.

	Hist 1951 – 1960	Curr 1995 – 2004	RCP 2.6 2090 – 2099	RCP 4.5 2090 – 2099	RCP 8.5 2090 – 2099
CH_4	-1	-2	-5	-17	-32
CO_2+CH_4	0	0	0	0	0

Change compared to carbon dioxide of the end dates of the main emission seasons of the modelled hourly soil respiration fluxes field means for a mean year of 10 years periods of the historic, the current and three future scenarios in days. Positive values indicate a later end.

Table B.26: Change compared to the historic period of the end dates of the main emission seasons of the hourly soil respiration fluxes for a mean year.

	Curr	RCP 2.6	RCP 4.5	RCP 8.5
	$1995 - 2004$	$2090 - 2099$	$2090 - 2099$	$2090 - 2099$
CH_4	6	12	17	30
CO_2	7	16	33	61
CO_2+CH_4	7	16	33	61

Change compared to the historic period of the end dates of the main emission seasons of the modelled hourly soil respiration fluxes field means for a mean year of 10 years periods of the historic, the current and three future scenarios in days. Positive values indicate a later end.

Table B.27: Change compared to carbon dioxide of the length of the main emission seasons of the hourly soil respiration fluxes for a mean year.

	Hist	Curr	RCP 2.6	RCP 4.5	RCP 8.5
	$1951 - 1960$	$1995 - 2004$	$2090 - 2099$	$2090 - 2099$	$2090 - 2099$
CH_4	10	5	-9	-19	-42
CO_2+CH_4	0	0	0	0	0

Change compared to carbon dioxide of the length of the main emission seasons of the modelled hourly soil respiration fluxes field means for a mean year of 10 years periods of the historic, the current and three future scenarios in days. Positive values indicate a longer main emission season.

Table B.28: Change compared to the historic period of the length of the main
emission seasons of the hourly soil respiration fluxes for a mean year.

	Curr 1995–2004	RCP 2.6 2090–2099	RCP 4.5 2090–2099	RCP 8.5 2090–2099
CH_4	14	30	41	64
CO_2	19	49	70	116
CO_2+CH_4	19	49	70	116

Change compared to the historic period of the length of the main emission seasons of the
modelled hourly soil respiration fluxes field means for a mean year of 10 years periods
of the current and three future scenarios in days. Positive values indicate a longer main
emission season.
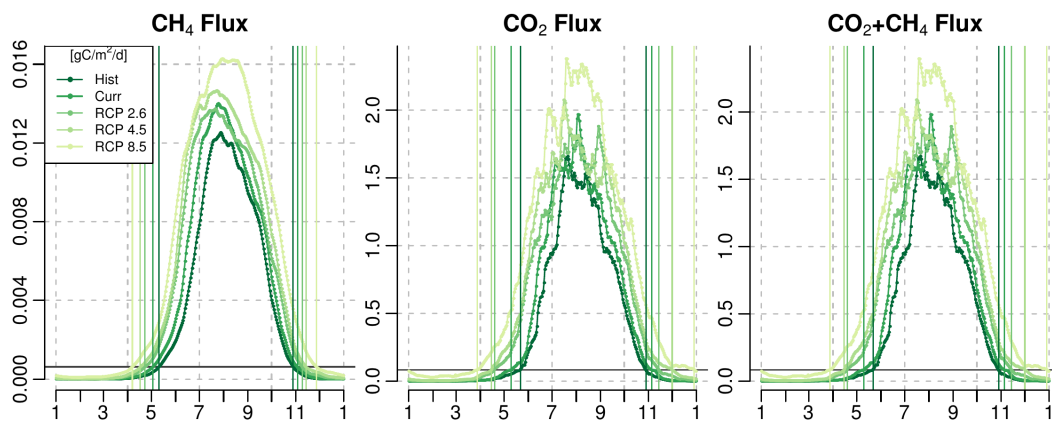
Figure B.9: Modelled soil respiration fluxes field means as hourly data (points) and
daily means (lines) for a mean year of the historic ($1951-1960$), the current
($1995-2004$) and the three RCP scenarios ($2090-2099$) in $gC\,m^{-2}\,d^{-1}$. X
axes indicate the first day of the respective month of the year. The solid
horizontal line is 5% of the maximum in the historic period as indicator of
the timing of the main emission seasons. The coloured vertical lines show
the intersections of the fluxes with this line.

B.7 Development of the seasonal cycle of methane

Table B.29: Increase compared to the historic period of the maxima of the hourly methane process fluxes for a mean year.

	Curr 1995 − 2004	RCP 2.6 2090 − 2099	RCP 4.5 2090 − 2099	RCP 8.5 2090 − 2099
Prod	11.9	9.8	17.6	31.9
Oxid	16.4	17.3	35.4	99.2
Plox	17.9	18.4	39.3	98.4
Plant	10.1	0.0	4.3	12.5
Ebul	14.1	25.7	36.8	55.3
Diff	16.0	30.7	44.2	67.2
SnowS	11.0	24.2	29.7	79.1
SnowA	-21.6	54.8	4.8	59.3
AllTrans	11.7	9.6	17.0	29.9

Increase compared to the historic period of the maxima of the modelled hourly methane process fluxes field means for a mean year of 10 years periods of the historic, the current and three future scenarios in %, rounded to one decimal place. For the meaning of the short names, see Sect. 3.2.

Table B.30: Dates of the maxima of the hourly methane process fluxes for a mean year.

	Hist 1951 − 1960	Curr 1995 − 2004	RCP 2.6 2090 − 2099	RCP 4.5 2090 − 2099	RCP 8.5 2090 − 2099
Prod	28.07.	25.07.	21.07.	23.07.	30.07.
Oxid	27.07.	24.07.	13.07.	23.07.	17.08.
Plox	27.07.	24.07.	14.07.	23.07.	17.08.
Plant	29.07.	26.07.	13.07.	19.07.	31.07.
Ebul	29.07.	25.07.	22.07.	24.07.	29.07.
Diff	28.07.	25.07.	21.07.	23.07.	29.07.
SnowS	30.05.	21.05.	14.05.	12.05.	13.05.
SnowA	11.10.	17.10.	16.10.	20.10.	28.10.
AllTrans	29.07.	26.07.	22.07.	24.07.	30.07.

Dates of the maxima of the modelled hourly methane process fluxes field means for a mean year of 10 years periods of the historic, the current and three future scenarios. For the meaning of the short names, see Sect. 3.2.

Table B.31: Change compared to production of the dates of the maxima of the hourly methane process fluxes for a mean year.

	Hist 1951 – 1960	Curr 1995 – 2004	RCP 2.6 2090 – 2099	RCP 4.5 2090 – 2099	RCP 8.5 2090 – 2099
Oxid	-1	-1	-8	0	18
Plox	-1	-1	-7	0	18
Plant	1	1	-8	-4	1
Ebul	1	0	1	1	-1
Diff	0	0	0	0	-1
SnowS	-59	-65	-68	-72	-78
SnowA	75	84	87	89	90
AllTrans	1	1	1	1	0

Change compared to production of the dates of the maxima of the modelled hourly methane process fluxes field means for a mean year of 10 years periods of the historic, the current and three future scenarios in days. Positive values indicate a later maximum. For the meaning of the short names, see Sect. 3.2.

Table B.32: Change compared to the historic period of the dates of the maxima of the hourly methane process fluxes for a mean year.

	Curr 1995 – 2004	RCP 2.6 2090 – 2099	RCP 4.5 2090 – 2099	RCP 8.5 2090 – 2099
Prod	-3	-7	-5	2
Oxid	-3	-14	-4	21
Plox	-3	-13	-4	21
Plant	-3	-16	-10	2
Ebul	-4	-7	-5	0
Diff	-3	-7	-5	1
SnowS	-9	-16	-18	-17
SnowA	6	5	9	17
AllTrans	-3	-7	-5	1

Change compared to the historic period of the dates of the maxima of the modelled hourly methane process fluxes field means for a mean year of 10 years periods of the current and three future scenarios in days. Positive values indicate a later maximum. For the meaning of the short names, see Sect. 3.2.

Table B.33: Change compared to production of the start dates of the main emission seasons of the hourly methane process fluxes for a mean year.

	Hist 1951 – 1960	Curr 1995 – 2004	RCP 2.6 2090 – 2099	RCP 4.5 2090 – 2099	RCP 8.5 2090 – 2099
Oxid	22	22	23	26	31
Plox	24	25	24	29	39
Plant	22	22	23	27	38
Ebul	21	19	20	24	34
Diff	22	21	21	24	34
SnowS	-29	-26	-29	-30	-65
SnowA	132	150	155	175	191
AllTrans	0	-1	-1	-1	0

Change compared to production of the start dates of the main emission seasons of the modelled hourly methane process fluxes field means for a mean year of 10 years periods of the historic, the current and three future scenarios in days. Positive values indicate a later start. For the meaning of the short names, see Sect. 3.2.

Table B.34: Change compared to the historic period of the start dates of the main emission seasons of the hourly methane process fluxes for a mean year.

	Curr 1995 – 2004	RCP 2.6 2090 – 2099	RCP 4.5 2090 – 2099	RCP 8.5 2090 – 2099
Prod	-7	-17	-23	-34
Oxid	-7	-16	-19	-25
Plox	-6	-17	-18	-19
Plant	-7	-16	-18	-18
Ebul	-9	-18	-20	-21
Diff	-8	-18	-21	-22
SnowS	-4	-17	-24	-70
SnowA	11	6	20	25
AllTrans	-8	-18	-24	-34

Change compared to the historic period of the start dates of the main emission seasons of the modelled hourly methane process fluxes field means for a mean year of 10 years periods of the historic, the current and three future scenarios in days. Positive values indicate a later start. For the meaning of the short names, see Sect. 3.2.

Table B.35: Change compared to production of the end dates of the main emission seasons of the hourly methane process fluxes for a mean year.

	Hist 1951 – 1960	Curr 1995 – 2004	RCP 2.6 2090 – 2099	RCP 4.5 2090 – 2099	RCP 8.5 2090 – 2099
Oxid	-12	-12	-12	-14	-16
Plox	-19	-18	-22	-20	-31
Plant	-16	-15	-21	-18	-30
Ebul	-17	-15	-21	-18	-29
Diff	-19	-18	-22	-19	-29
SnowS	-140	-150	-161	-167	-183
SnowA	20	20	30	40	61
AllTrans	0	1	1	1	0

Change compared to production of the end dates of the main emission seasons of the modelled hourly methane process fluxes field means for a mean year of 10 years periods of the historic, the current and three future scenarios in days. Positive values indicate a later end. For the meaning of the short names, see Sect. 3.2.

Table B.36: Change compared to the historic period of the end dates of the main emission seasons of the hourly methane process fluxes for a mean year.

	Curr 1995 – 2004	RCP 2.6 2090 – 2099	RCP 4.5 2090 – 2099	RCP 8.5 2090 – 2099
Prod	5	11	16	30
Oxid	5	11	14	26
Plox	6	8	15	18
Plant	6	6	14	16
Ebul	7	7	15	18
Diff	6	8	16	20
SnowS	-5	-10	-11	-13
SnowA	5	21	36	71
AllTrans	6	12	17	30

Change compared to the historic period of the end dates of the main emission seasons of the modelled hourly methane process fluxes field means for a mean year of 10 years periods of the historic, the current and three future scenarios in days. Positive values indicate a later end. For the meaning of the short names, see Sect. 3.2.

Table B.37: Change compared to production of the length of the main emission seasons of the hourly methane process fluxes for a mean year.

| | Hist | Curr | RCP 2.6 | RCP 4.5 | RCP 8.5 |
	$1951-1960$	$1995-2004$	$2090-2099$	$2090-2099$	$2090-2099$
Oxid	-34	-34	-35	-40	-47
Plox	-43	-43	-46	-49	-70
Plant	-38	-37	-44	-45	-68
Ebul	-38	-34	-41	-42	-63
Diff	-41	-39	-43	-43	-63
SnowS	-111	-124	-132	-137	-118
SnowA	-112	-130	-125	-135	-130
Snow	-53	-72	-59	-63	-14
AllTrans	0	2	2	2	0

Change compared to production of the length of the main emission seasons of the modelled hourly methane process fluxes field means for a mean year of 10 years periods of the historic, the current and three future scenarios in days. Positive values indicate a longer main emission season. For the meaning of the short names, see Sect. 3.2.

Table B.38: Change compared to the historic period of the length of the main emission seasons of the hourly methane process fluxes for a mean year.

| | Curr | RCP 2.6 | RCP 4.5 | RCP 8.5 |
	$1995-2004$	$2090-2099$	$2090-2099$	$2090-2099$
Prod	12	28	39	64
Oxid	12	27	33	51
Plox	12	25	33	37
Plant	13	22	32	34
Ebul	16	25	35	39
Diff	14	26	37	42
SnowS	-1	7	13	57
SnowA	-6	15	16	46
Snow	-7	22	29	103
AllTrans	14	30	41	64

Change compared to the historic period of the length of the main emission seasons of the modelled hourly methane process fluxes field means for a mean year of 10 years periods of the current and three future scenarios in days. Positive values indicate a longer main emission season. For the meaning of the short names, see Sect. 3.2.
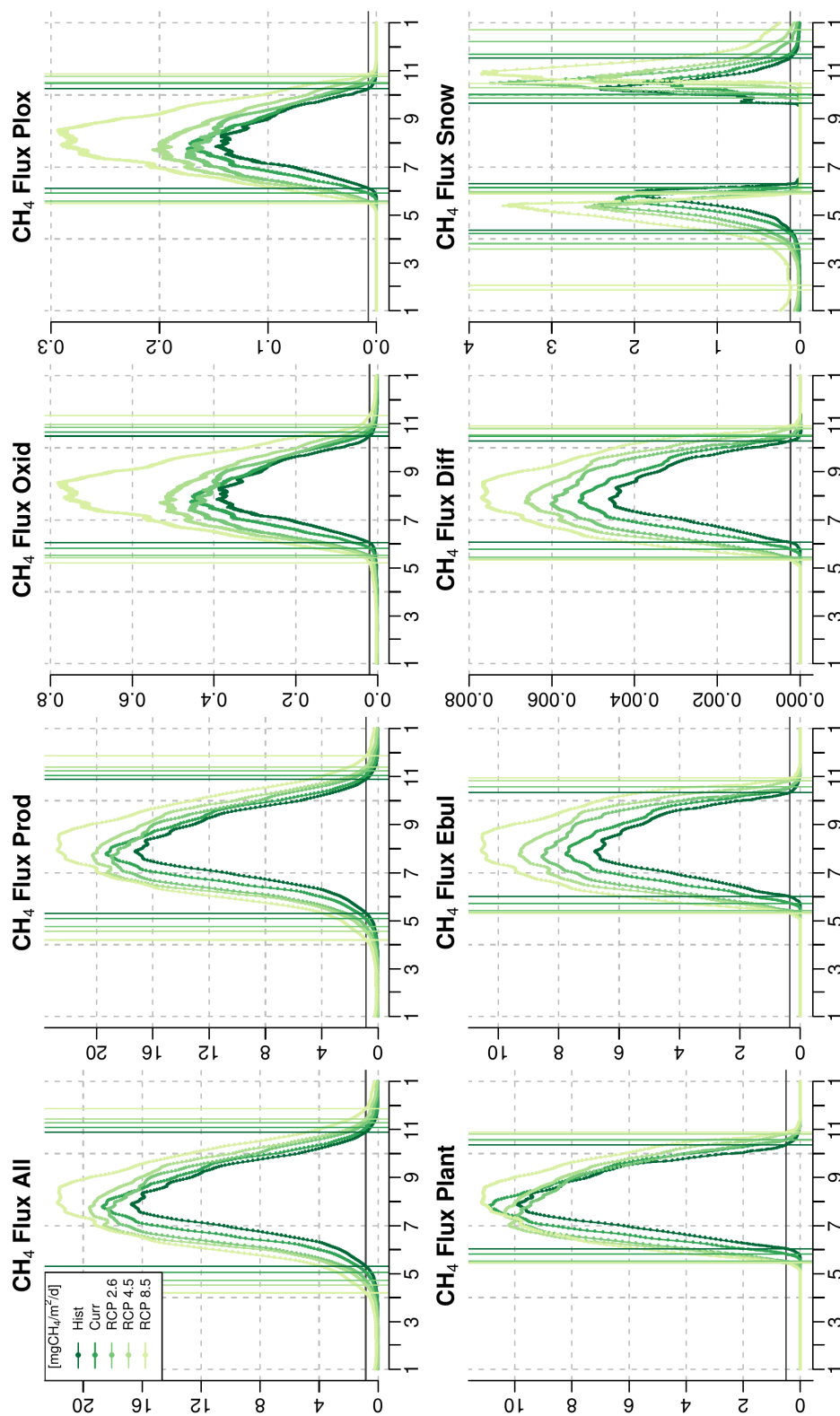
Figure B.10: Modelled methane process fluxes field means as hourly data (points) and daily means (lines) for a mean year of the historic (1951 − 1960), the current (1995 − 2004) and the three RCP scenarios (2090 − 2099) in mgCH$_4$ m^{-2} d^{-1}. X axes indicate the first day of the respective month of the year. The solid horizontal line is 5 % of the maximum in the historic period as indicator of the timing of the main emission seasons. The coloured vertical lines show the intersections of the fluxes with this line.
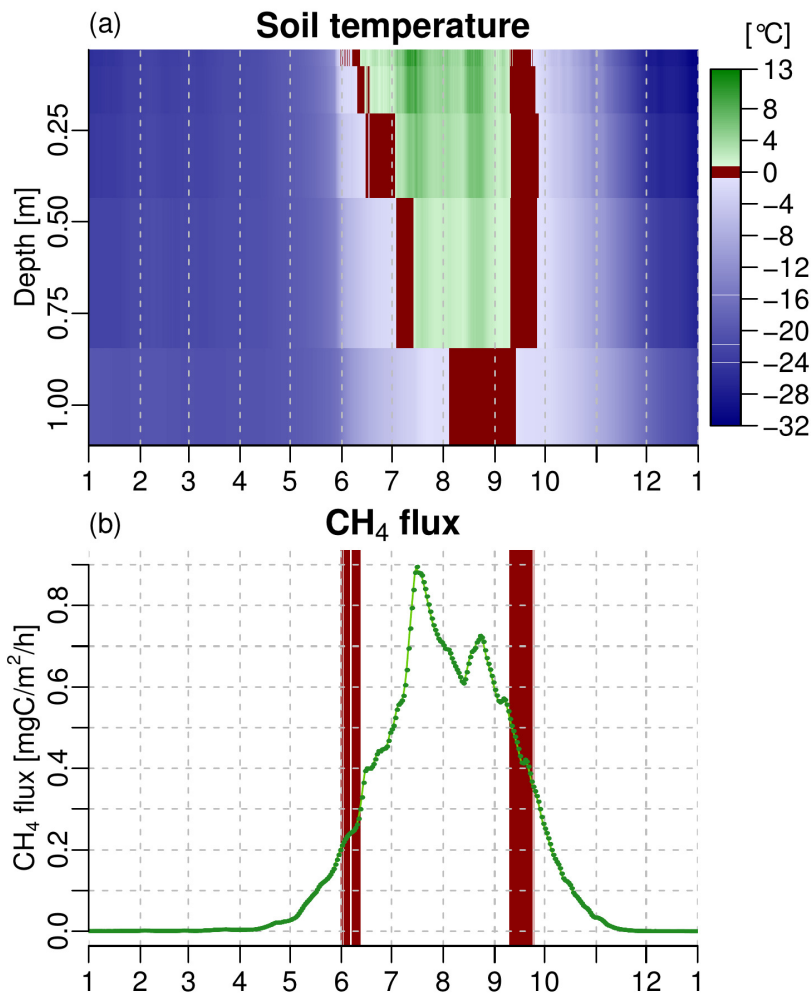
Figure B.11: Modelled **(a)** soil temperature of the uppermost five soil layers and **(b)** methane emissions as hourly data (points) and daily means (lines) in mgC m^{-2} h^{-1} for the grid cell containing Samoylov and for the year 1985. This grid cell has medium methane emissions within the model domain and its seasonal fractionation in 1985 is with 10.2 % in the zero curtain and 14.6 % in the cold season nearly mean within the historic period (compare Table 4.3). X axes and dashed vertical lines indicate the first day of the respective month of the year. In **(a)**, red colour indicates temperatures between -0.75 and 0.75 °C. In **(b)**, red background indicates, when the first soil layer shows these temperatures.

List of Figures

List of Tables

Acknowledgement

This work was done with the help of the following people:

Christian Beer

Karel Castro-Morales

Altug Ekici

Mathias Göckede

Uwe-Jens Görke

Martin Heimann

Thomas Kleinen

Christian Knoblauch

Guido Krämer

Torsten Sachs

Christian Wille

Sebastian Zubrzycki

Thank you!

Bibliography

Arctic Climate Impact Assessment (ACIA): Impacts of a Warming Arctic: Arctic Climate Impact Assessment, ACIA Overview report, Cambridge University Press, ISBN 0-521-61778-2, 2004.

Bartlett, K. B., Crill, P. M., Sass, R. L., Harriss, R. C., Dise, N. B.: Methane emissions from tundra environments in the Yukon-Kuskokwim delta, Alaska, J. Geophys. Res., 97, D15, 16645 – 16660, doi:10.1029/91JD00610, 1992.

Beer, C., Weber, U., Tomelleri, E., Carvalhais, N., Mahecha, M., Reichstein, M.: Harmonized European Long-Term Climate Data for Assessing the Effect of Changing Temporal Variability on Land–Atmosphere CO_2 Fluxes, J. Clim., 27, 13, 4815 – 4834, doi: http://dx.doi.org/10.1175/JCLI-D-13-00543.1, 2014.

Beer, C.: Permafrost Sub-grid Heterogeneity of Soil Properties Key for 3-D Soil Processes and Future Climate Projections, Front. Earth Sci., 4, 1 – 81, doi:10.3389/feart.2016.00081, 2016.

Beerman, F., Teltewskoi, A., Fiencke, C., Pfeiffer, E.-M., Kutzbach, L.: Stoichiometric analysis of nutrient availability (N,P,K) within soils of polygonal tundra, Biogeochemistry, 122, 2, 211 – 227, doi:10.1007/s10533-014-0037-4, 2015.

Berchet, A., Pison, I., Chevallier, F., Paris, J.-D., Bousquet, P., Bonne, J.-L., Arshinov, M. Y., Belan, B. D., Cressot, C., Davydov, D. K., Dlugokencky, E. J., Fofonov, A. V., Galanin, A., Lavrič, J., Machida, T., Parker, R., Sasakawa, M., Spahni, R., Stocker, B. D., Winderlich, J.: Natural and anthropogenic methane

fluxes in Eurasia: a mesoscale quantification by generalized atmospheric inversion, Biogeosciences, 12, 18, 5393 – 5414, doi:10.5194/bg-12-5393-2015, 2015.

Bloom, A. A., Palmer, P. I., Fraser, A., Reay, D. S., Frankenberg, C.: Large-Scale Controls of Methanogenesis Inferred from Methane and Gravity Space-borne Data, Science, 327, 322 – 325, doi:10.1126/science.1175176, 2010.

Boike, J., Kattenstroth, B., Abramova, K., Bornemann, N., Chetverova, A., Fedorova, I., Fröb, K., Grigoriev, M., Grüber, M., Kutzbach, L., Langer, M., Minke, M., Muster, S., Piel, K., Pfeiffer, E.-M., Stoof, G., Westermann, S., Wischnewski, K., Wille, C., Hubberten, H.-W.: Baseline characteristics of climate, permafrost and land cover from a new permafrost observatory in the Lena River Delta, Siberia (1998 – 2011), Biogeosciences, 10, 3, 2105 – 2128, doi:10.5194/bg-10-2105-2013, 2013.

Boudreau, B. P.: Diagenetic Models and their Implementation. Modelling Transport and Reactions in Aquatic Sediments, Springer, Berlin, doi:10.1007/978-3-642-60421-8, 1997.

Bousquet, P., Ringeval, B., Pison, I., Dlugokencky, E. J., Brunke, E.-G., Carouge, C., Chevallier, F., Fortems-Cheiney, A., Frankenberg, C., Hauglustaine, D. A., Krummel, P. B., Langenfelds, R. L., Ramonet, M., Schmidt, M., Steele, L. P., Szopa, S., Yver, C., Viovy, N., Ciais, P.: Source attribution of the changes in atmospheric methane for 2006 – 2008, Atmos. Chem. Phys., 11, 8, 3689 – 3700, doi:10.5194/acp-11-3689-2011, 2011.

Braakhekke, M. C., Beer, C., Hoosbeek, M. R., Reichstein, M., Kruijt, B., Schrumpf, M., Kabat, P.: SOMPROF: A vertically explicit soil organic matter model, Ecol. Model., 222, 10, 1712 – 1730, doi:10.1016/j.ecolmodel.2011.02.015, 2011.

Braakhekke, M. C., Beer, C., Schrumpf, M., Ekici, A., Ahrens, B., Hoosbeek, M. R., Kruijt, B., Kabat, P., Reichstein, M.: The use of radiocarbon to constrain current and future soil organic matter turnover and transport in a temperate

forest, J. Geophys. Res.-Biogeo., 119, 3, 372 – 391, doi:10.1002/2013JG002420, 2014.

Brown, J., Ferrians, O. J. Jr, Heginbottom, J. A., Melnikov, E. S.: Circum-Arctic Map of Permafrost and Ground Ice Conditions, Boulder, CO: National Snow and Ice Data Center, 1998, revised 2001.

CAVM Team: Circumpolar Arctic Vegetation Map. (1:7,500,000 scale), Conservation of Arctic Flora and Fauna (CAFF) Map No. 1, U.S. Fish and Wildlife Service, Anchorage, Alaska, ISBN 0-9767525-0-6, ISBN-13 978-0-9767525-0-9, 2003.

Ciais, P., Sabine, C., Bala, G., Bopp, L., Brovkin, V., Canadell, J., Chhabra, A., DeFries, R., Galloway, J., Heimann, M., Jones, C., Le Quéré, C., Myneni, R. B., Piao, S., Thornton, P.: Carbon and Other Biogeochemical Cycles. In: Climate Change 2013: The Physical Science Basis. Contribution of Working Group I to the Fifth Assessment Report of the Intergovernmental Panel on Climate Change [Stocker, T.F., Qin, D., Plattner, G.-K., Tignor, M., Allen, S.K., Boschung, J., Nauels, A., Xia, Y., Bex, V., Midgley, P.M. (eds.)], Cambridge University Press, Cambridge, United Kingdom and New York, NY, USA, 2013.

Christensen, T. R., Jonasson, S., Callaghan, T. V., Havström, M.: Spatial variation in high-latitude methane flux along a transect across Siberian and European tundra environments, J. Geophys. Res.-Atmos., 100, D10, 21035 – 21045, doi:10.1029/95JD02145, 1995.

Christensen, T. R., Prentice, I. C., Kaplan, J., Haxeltine, A., Sitch, S.: Methane flux from northern wetlands and tundra, An ecosystem source modelling approach, Tellus B, 48, 5, 652 – 661, doi:10.1034/j.1600-0889.1996.t01-4-00004.x, 1996.

Collin, M., Rasmuson, A.: A comparison of gas diffusivity models for unsaturated porous media, Soil Sci. Soc. Am. J., 52, 6, 1559 – 1565, doi:10.2136/sssaj1988.03615995005200060007x, 1988.

Dean, J. A.: Lange's Handbook of Chemistry, McGraw-Hill, Inc., ISBN 0-07-016384-7, 1992.

Desyatkin, A. R., Takakai, F., Fedorov, P. P., Nikolaeva, M. C., Desyatkin, R. V., Hatano, R.: CH_4 emission from different stages of thermokarst formation in Central Yakutia, East Siberia, Soil Science Plant Nutr., 55, 4, 558–570, doi:10.1111/j.1747-0765.2009.00389.x, 2009.

Ekici, A., Beer, C., Hagemann, S., Boike, J., Langer, M., Hauck, C.: Simulating high-latitude permafrost regions by the JSBACH terrestrial ecosystem model, Geosci. Model Dev., 7, 2, 631–647, doi:10.5194/gmd-7-631-2014, 2014.

EPA (United States Environmental Protection Agency): Methane and nitrous oxide emissions from natural sources, United States Environmental Protection Agency (EPA) Report, Washington, DC, https://nepis.epa.gov/Exe/ZyPDF.cgi/P100717T.PDF?Dockey=P100717T.PDF, 2010.

French, H.: The periglacial environment, 3rd Edn., Wiley, New York, ISBN 978-0-470-86588-0, 2007.

Friborg, T., Christensen, T. R., Sogaard, H.: Rapid response of greenhouse gas emission to early thaw in a subarctic mire as shown by micrometeorological techniques, Geophys. Res. Lett., 24, 23, 3061–3064, doi:10.1029/97GL03024, 1997.

Goll, D. S., Brovkin, V., Liski, J., Raddatz, T., Thum, T., Todd-Brown, K. E. O.: Strong dependence of CO_2 emissions from anthropogenic land cover change on initial land cover and soil carbon parametrization, Glob. Biogeochem. Cycles, 29, 9, 1511–1523, doi:10.1002/2014GB004988, 2015.

Gurevitch, J., Scheiner, S. M., Fox, G. A.: The Ecology of Plants, 2nd Edn., Sinauer Associates, Inc., Sunderland, ISBN: 0878932941, 2006.

Hagemann, S., Stacke, T.: Impact of the soil hydrology scheme on simulated soil moisture memory, Clim. Dyn., 44, 7, 1731 – 1750, doi:10.1007/s00382-014-2221-6, 2014.

Harden, J. W., Koven, C. D., Ping, C.-L., Hugelius, G., McGuire, A. D., Camill, P., Jorgenson, T., Kuhry, P., Michaelson, G. J., O'Donnell, J. A., Schuur, E. A. G., Tarnocai, C., Johnson, K., Grosse, G.: Field information links permafrost carbon to physical vulnerabilities of thawing, Geophys. Res. Lett., 39, 15, L15704, 1 – 6, doi:10.1029/2012GL051958, 2012.

Hargreaves, K. J., Fowler, D., Pitcairn, C. E. R., Aurela, M.: Annual methane emission from Finnish mires estimated from eddy covariance campaign measurements, Theor. Appl. Climatol., 70, 1, 203 – 213, doi:10.1007/s007040170015, 2001.

Heimann, M., Schulze, E.-D., Winderlich, J., Andreae, M. O., Chi, X., Gerbig, C., Kolle, O., Kübler, K., Lavric, J., Mikhailov, E., Panov, A., Park, S., Rödenbeck, C., Skorochod, A.: The Zotino Tall Tower Observatory (ZOTTO): Quantifying large scale biogeochemical changes in Central Siberia, Nova Acta Leopoldina NF, 117, 399, 51 – 64, doi:http://hdl.handle.net/11858/00-001M-0000-0025-69E7-9, 2014.

Hempel, S., Frieler, K., Warszawski, L., Schewe, J., Piontek, F.: A trend-preserving bias correction – the ISI-MIP approach, Earth Syst. Dynam., 4, 2, 219 – 236, doi:10.5194/esd-4-219-2013, 2013.

Houghton, J. T., Ding, Y., Griggs, D. J., Noguer, M., van der Linden, P. J., Dai, X., Maskell, K., Johnson, C. A. (eds.): Climate Change 2001: The Scientific Basis. Contribution of Working Group I to the Third Assessment Report of the Intergovernmental Panel on Climate Change, Cambridge University Press, Cambridge, United Kingdom and New York, NY, USA, 2001.

Hugelius, G., Strauss, J., Zubrzycki, S., Harden, J. W., Schuur, E. A. G., Ping, C.-L., Schirrmeister, L., Grosse, G., Michaelson, G. J., Koven, C. D., O'Donnell, J.

A., Elberling, B., Mishra, U., Camill, P., Yu, Z., Palmtag, J., Kuhry, P.: Estimated stocks of circumpolar permafrost carbon with quantified uncertainty ranges and identified data gaps, Biogeosciences, 11, 23, 6573 – 6593, doi:10.5194/bg-11-6573-2014, 2014.

Ito, A., Inatomi, M.: Use of a process-based model for assessing the methane budgets of global terrestrial ecosystems and evaluation of uncertainty, Biogeosciences, 9, 2, 759 – 773, doi:10.5194/bg-9-759-2012, 2012.

Jackowicz-Korczyński, M., Christensen, T. R., Bäckstrand, K., Crill, P., Friborg, T., Mastepanov, M., Ström, L.: Annual cycle of methane emission from a subarctic peatland, J. Geophys. Res., 115, G2, G02009, 1 – 10, doi:10.1029/2008JG000913, 2010.

Jähne, B., Heinz, G., Dietrich, W.: Measurement of the diffusion coefficients of sparingly soluble gases in water, J. Geophys. Res., 92, C10, 10767 – 10776, doi:10.1029/JC092iC10p10767, 1987.

Jammet, M., Crill, P., Dengel, S., Friborg, T.: Large methane emissions from a subarctic lake during spring thaw: Mechanisms and landscape significance, J. Geophys. Res.-Biogeo., 120, 11, 2289 – 2305, doi:10.1002/2015JG003137, 2015.

Jansson, P.-E., Karlberg, L.: COUP Manual, Coupled heat and mass transfer model for soil-plant-atmosphere systems, www.coupmodel.com, 2011.

Jones, A., Stolbovoy, V., Tarnocai, C., Broll, G., Spaargaren, O., Montanarella, L. (eds.): Soil Atlas of the Northern Circumpolar Region, European Commission, Publications Office of the European Union, Luxembourg, 144pp., ISBN 978-92-79-09770-6, doi:10.2788/95795, 2010.

Kaiser, S., Göckede, M., Castro-Morales, K., Knoblauch, C., Ekici, A., Kleinen, T., Zubrzycki, S., Sachs, T., Wille, C., Beer, C.: Process-based modelling of the methane balance in periglacial landscapes (JSBACH-methane), Geosci. Model Dev., 10, 1, 333 – 358, doi:10.5194/gmd-10-333-2017, 2017.

Kamat, S. S., Williams, H. J., Dangott, L. J., Chakrabarti, M., Raushel, F. M.:
The catalytic mechanism for aerobic formation of methane by bacteria, Nature,
497, 7447, 132 – 136, doi:10.1038/nature12061, 2013.

Karl, D. M., Beversdorf, L., Björkman, K. M., Church, M. J., Martinez, A., Delong,
E. F.: Aerobic production of methane in the sea, Nature Geosci, 1, 7, 473 – 478,
doi:10.1038/ngeo234, 2008.

Khalil, M.A.K.: Atmospheric Methane: Sources, Sinks, and Role in Global
Change, Nato ASI Subseries I, Springer Berlin Heidelberg, ISBN-13 978-3-642-
84607-6, doi:10.1007/987-3-642-84605-2, 1993.

Khvorostyanov, D. V., Krinner, G., Ciais, P., Heimann, M., Zimov, S. A.: Vul-
nerability of permafrost carbon to global warming, Part I: model description
and role of heat generated by organic matter decomposition, Tellus B, 60, 2,
250 – 264, doi:10.1111/j.1600-0889.2007.00333.x, 2008.

Khvorostyanov, D. V., Ciais, P., Krinner, G., Zimov, S. A., Corradi, C.: Vulnerab-
ility of permafrost carbon to global warming. Part II: sensitivity of permafrost
carbon stock to global warming, Tellus B, 60, 2, 265 – 275, doi:10.1111/j.1600-
0889.2007.00336.x, 2008.

Kleinen, T., Brovkin, V., Schuldt, R. J.: A dynamic model of wetland extent
and peat accumulation: results for the Holocene, Biogeosciences, 9, 1, 235 – 248,
doi:10.5194/bg-9-235-2012, 2012.

Knoblauch, C., Spott, O., Evgrafova, S., Kutzbach, L., Pfeiffer, E.-M.: Regu-
lation of methane production, oxidation, and emission by vascular plants and
bryophytes in ponds of the northeast Siberian polygonal tundra, J. Geophys.
Res., 120, 12, 2525 – 2541, doi:10.1002/2015JG003053, 2015.

Koelbener, A., Ström, L., Edwards, P. J., Venterink, H. O.: Plant species from
mesotrophic wetlands cause relatively high methane emissions from peat soils,
Plant Soil, 326, 1, 147 – 158, doi:10.1007/s11104-009-9989-x, 2010.

Končalová, H.: Anatomical adaptations to waterlogging in roots of wetland graminoids: limitations and drawbacks, Aquat. Bot., 38, 1, 127 – 134, doi:10.1016/0304-3770(90)90102-Q, 1990.

Koven, C. D., Schuur, E. A. G., Schädel, C., Bohn, T. J., Burke, E. J., Chen, G., Chen, X., Ciais, P., Grosse, G., Harden, J. W., Hayes, D. J., Hugelius, G., Jafarov, E. E., Krinner, G., Kuhry, P., Lawrence, D. M., MacDougall, A. H., Marchenko, S. S., McGuire, A. D., Natali, S. M., Nicolsky, D. J., Olefeldt, D., Peng, S., Romanovsky, V. E., Schaefer, K. M., Strauss, J., Treat, C. C., Turetsky, M.: A simplified, data-constrained approach to estimate the permafrost carbon – climate feedback, Phil. T. R. Soc. A, 373, 2054, 20140423, doi:10.1098/rsta.2014.0423, 2015.

Kuhry, P., Dorrepaal, E., Hugelius, G., Schuur, E. A. G., Tarnocai, C.: Potential remobilization of belowground permafrost carbon under future global warming, Permafrost Periglac., 21, 2, 208 – 214, doi:10.1002/ppp.684, 2010.

Kukulka, D. J., Gebhart, B., Mollendorf, J. C.: Thermodynamic and transport properties of pure and saline water, Adv. Heat Transfer, 18, 325 – 363, doi:10.1016/S0065-2717(08)70121-7, 1987.

Kutzbach, L., Wagner, D., Pfeiffer, E.-M.: Effect of microrelief and vegetation on methane emission from wet polygonal tundra, Lena Delta, Northern Siberia, Biogeochemistry, 69, 3, 341 – 362, doi:10.1023/B:BIOG.0000031053.81520.db, 2004.

Lessner, D. J.: Methanogenesis Biochemistry, Encyclopedia of life sciences (ELS), John Wiley & Sons, Ltd, doi:10.1002/9780470015902.a0000573.pub2, 2009.

Madigan, M. T., Martinko, J. M., Bender, K.: Brock Biology of Microorganisms, Global ed. of 14th revised ed., Addison-Wesley Longman, Amsterdam, ISBN 1292018313, 2014.

Martin, W.: Hydrothermalquellen und der Ursprung des Lebens. Alles hat einen Anfang, auch die Evolution, Biol. Unserer Zeit, 39, 3, 166 – 174, doi:10.1002/biuz.200910391, 2009.

Marushchak, M. E., Friborg, T., Biasi, C., Herbst, M., Johansson, T., Kiepe, I., Liimatainen, M., Lind, S. E., Martikainen, P. J., Virtanen, T., Soegaard, H., Shurpali, N. J.: Methane dynamics in the subarctic tundra: combining stable isotope analyses, plot- and ecosystem-scale flux measurements, Biogeosciences, 13, 2, 597 – 608, doi:10.5194/bg-13-597-2016, 2016.

Massman, W. J.: A review of the molecular diffusivities of H_2O, CO_2, CH_4, CO, O_3, SO_2, NH_3, N_2O, NO, and NO_2 in air, O_2 and N_2 near STP, Atmos. Environ., 32, 6, 1111 – 1127, doi:10.1016/S1352-2310(97)00391-9, 1998.

Matthews, E., Fung, I.: Methane emission from natural wetlands: Global distribution, area, and environmental characteristics of sources, Glob. Biogeochem. Cycles, 1, 1, 61 – 86, doi:10.1029/GB001i001p00061, 1987.

Meinshausen, M., Smith, S. J., Calvin, K., Daniel, J. S., Kainuma, M. L. T., Lamarque, J.-F., Matsumoto, K., Montzka, S. A., Raper, S. C. B., Riahi, K., Thomson, A., Velders, G. J. M., van Vuuren, D. P. P.: The RCP greenhouse gas concentrations and their extensions from 1765 to 2300, Climatic Change, Springer, 109, 213 – 241, doi:10.1007/s10584-011-0156-z, 2011.

Melle, C., Wallenstein, M., Darrouzet-Nardi, A., Weintraub, M. N.: Microbial activity is not always limited by nitrogen in Arctic tundra soils, Soil. Biol. Biochem., 90, 1, 52 – 61, doi:10.1016/j.soilbio.2015.07.023, 2015.

Mi, Y., van Huissteden, J., Parmentier, F. J. W., Gallagher, A., Budishchev, A., Berridge, C. T., Dolman, A. J.: Improving a plot-scale methane emission model and its performance at a northeastern Siberian tundra site, Biogeosciences, 11, 14, 3985 – 3999, doi:10.5194/bg-11-3985-2014, 2014.

Mitsch, W.J., Gosselink, J.G.: Wetlands, 4th edn., Wiley, Hoboken, ISBN-10 0471699675, ISBN-13 978-0471699675, 2007.

Muster, S., Langer, M., Heim, B., Westermann, S., Boike, J.: Subpixel heterogeneity of ice-wedge polygonal tundra: a multi-scale analysis of land cover and evapotranspiration in the Lena River Delta, Siberia, Tellus B, 64, 0, 17301 – 17319, doi:10.3402/tellusb.v64i0.17301, 2012.

Myhre, G., Shindell, D., Bréon, F.-M., Collins, W., Fuglestvedt, J., Huang, J., Koch, D., Lamarque, J.-F., Lee, D., Mendoza, B., Nakajima, T., Robock, A., Stephens, G., Takemura, T., Zhang, H.: Anthropogenic and Natural Radiative Forcing, in: Climate Change 2013: The Physical Science Basis, Contribution of Working Group I to the Fifth Assessment Report of the Intergovernmental Panel on Climate Change, edited by: Stocker, T. F., Qin, D., Plattner, G.-K., Tignor, M., Allen, S. K., Boschung, J., Nauels, A., Xia, Y., Bex, V., Midgley, P. M., Cambridge University Press, Cambridge, UK, New York, NY, USA, doi:10.1017/CBO9781107415324.018, 2013.

Nakano, T., Kuniyoshi, S., Fukuda, M.: Temporal variation in methane emission from tundra wetlands in a permafrost area, northeastern Siberia, Atm. Env., 34, 8, 1205 – 1213, doi:10.1016/S1352-2310(99)00373-8, 2000.

Nisbet, E. G., Dlugokencky, E. J., Manning, M. R., Lowry, D., Fisher, R. E., France, J. L., Michel, S. E., Miller, J. B., White, J. W. C., Vaughn, B., Bousquet, P., Pyle, J. A., Warwick, N. J., Cain, M., Brownlow, R., Zazzeri, G., Lanoisellé, M., Manning, A. C., Gloor, E., Worthy, D. E. J., Brunke, E.-G., Labuschagne, C., Wolff, E. W., Ganesan, A. L.: Rising atmospheric methane: 2007 – 2014 growth and isotopic shift, Glob. Biogeochem. Cy., 30, 9, 1356 – 1370, doi:10.1002/2016GB005406, 2016.

Osterkamp, T. E.: Sub-sea permafrost, Academic Press, 2902 – 2912, doi:10.1006/rwos.2001.0008, 2001.

Péwé, T. L.: Britannica Online Encyclopedia: Permafrost: Ice wedges: Origins, https://www.britannica.com/science/permafrost, 2016.

Press, W. H., Teukolsky, S. A., Vetterling, W. T., Flannery, B. P.: Numerical Recipes in Fortran 90, The Art of Parallel Scientific Computing, 2nd Edn., Cambridge University Press, ISBN 0-521-57439-0, 1996.

Proskurowski, G., Lilley, M. D., Seewald, J. S., Früh-Green, G. L., Olson, E. J., Lupton, J. E., Sylva, S. P., Kelley, D. S.: Abiogenic Hydrocarbon Production at Lost City Hydrothermal Field, Science, 319, 5863, 604 – 607, doi:10.1126/science.1151194, 2008.

Reick, C. H., Raddatz, T., Brovkin, V., Gayler, V.: Representation of natural and anthropogenic land cover change in MPI-ESM, J. Adv. Model. Earth Sys., 5, 3, 459 – 482, doi:10.1002/jame.20022, 2013.

Riley, W. J., Subin, Z. M., Lawrence, D. M., Swenson, S. C., Torn, M. S., Meng, L., Mahowald, N. M., Hess, P.: Barriers to predicting changes in global terrestrial methane fluxes: analyses using CLM4Me, a methane biogeochemistry model integrated in CESM, Biogeosciences, 8, 7, 1925 – 1953, doi:10.5194/bg-8-1925-2011, 2011.

Sachs, T., Wille, C., Boike, J., Kutzbach, L.: Environmental controls on ecosystem-scale CH_4 emission from polygonal tundra in the Lena River Delta, Siberia, J. Geophys. Res., 113, G3, G00A03, 1 – 12, doi:10.1029/2007JG000505, 2008.

Sachs, T., Giebels, M., Boike, J., Kutzbach, L.: Environmental controls on CH_4 emission from polygonal tundra on the microsite scale in the Lena river delta, Siberia, Glob. Change Biol., 16, 11, 3096 – 3110, doi:10.1111/j.1365-2486.2010.02232.x, 2010.

Sander, R.: Compilation of Henry's Law Constants for Inorganic and Organic Species of Potential Importance in Environmental Chemistry, (version 3), available at: http://www.henrys-law.org/henry-3.0.pdf, 1999.

Saunois, M., Bousquet, P., Poulter, B., Peregon, A., Ciais, P., Canadell, J. G., Dlugokencky, E. J., Etiope, G., Bastviken, D., Houweling, S., Janssens-

Maenhout, G., Tubiello, F. N., Castaldi, S., Jackson, R. B., Alexe, M., Arora, V. K., Beerling, D. J., Bergamaschi, P., Blake, D. R., Brailsford, G., Brovkin, V., Bruhwiler, L., Crevoisier, C., Crill, P., Covey, K., Curry, C., Frankenberg, C., Gedney, N., Höglund-Isaksson, L., Ishizawa, M., Ito, A., Joos, F., Kim, H.-S., Kleinen, T., Krummel, P., Lamarque, J.-F., Langenfelds, R., Locatelli, R., Machida, T., Maksyutov, S., McDonald, K. C., Marshall, J., Melton, J. R., Morino, I., Naik, V., O'Doherty, S., Parmentier, F.-J. W., Patra, P. K., Peng, C., Peng, S., Peters, G. P., Pison, I., Prigent, C., Prinn, R., Ramonet, M., Riley, W. J., Saito, M., Santini, M., Schroeder, R., Simpson, I. J., Spahni, R., Steele, P., Takizawa, A., Thornton, B. F., Tian, H., Tohjima, Y., Viovy, N., Voulgara- kis, A., van Weele, M., van der Werf, G. R., Weiss, R., Wiedinmyer, C., Wilton, D. J., Wiltshire, A., Worthy, D., Wunch, D., Xu, X., Yoshida, Y., Zhang, B., Zhang, Z., Zhu, Q.: The global methane budget 2000 – 2012, Earth Syst. Sci. Data, 8, 2, 697 – 751, doi:10.5194/essd-8-697-2016, 2016.

Schaefer, K., Zhang, T., Bruhwiler, L., Barrett, A. P.: Amount and timing of permafrost carbon release in response to climate warming, Tellus B, 63, 2, 165 – 180, doi:10.1111/j.1600-0889.2011.00527.x, 2011.

Schikora, J.: Simulation von Diffusions-Adsorptionsprozessen in natürlichem Gesteinsmaterial mit COMSOL Multiphysics, (Simulation of diffusion adsorp- tion processes in natural stones material with COMSOL Multiphysics), Diploma thesis, University of Dresden, 2012.

Schirrmeister, L., Grosse, G., Wetterich, S., Overduin, P. P., Strauss, J., Schuur, E. A. G., Hubberten, H.-W.: Fossil organic matter characteristics in permafrost deposits of the northeast Siberian Arctic, J. Geophys. Res., 116, G2, G00M02, 1 – 16, doi:10.1029/2011JG001647, 2011.

Schneider, J., Grosse, G., Wagner, D.: Land cover classification of tundra en- vironments in the Arctic Lena Delta based on Landsat 7 ETM+ data and its application for upscaling of methane emissions, Remote Sens. Environ., 113, 2, 380 – 391, doi:10.1016/j.rse.2008.10.013, 2009.

Schneider von Deimling, T., Grosse, G., Strauss, J., Schirrmeister, L., Morgenstern, A., Schaphoff, S., Meinshausen, M., Boike, J.: Observation-based modelling of permafrost carbon fluxes with accounting for deep carbon deposits and thermokarst activity, Biogeosciences, 12, 11, 3469 – 3488, doi:10.5194/bg-12-3469-2015, 2015.

Schuldt, R. J., Brovkin, V., Kleinen, T., Winderlich, J.: Modelling Holocene carbon accumulation and methane emissions of boreal wetlands – an Earth system model approach, Biogeosciences, 10, 3, 1659 – 1674, doi:10.5194/bg-10-1659-2013, 2013.

Schütz, H., Seiler, W., Conrad, R.: Processes involved in formation and emission of metane in rice paddies, Biogeochem., 7, 1, 33 – 53, doi:10.1007/BF00000896, 1989.

Schuur, E. A. G., McGuire, A. D., Schädel, C., Grosse, G., Harden, J. W., Hayes, D. J., Hugelius, G., Koven, C. D., Kuhry, P., Lawrence, D. M., Natali, S. M., Olefeldt, D., Romanovsky, V. E., Schaefer, K., Turetsky, M. R., Treat, C. C., Vonk, J. E.: Climate change and the permafrost carbon feedback, Nature, 520, 7546, 171 – 179, doi:10.1038/nature14338, 2015.

Schwietzke, S., Sherwood, O. A., Bruhwiler, L. M. P., Miller, J. B., Etiope, G., Dlugokencky, E. J., Michel, S. E., Arling, V. A., Vaughn, B. H., White, J. W. C., Tans, P. P.: Upward revision of global fossil fuel methane emissions based on isotope database, Nature, 538, 7623, 88 – 91, doi:10.1038/nature19797, 2016.

Segers, R.: Methane production and methane consumption: a review of processes underlying wetland methane fluxes, Biogeochemistry, 41, 1, 23 – 51, doi:10.1023/A:1005929032764, 1998.

Shaver, G. R., Billings, W. D.: Root Production and Root Turnover in a Wet Tundra Ecosystem, Barrow, Alaska, Ecology, 56, 2, 401 – 409, doi:10.2307/1934970, 1975.

Smagin, A. V., Shnyrev, N. A.: Methane Fluxes during the Cold Season: Distribution and Mass Transfer in the Snow Cover of Bogs, Eurasian Soil Sci., 48, 8, 823–830, doi:10.1134/S1064229315080086, 2015.

Song, C., Xu, X., Sun, X., Tian, H., Sun, L., Miao, Y., Wang, X., Guo, Y.: Large methane emission upon spring thaw from natural wetlands in the northern permafrost region, Environ. Res. Lett., 7, 3, 034009, 1–8, doi:10.1088/1748-9326/7/3/034009, 2012.

Sonntag, D., Heinze, D.: Sättigungsdampfdruck- und Sättigungsdampfdichtetafeln für Wasser und Eis, (Saturated Vapor Pressure and Saturated Vapor Density Tables for Water and Ice), 1st Edn., VEB Deutscher Verlag für Grundstoffindustrie, 1982.

Stacke, T., Hagemann, S.: Development and evaluation of a global dynamical wetlands extent scheme, Hydrol. Earth Syst. Sci., 16, 8, 2915–2933, doi:10.5194/hess-16-2915-2012, 2012.

Stieglitz, M., Rind, D., Famiglietti, J., Rosenzweig, C.: An efficient approach to modeling the topographic control of surface hydrology for regional and global climate modeling, J. Clim., 10, 1, 118–137, doi:10.1175/1520-0442(1997)010<0118:AEATMT>2.0.CO;2, 1997.

Ström, L., Tagesson, T., Mastepanov, M., Christensen, T. R.: Presence of *Eriophorum schuchzeri* enhances substrate availability and methane emission in an Arctic wetland, Soil. Biol. Biochem., 45, 1, 61–70, doi:10.1016/j.soilbio.2011.09.005, 2012.

Tagesson, T., Mölder, M., Mastepanov, M., Sigsgaard, C., Tamstorf, M. P., Lund, M., Falk, J. M., Lindroth, A., Christensen, T. R., Ström, L.: Land-atmosphere exchange of methane from soil thawing to soil freezing in a high-Arctic wet tundra ecosystem, Glob. Change Biol., 18, 6, 1928–1940, doi:10.1111/j.1365-2486.2012.02647.x, 2012.

Tan, Z., Zhuang, Q.: Methane emissions from pan-Arctic lakes during the 21st century: An analysis with process-based models of lake evolution and biogeochemistry, J. Geophys. Res. Biogeo., 120, 12, 2641–2653, doi:10.1002/2015JG003184, 2015.

Thauer, R. K.: Biochemistry of methanogenesis: a tribute to Marjory Stephenson, Microbiology, 144, 9, 2377–2406, doi:10.1099/00221287-144-9-2377, 1998.

Tokida, T., Miyazaki, T., Mizoguchi, M., Nagata, O., Takakai, F., Kagemoto, A., Hatano, R.: Falling atmospheric pressure as a trigger for methane ebullition from peatland, Global Biogeochem. Cy., 21, 2, GB2003, 1–8, doi:10.1029/2006GB002790, 2007.

Tokida, T., Mizoguchi, M., Miyazaki, T., Kagemoto, A., Nagata, O., Hatano, R.: Episodic release of methane bubbles from peatland during spring thaw, Chemosphere, 70, 2, 165–171, doi:10.1016/j.chemosphere.2007.06.042, 2007.

Walter, B. P., Heimann, M.: A process-based, climate-sensitive model to derive methane emissions from natural wetlands: Application to five wetland sites, sensitivity to model parameters, and climate, Global Biogeochem. Cy., 14, 3, 745–765, doi:10.1029/1999GB001204, 2000.

Walter, B. P., Heimann M., Matthews, E.: Modeling modern methane emissions from natural wetlands 1. Model description and results, J. Geophys. Res., 106, D24, 34189–34206, doi:10.1029/2001JD900165, 2001.

Wania, R.: Modelling northern peatland land surface processes, vegetation dynamics and methane emissions, PhD thesis, University of Bristol, 2007.

Wania, R., Ross, I., Prentice, I. C.: Implementation and evaluation of a new methane model within a dynamic global vegetation model: LPJ-WHyMe v1.3.1, Geosci. Model Dev., 3, 2, 565–584, doi:10.5194/gmd-3-565-2010, 2010.

Warszawski, L., Frieler, K., Huber, V., Piontek, F., Serdeczny, O., Schewe, J.: The Inter-Sectoral Impact Model Intercomparsion Pro-

ject (ISI-MIP): Project framework, PNAS, 111, 9, 3228–3232, doi:www.pnas.org/cgi/doi/10.1073/pnas.1312330110, 2014.

Wille, C., Kutzbach, L., Sachs, T., Wagner, D., Pfeiffer, E.-M.: Methane emission from Siberian arctic polygonal tundra: eddy covariance measurements and modeling, Glob. Change Biol., 14, 6, 1395–1408, doi:10.1111/j.1365-2486.2008.01586.x, 2008.

World Meteorological Organization: WMO Greenhouse Gas Bulletin, 11, ISSN 2078-0796, 2015.

Woo, M. K.: Permafrost Hydrology, Springer, Heidelberg, ISBN 3642234615, 2012.

Xu, X., Elias, D. A., Graham, D. E., Phelps, T. J., Carroll, S. L., Wullschleger, S. D., Thornton, P. E.: A microbial functional group-based module for simulating methane production and consumption: Application to an incubated permafrost soil, J. Geophys. Res.-Biogeo., 120, 7, 1315–1333, doi:10.1002/2015JG002935, 2015.

Yamamoto, S., Alcauskas, J. B., Crozier, T. E.: Solubility of methane in distilled water and seawater, J. Chem. Eng. Data, 21, 1, 78–80, doi:10.1021/je60068a029, 1976.

Yershov, E. D.: General Geocryology, Cambridge University Press, Cambridge, ISBN 0-521-47344-9, 1998.

Zhu, Q., Liu, J., Peng, C., Chen, H., Fang, X., Jiang, H., Yang, G., Zhu, D., Wang, W., Zhou, X.: Modelling methane emissions from natural wetlands by development and application of the TRIPLEX-GHG model, Geosci. Model Dev., 7, 3, 981–999, doi:10.5194/gmd-7-981-2014, 2014.

Zhuang, Q., Melillo, J. M., Kicklighter, D. W., Prinn, R. G., McGuire, A. D., Steudler, P. A., Felzer, B. S., Hu, S.: Methane fluxes between terrestrial ecosystems and the atmosphere at northern high latitudes during the past century: A retrospective analysis with a process-based biogeochemistry model, Global Biogeochem. Cy., 18, 3, GB3010, 1–23, doi:10.1029/2004GB002239, 2004.

Zona, D., Oechel, W. C., Kochendorfer, J., Paw U, K. T., Salyuk, A. N., Olivas, P. C., Oberbauer, S. F., Lipson, D. A.: Methane fluxes during the initiation of a large-scale water table manipulation experiment in the Alaskan Arctic tundra, Global Biogeochem. Cy., 23, 2, GB2013, 1 – 11, doi:10.1029/2009GB003487, 2009.

Zona, D., Gioli, B., Commane, R., Lindaas, J., Wofsy, S. C., Miller, C. E., Dinardo, S. J., Dengel, S., Sweeney, C., Karion, A., Chang, R. Y.-W., Henderson, J. M., Murphy, P. C., Goodrich, J. P., Moreaux, V., Liljedahl, A., Watts, J. D., Kimball, J. S., Lipson, D. A., Oechel, W. C.: Cold season emissions dominate the Arctic tundra methane budget, P. Natl. Acad. Sci. USA, 113, 1, 40 – 45, doi:10.1073/pnas.1516017113, 2016.

Zubrzycki, S., Kutzbach, L., Grosse, G., Desyatkin, A., Pfeiffer, E.-M.: Organic carbon and total nitrogen stocks in soils of the Lena River Delta, Biogeosciences, 10, 6, 3507 – 3524, doi:10.5194/bg-10-3507-2013, 2013.

Selbstständigkeitserklärung

Ich erkläre, daß ich die vorliegende Arbeit selbstständig und nur unter Verwendung der angegebenen Hilfsmittel, persönlichen Mitteilungen und Quellen angefertigt habe.

Wildenfels, den 23. Juni 2017   Sonja Kaiser